Mononuclear Zinc(II) Complexes with Intramolecular Hydrogen Bonding Interactions as Models of Peptidases

A Thesis Submitted for the Degree of

Doctor of Philosophy

by

Emiliano Salvagni

School of Chemistry
University of Edinburgh
King's Buildings
West Mains Road
Edinburgh, EH9 3JJ

July 2005

To my mother

Abstract

Metallopeptidases are enzymes that hydrolyse peptide bonds of polypeptides and proteins; they play vital roles in biological processes including protein digestion and viral defence. In their active-site, in addition to the metal(s) which is an essential cofactor for catalysis, there are amino acid residues that appear to be essential in proton transfer events, substrate activation, positioning and transition state stabilization. However, the role of metal ions and mechanistic details of hydrolysis are often unclear. Synthetic models mimicking the main features of the enzyme active sites were used to elucidate some of these aspects.

As an approach to explore the amide cleavage reaction, we designed, synthesised, fully characterised and investigated different model systems resembling the catalytic zinc sites of peptidases. The models are mononuclear zinc(II) complexes containing the unit (6-NHR-2-pyridylmethyl)amine (R=CO^{t}Bu, H) as a common feature. This unit supplies an N_2 coordination motif and an intramolecular amide oxygen capable of binding the metal ion (Zn···O=C(amide)); such event has been proposed to be crucial for the cleavage of peptide bonds in peptidases. Besides, these models offer different types and numbers of metal binding sites, which affect electronically and sterically the zinc(II) ion as well as its Lewis acidity. Indeed, the effect of the first coordination sphere influences the cleavage of the intramolecular amide bond. Specifically, amide cleavage was found to occur at an N_4 environment 300-fold faster than an N_2S_2 environment. This result is consistent with the natural abundance of nitrogen ligands in catalytic zinc sites.

The unit (6-NHR-2-pyridylmethyl)amine also provides amide/amine groups that can hydrogen bond other zinc-bound ligands. Some of these complexes were, therefore, used to explore strategies to induce and manipulate hydrogen bond interactions, and to investigate the factors that influence their strength. These hydrogen bond interactions occur both in solution and in the solid state and their strength was determined by IR spectroscopy and correlated with the X-ray crystal structures.

We also report two strategies to position NH groups in the proximity of a zinc(II)-bound amide oxygen N-H···O=C(amide), and we investigate their effect on the stability of the amide group. These model systems showed how the effect of different hydrogen bonding microenvironments can both accelerate and slow down amide bond cleavage reactions at zinc(II) sites. Importantly, the magnitude of the effect exerted by the hydrogen bonding environments was found to be significant; 800-fold rate difference.

Lastly, one of these synthetic zinc(II) complexes promote hydrolysis of an unactivated peptide bond (Gly-Gly) at neutral pH at a site that remarkably resembles the active site and reaction intermediates proposed for aminopeptidase A.

In summary, this work highlights the importance of first coordination sphere and hydrogen bonding environments around metal centres in amide cleavage reactions. This study may be relevant to the chemistry of natural metalloproteases and applicable to the design and development of more efficient artificial protein cleaving agents.

Acknowledgements

First of all, I would like to express all my thanks to my supervisor Dr. Juan Mareque for his guidance, encouragement, criticism and mainly for the enthusiasm and motivation he conveyed to me all over my PhD. Working in his group offered me the opportunity to spend three stimulating years on an interesting area of research.

Many thanks to the members of Mareque's group, especially, Rafael Martin Torres De Rosales and Laurent Metteau who helped me as colleagues and friends. Thanks to the new *"arrivals"* Daniela Natale and Pilar Calatayud, for the enjoyable time spent together.

I would like also to thank all my *"in/or-ganic"* friends Michele, Alex, Davide, Chiara, Elaine, spiky Mike, Robert, Pedro, Iria, Maria, Pekka, Isa and Gordon for making the corridor a pleasant environment. Special thanks to Salma for letting me help her with the NMR.

Many thanks to Ale, Andrea A. and B., Ana, Dana, Diego, Cecile, Elena, Fred, Gianni, Ione, Jesus, Murad, Marc, Maria, Popi, Rafa, Romain, Smilja, Viviana, Winz and all the people like them who contributed to turn a cold building in a warm place. Thanks to Xavier for helping me with HPLC studies.

I wish to acknowledge also the School of Chemistry (UoE), EPSRC, Nuffield Foundation and the RSC for funding and also all the technical staff. Above all, Mr. John Millar from the NMR services whose help and kindness were

incommensurable. Special thanks also to Simon Parsons and his group for solving the crystal structures.

Thanks to Steph, for being close during these years of my PhD.

Finally, I would like to thank my family for supporting and encouraging me throughout my studies.

Abbreviations

AIBN	2,2'-azobis(2-methyl-propionitrile)
AMP	adenosine monophosphate
APA	aminopeptidase A
BNPP	bis(4-nitrophenyl)phosphate
ca.	circa
CCDC	Cambridge Crystallographic Data Centre
CPA	carboxypeptidase A
CSD	Cambridge Structural Database
DABS-Cl	(dimethylamino)azobenzensulfonyl chloride
DCM	dichloromethane
DMF	dimethylformamide
DMSO	dimethylsulfoxide
DNA	deoxyribonucleic acid
ESI-MS	electrospray ionisation mass spectroscopy
et al.	and others
FT	Fourier transform
Gly	Glycine
Gly-Gly	Glycylglycine
h	Planck´s constant
HEPES	4-(2-hydroxyethyl)-1-piperazineethanesulfonic acid
HPLC	high performance liquid chromatography
HSAB	hard and soft acid-base theory
i. e.	that is
IR	infrared
L	ligand
N	Avogadro´s number
NBS	*N*-bromosuccinimide
NMR	nuclear magnetic resonance
R	universal gas constant
RNA	ribonucleic acid
tach	1,3,5-triaminocyclohexane
T_c	coalescence temperature
tpa	tris-pyridylmethylamine
TS	transition state
vide infra	see below
vide supra	see above
vs.	in contrast to
VT	variable temperature

Courses attended:

1. Weekly *Inorganic Section Seminars* during terms 2001-2004.

2. Weekly *School of Chemistry Colloquia* during terms 2001-2004.

3. *Induction Course for Laboratory Demonstrators in Chemistry*, Centre for Teaching, Learning and assessment, University of Edinburgh, October 2001.

4. *Scientific Paper Production* by Prof. Bill Earnshaw (Institute of Cell & Molecular Biology), Transferable Skills Programme, University of Edinburgh. 8 May 2002.

5. *Transition Metal Chemistry I and II* by Dr. N. Robertson, undergraduate course, School of Chemistry, University of Edinburgh, 2002.

Publications:

1. **"Investigating the effect of hydrogen bonding environments in amide cleavage reactions at zinc(II) complexes with intramolecular amide oxygen co-ordination"** J. C. Mareque Rivas, E. Salvagni and S. Parsons, *Dalton Trans.*, 4185 (2004)

2. **"Structure and reactivity of synthetic zinc(II) complexes resembling the active site and intermediates of aminopeptidases"** J. C. Mareque Rivas, E. Salvagni and S. Parsons, *Chem. Commun.*, 460 (2004)

3. **"Zinc(II) complexes with intramolecular amide oxygen coordination as models of metalloamidases"** J. C. Mareque Rivas, E. Salvagni, R. Torres Martin de Rosales, Ravi Prabaharan and S. Parsons, *Dalton Trans.*, 172 (2004)

4. **"Internal hydrogen bonding in tetrahedral and trigonal bipyramidal zinc(II) complexes of pyridine-based ligands"** J. C. Mareque Rivas, E. Salvagni, R. Torres Martin de Rosales and S. Parsons, *Dalton Trans.*, 3339 (2003)

Structures Summary

Chapter 2

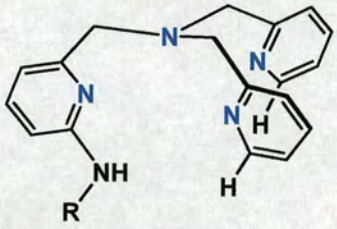

R= CO^tBu ($L^{2.1}$)
R = H ($L^{2.1'}$)

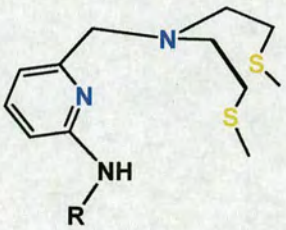

R= CO^tBu ($L^{2.2}$)
R = H ($L^{2.2'}$)

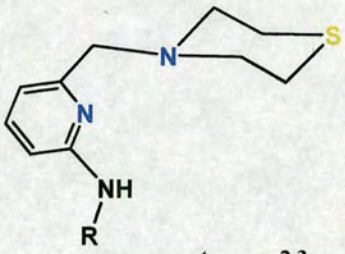

R= CO^tBu ($L^{2.3}$)
R = H ($L^{2.3'}$)

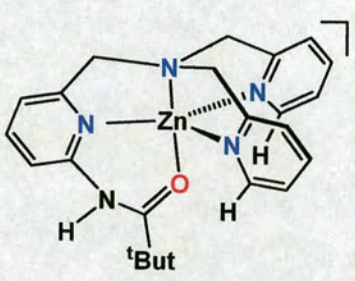

$C^{2.1}$

X = ClO_4, PF_6

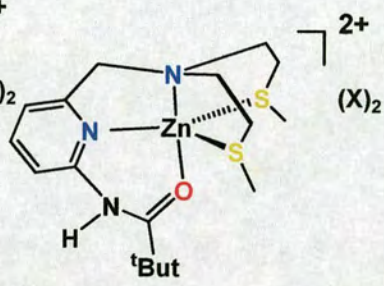

$C^{2.2}$

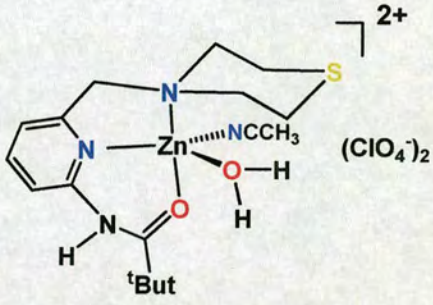

$C^{2.3}$

Chapter3

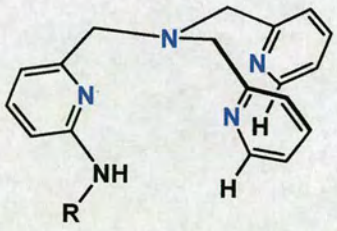

R = CO^tBu ($L^{3.1}$); H ($L^{3.2}$)

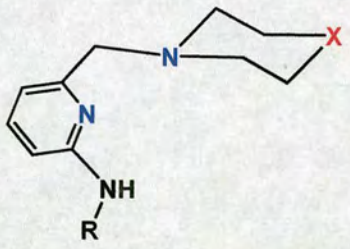

X = N-Me; R = CO^tBu ($L^{3.3}$); H ($L^{3.4}$)
X = O; R = CO^tBu ($L^{3.5}$); H ($L^{3.6}$)

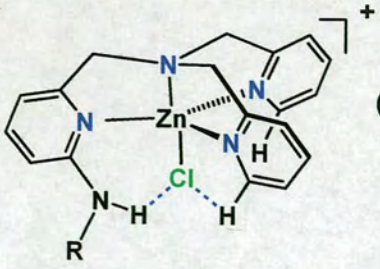

R = CO^tBu; Y = Cl ($C^{3.1'}$), BPh_4 ($C^{3.1}$)
R = H; Y = Cl ($C^{3.2'}$), BPh_4 ($C^{3.2}$)

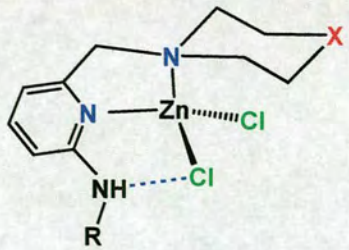

R = CO^tBu; X = N-Me ($C^{3.3}$), O ($C^{3.5}$)
R = H; X = N-Me ($C^{3.4}$), O ($C^{3.6}$)

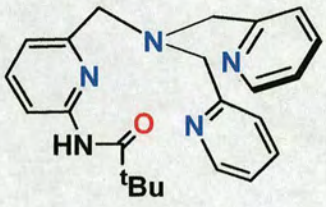

$L^{4.1}$

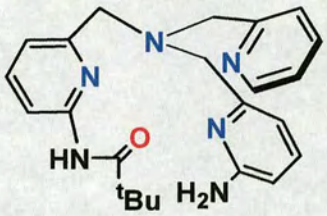

$L^{4.2}$

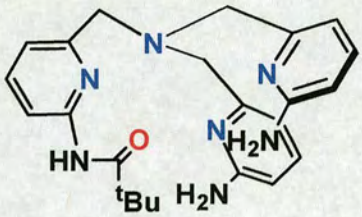

$L^{4.3}$

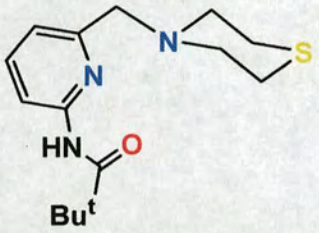

$L^{4.4}$

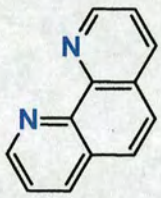

$L^{4.5}$

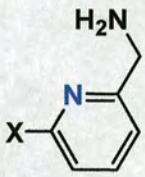

X =H; $L^{4.6}$

X = NH_2; $L^{4.7}$

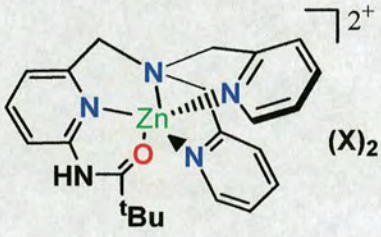

$C^{4.1}$

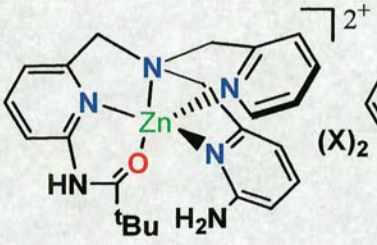

$C^{4.2}$

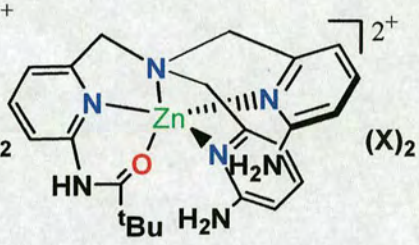

$C^{4.3}$

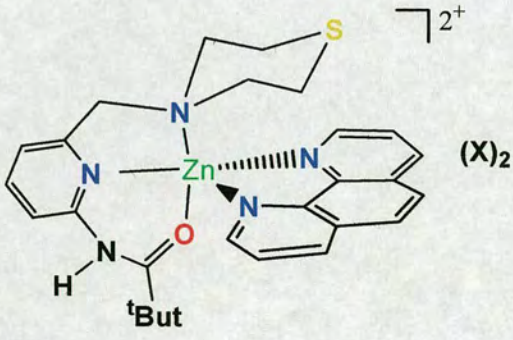

$C^{4.5}$

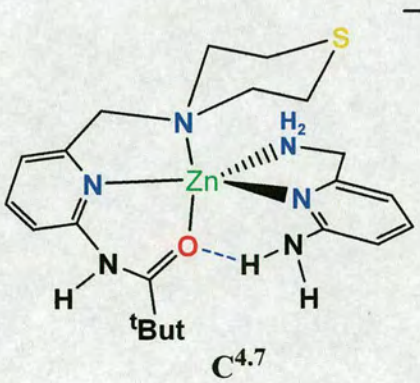

$C^{4.7}$

X= ClO_4

Chapter 5

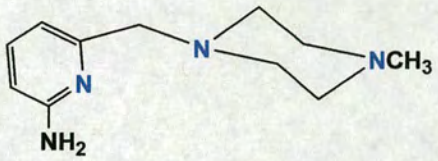

$L^{5.1}$

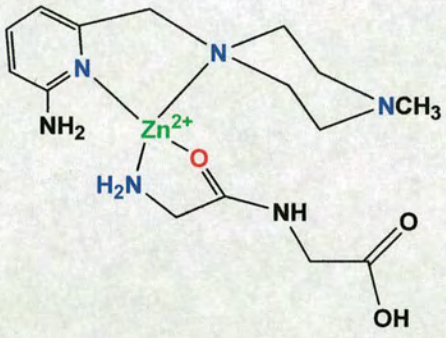

$C^{5.1}$

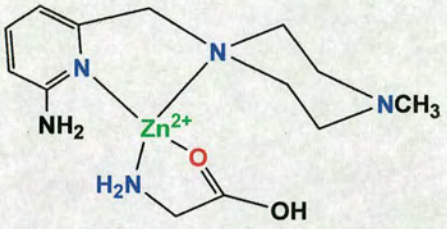

$C^{5.2}$

TABLE OF CONTEXTS

Chapter 1

Introduction

1.1 Thesis Aim

The aim of this research is the synthesis and development of novel zinc(II) complexes as models for peptidases. Metallopeptidases and proteases are hydrolases that cleave peptide bonds of polypeptides and proteins. These enzymes are of fundamental importance due to their vital biological roles including protein digestion, viral defence, and have also great technological importance e.g. for protein sequencing. Many of them require zinc(II) ions as cofactors, which are involved in the activation of the nucleophile (water) and/or substrate (peptide). In addition to the metal(s), the participation of active-site residues in proton transfer events, substrate activation and positioning and transition state stabilisation appears to be also essential. Although the zinc(II) ion and second sphere residues are believed to play an important role in catalysis, the exact mechanistic details are not fully understood.

Mimicking and modelling these enzymes, by focusing on the features of their active site, will lead to a better understanding of the mechanism by which these metallo-enzymes operate and the requirements to achieve efficient catalysis. This information may facilitate the design of mechanism-based inhibitors that could be used as therapeutic drugs and lead to useful artificial peptide cleaving agents.[1,2]

With this in mind, we have examined ligands capable of providing the electronic and steric properties at and around a zinc(II) ion and the intermolecular interactions, similar to those in the active site of these enzymes. To achieve strong binding we are using the cooperation of metal ions and internal hydrogen bonding interactions. It should be noted

that, although nature delivers specific molecular units to enzyme active sites using non-covalent interactions with incredible ease and precision, this exercise still poses an incredible challenge for chemists. Hence, one objective of this study was also to develop strategies to induce hydrogen bonds to metal bound ligands.

In view of that, metal complexes of pyridine-based ligands have been designed and synthesised. These ligands constitute a good platform that can be readily modified in order to provide different numbers and types of metal binding sites. They can also incorporate functional groups to mimic the intermolecular interactions, mainly hydrogen bonds, which enable the substrate molecules to react at the zinc sites. The interest of this research resides in how functional groups of these ligands and changes in the ligand environments and microenvironments affect binding and cleavage of peptide bonds.

This chapter presents a short overview on enzymes, their active site, the importance of zinc(II) in life and in enzymes. A brief description of peptidases will then be discussed along with an outline of peptide cleaving agents, the criteria for the choice of the ligands and a summary of the contents of this thesis.

1.2 Enzymes

The term enzyme comes from the Greek words *en*, "in", and *zymē*, "leaven", it was coined by Friedrich Wilhelm Kühne in 1878 to indicate substances previously defined as ferments.[3] Enzymes are catalysts that play a vital role in biology, since they facilitate all the biochemical transformations required for life. Unique enzyme features include high catalytic efficiency and specificity. Specificity refers to their ability to choose a specific substrate and/or to catalyse only a particular reaction. Efficiency refers to their remarkable ability to greatly lower the activation barrier of the reaction they catalyse. As a result, they can increase the rate of a reaction by as much as a million times.[4]

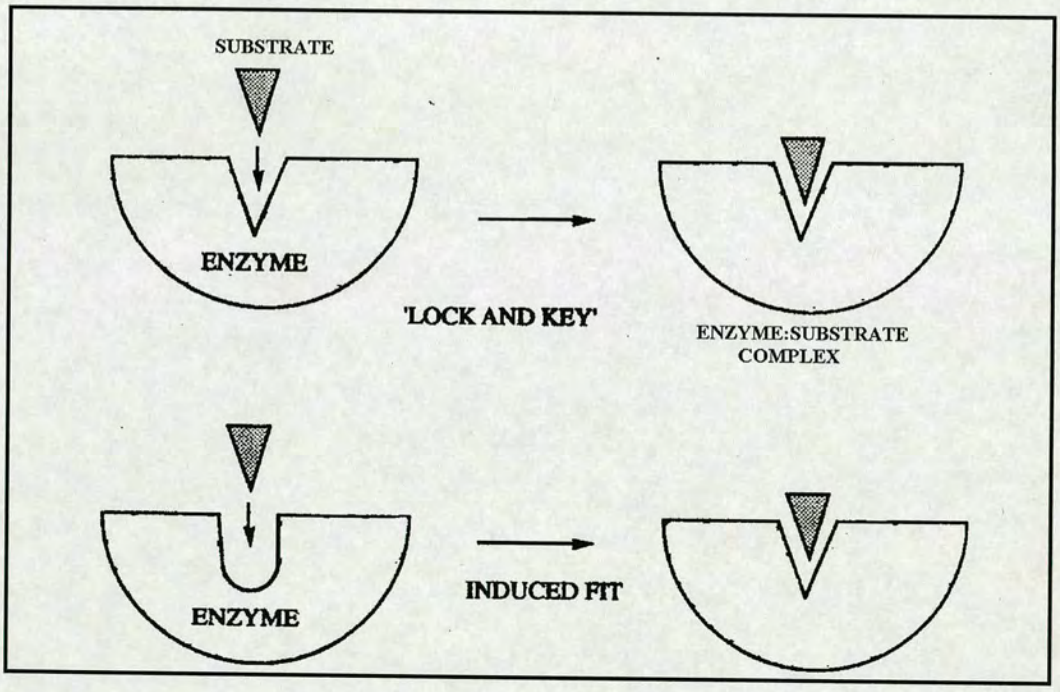

Fig. 1.1 Schematic representation of the 'lock and key' and 'induced fit' theories.

Both specificity and efficiency rely on the positioning of atoms within the active site. In 1890 Emil Fischer suggested that enzyme active site and substrate fit like 'lock and key', and that this accounts for enzyme efficiency and selectivity. The 'lock and key theory' evolved into the 'induced fit theory', which was postulated by Daniel E. Koshland in 1958.[5] According to this theory enzymes assume forms complementary to the substrate only after that the substrate has been bound and the full complement of the interactions are formed only when the transition state is reached (Fig. 1.1). In other words, the enzyme binds the transition state more strongly than the substrate.

1.2.1 Enzyme Catalysis

In the chemical process that converts the substrate (S) to the product (P) the substrate goes through the transition state (TS). Enzymes catalyse a reaction by stabilising the transition state more than the ground state.

This is illustrated diagrammatically in Fig. 1.2, which shows an energy profile for a catalysed and uncatalysed reaction.[6] In this diagram $TS_{(cat)}$ and $TS_{(uncat)}$ represent the transition states of the catalysed and uncatalysed reaction, respectively. The stabilisation of $TS_{(cat)}$ by $\Delta G^{0}_{(TS)}$, makes the activation barrier for the catalysed reaction, $\Delta G^{+}_{(cat)}$, lower than the uncatalysed, $\Delta G^{+}_{(uncat)}$. Moreover, this drop in the activation energy is only possible if the interactions occurring between the active site and substrate are weaker than with the transition state.

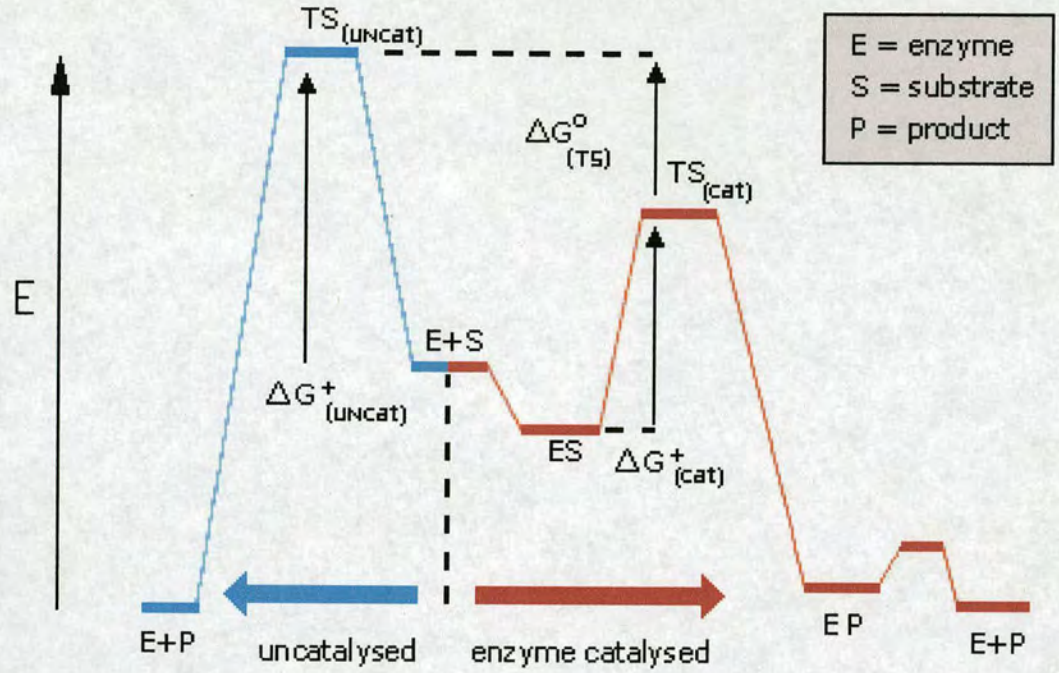

Fig. 1. 2 Energy profile diagram for the reaction of a substrate both catalysed and un-catalysed.

1.2.2 Enzyme Active Sites

The active site of an enzyme is the region where the substrate binds. It contains the amino acid residues and co-factors that take part in catalysis. Although enzymes are made up of hundreds of amino acid residues, only a minor part of these residues is in contact with the substrate. Thus, the active site is a cavity or a groove that occupies only a relatively small part of the entire volume of the enzyme. Water is normally excluded from the active site, unless it is involved in the reaction. This results in a non-polar character that promotes substrate binding. However, there can be polar residues that may play an important role in catalysis. At the same time, binding between the enzyme and the substrate must be strong enough for reaction to proceed yet weak enough to

allow rapid release of the product. Enzymes achieve this difficult balance by providing functional groups for ionic, hydrogen-bonding, and hydrophobic interactions.

1.2.3 Interactions at Active Sites

Non-covalent interactions, such as hydrogen bonding, and hydrophobic effects play an important role in the recognition and binding events between the active site of an enzyme and substrate/transition state species. Although these interactions are much weaker than the covalent bonds they can result in strong substrate binding or transition state stabilisation when several of them make a contribution. Because non-covalent interactions are relatively weak, they can be broken easily. Thus, non-covalent interactions provide the means to achieve the aforementioned strength-weakness balance in terms of binding between enzyme and substrate, transition state and product species that is required in enzyme catalysis. Hydrogen bonds can be formed both between charged and non-charged molecules. In a hydrogen bond, a hydrogen atom is 'shared' between two other atoms called the donor and the acceptor (see chapter 3). The acceptor is an electron rich atom that attracts the hydrogen atom, whereas the donor is also an electron rich atom, which is more tightly bound to the hydrogen. In biological systems hydrogen bonds donors and acceptors are generally oxygen or nitrogen atoms and the energy of hydrogen bond interactions ranges between 8 and 22 kcal/mol.[7] Therefore, they can be considered weaker than covalent bonds, but stronger than van der Waals interactions. It is also important to underline that hydrogen bonds are highly directional. In other words, their strength decreases with deviation of the bond angle from 180°. The directionality of hydrogen bonding means that multiple hydrogen bonding sites can be aligned in such a way to complement each other.

Two factors are important to understand the hydrophobic effect.[8,9] First, water molecules have tendency to interact with one another through hydrogen bonding specially in non-polar environments. In addition, apolar molecules prefer the association with other apolar molecules. Thus, the hydrophobic effect primarily refers to the exclusion of water molecules from a hydrophobic cavity as these will facilitate stronger polar with polar and apolar with apolar interactions.

1.2.4 Metals in Active Sites

Metal ions, such as Mg^{2+}, Ca^{2+}, Co^{2+}, Cu^{2+}, Fe^{2+}, Mn^{2+}, Ni^{2+} and Zn^{2+}, are essential for life and are generally found as natural constituents of proteins, they can be involved in diverse biological functions.[10,11] One of those roles involves acting as co-factors in enzyme catalysis, in this case metalloproteins are termed matalloenzymes. A class of metalloenzymes relevant to this study are hydrolytic enzymes, which are proteins that catalyse addition or removal of water in substrate molecules. Typical examples are carbonic anhydrase that promote hydrolysis of CO_2, alkaline phosphatase, which catalyse the hydrolysis of phosphate esters, and peptidases that catalyse the cleavage of peptide bonds of polypeptides and proteins.[10] The latter enzymes are subject of interest of this thesis and will be discussed later on. Since many of hydrolytic enzymes utilise zinc (II) to perform their catalytic action and, more specifically, Zn^{2+} is the most commonly used metal ion in natural peptidases,[12] only this metal will be discussed in the following sections.

1.3 Zinc in Life

The natural abundance of zinc may be one factor that induced organisms to select this element for their needs. In fact, the level of zinc in organisms is comparable or higher to that in the environment.[11,13] Zinc is the second most abundant transition metal in biology, it is second only to iron and is essential in all forms of life, from bacteria to humans.[14] For instance, the tissues of a 70 kg human body contain between 2 and 3 g of zinc. Zinc is an essential component of more than 300 enzymes isolated from different species.[15]

1.3.1 Properties of Zinc(II)

Zinc belongs to group 12 of the periodic table and as such has a completed 3d subshell with two additional 4s electrons. The most stable oxidation state for zinc is +2. Zinc(II) is a d^{10} system and as such, it is diamagnetic, spectroscopically silent and lacks redox activity.[11,13] Zinc(II) has an intermediate polarizability thus according to the hard-soft acid base (HSAB) theory is a borderline-to-soft acid.[16] This relatively soft acid character of zinc(II) explains its affinity for N or S donors in biological systems. Zinc(II) is a strong Lewis acid and as such can exert a strong polarising effect on bound molecules. Compared to Mg^{2+}, for instance, Zn^{2+} has a lower charge density and is consequently a stronger Lewis acid. Therefore, Zn^{2+} is more effective at polarizing carbonyl bonds than Mg^{2+}. In addition, it is important to underline that zinc(II) undergoes relatively fast ligand exchange. Moreover, it is also worth noting that the coordination number (CN) of zinc can fluctuate between 4 and 6, and that zinc(II) complexes are characterized by an ability to adopt different geometries *via* an energy

free process fundamental in stabilizing the transition state. Indeed, the filled d-shell of zinc indicates that zinc complexes are not subject to ligand field stabilisation effects and so the coordination number and geometry adopted is largely dictated by ligand size and charge. All these physicochemical properties make zinc a very useful metal in biocatalysis.[11,13]

1.3.2 Zinc in Enzymes

Zinc can play different roles in enzymes; these can be divided into four main classes: structural, regulatory or modulatory, noncatalytic, and catalytic.[13]

-*Structural.* Zinc stabilises the structure of the protein, but it does not affect catalysis.

-*Regulatory or Modulatory.* Zinc regulates the enzymatic activity and the stability of the protein. In this case zinc is not essential for catalysis, but its replacement for other metal ions can affect catalysis.

-*Noncatalytic.* The function of zinc in this role is still unclear. It is not directly involved in catalysis, it may stabilise the tertiary structure, but is not essential for it.

-*Catalytic.* Zinc is directly involved in catalysis by the enzyme. Zinc is essential for this role and its removal generates an inactive apoenzyme.

1.3.3 Zinc in Enzymatic Catalysis

The coordination chemistry of zinc in enzymes and 'simple' small-molecule ligand environments can be very different. Typically, the single divalent zinc metal ion, in biological systems, is tetra-coordinated in a tetrahedral-like arrangement: the active site

offers three amino acid residues as ligands and water gives the fourth one which participates in the catalytic process (Fig 1.3).

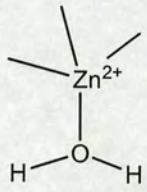

Fig. 1.3 Typical arrangement for Zn^{2+} in enzyme active site.

Enzymes are able to bind zinc(II) ions with distorted geometries, unusual bond lengths and an odd number of ligands. In this situation of stress zinc is said to be in an *entatic* state and often occurs prior to binding the substrate.[13] In this entatic state the zinc(II) centre has higher energy thus favouring lower activation barriers. In other words, *entasis* makes catalysis more favourable.

There are three proposed mechanisms by which zinc can influence catalysis.[13,17] The first one is known as the zinc-carbonyl mechanism (Fig. 1.4). In this case, the substrate binds the metal displacing a metal-bound water molecule. The zinc(II) centre acts as a Lewis acid to polarise the bound substrate resulting in activating the electrophile.

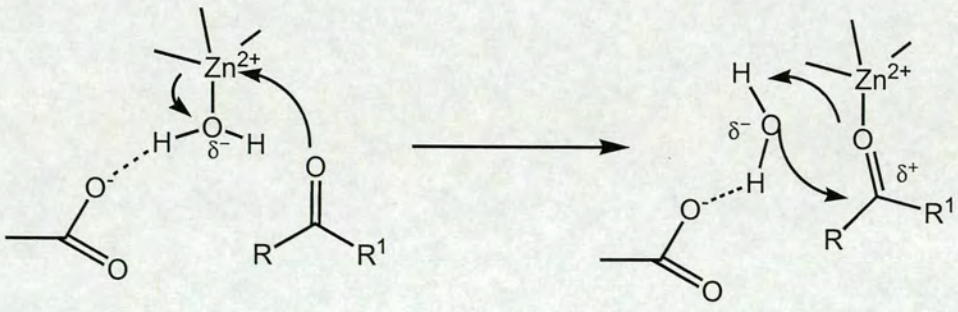

Fig. 1.4 The zinc-carbonyl mechanism.

At the same time, a carboxylate group belonging to one of the active site second-sphere amino acid residues generally acts as general base to make a water molecule a better nucleophile. The water can then attack the activated electrophilic carbon. The second mechanism is known as the zinc-hydroxide mechanism (Fig. 1.5). In this case, zinc(II) acts as a Lewis acid to activate the bound water molecule, which is not displaced by the approaching substrate.

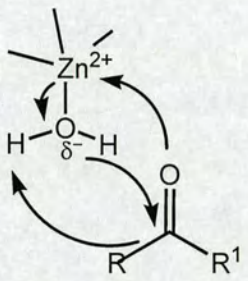

Fig. 1.5 The zinc-hydroxide mechanism.

The third proposed mechanism is an integrated mechanism of the previous two (Fig. 1.6). Thus, zinc coordinates both the substrate and the water molecule, resulting in a pentacoordinate intermediate. In this way zinc not only activates the nucleophile and polarises the substrate, but also brings them in close proximity, thus making the reaction more favourable.

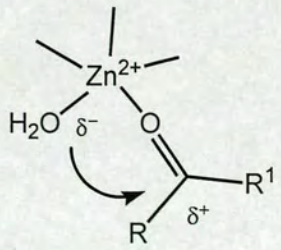

Fig. 1.6 The zinc activates the nucleophile and polarises the substrate.

1. 4 Peptidases

Peptidases, also known as proteases, are enzymes that catalyse the cleavage of peptide bonds (proteolysis).[1,2] Peptidases are involved in many physiological events such as infection, inflammation, allergic reactions, blood clotting, cell growth and death, tumour growth and bone remodelling. Peptidases can, therefore, be also therapeutically helpful for several health conditions or diseases.[18,19]

Amino acids can combine together through amide bonds. The condensation of two amino acids affords a dipeptide, whereas the build up of several amino acids gives rise to polypeptides and proteins. The linkage between two adjacent amino acids (amide bond) is the fundamental bond in polypeptide and proteins and it is also referred to as peptide bond. In a protein of *n* amino acids there are *n* -1 peptide bonds in the backbone.[20] Although the hydrolysis of proteins in their constituent amino acids is thermodynamically favoured, peptide bonds or amide bonds are very stable at pH 7 and 25 ^{O}C. They exhibit half-lives for hydrolysis of at least 7 years. In fact, the half-life of the peptide bond is subjected to controversy as estimated by several research groups to be only seven years,[21] between 350 and 600 years[22] or up to 2000.[23]

In physiological conditions, these linking bonds are subject to degradation, digestion and modification in the protein backbone. In order for these biological processes to be accomplished in a physiologically acceptable timescale, nature uses peptidases, a type of enzymes that cleaves the amide bond between two amino acid residues.

There are three types of peptidases: the endopeptidases cleave an amide bond within a polypeptide chain, the exopeptidases and peptidases cleave *N*- and *C*-terminal amino

acids of a polypeptide chain, respectively. In this discussion the attention will be focused on the case of the peptidases only.

In most metallo-peptidases amino acid side chains are involved in the substrate transformation as general acid, base or nucleophile. The high catalytic efficiency of the metallo-peptidases is the result of a perfectly coordinated catalytic cooperation of the metal ion and one or several of these functional organic groups.

1.4.1 Carboxypeptidase A

One of the most studied peptidases which can also be taken as a representative example of metallopeptidases is the carboxypeptidase A (CPA) from the bovine pancreas.[24] CPA hydrolyses the amide bonds of the C-terminal amino acid of peptides. In the active site a zinc(II) ion is coordinated in a tetrahedral geometry to two histidine amino acid residues (His-69 and His-196), a glutamate (Glu-72) and a water molecule (Fig. 1.7).

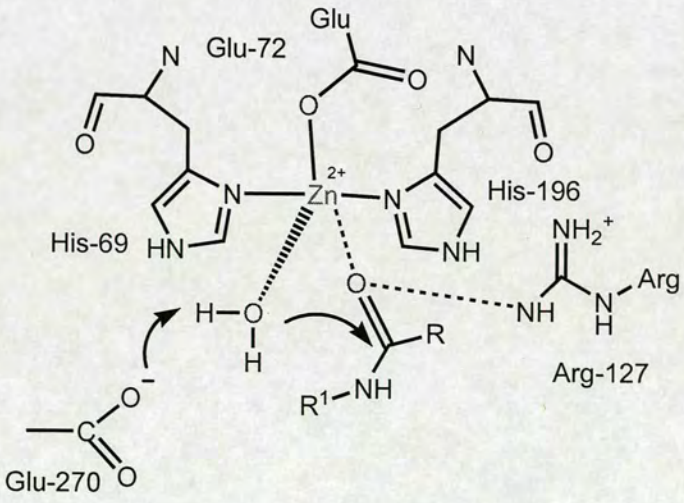

Fig. 1.7 The Carboxypeptidase A active site.

CPA is a typical example of peptidase in which amino acid residues appear to co-operate with the zinc(II) ion to make the reaction more favourable (Fig. 1.7). Thus, active site residues provide hydrogen bonding interactions to position/activate the substrate. In addition, a carboxylate group of a glutamate residue (Glu-270) acts as a general base to generate a hydroxide ion, which then attacks the activated electrophilic amide carbon.

The mechanism of carboxypeptidase A hydrolysis is subject of controversy despite many investigations. The first postulated mechanism (Fig. 1.8) includes the ground state activation of the amide by coordination of the carbonyl oxygen to Zn^{2+}. Then it follows the nucleophilic attack of Glu-carboxylate on the carbonyl carbon leading to an anhydride intermediate further hydrolyzed *via* a zinc-coordinated hydroxide.[25]

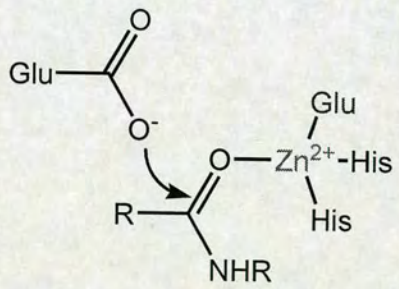

Fig. 1.8 Hydrolysis mechanism for carboxypeptidase A *via* carboxylate nucleophile.

A more favoured mechanism (Fig. 1.9) implies the direct attack of a Zn-OH nucleophile on the amide group.[24] The carbonyl group is activated by hydrogen bonding with Arg-127 (Fig. 1.9 A). Catalytically essential Glu-270 carboxylate acts as a general base attracting a proton from the zinc-coordinated water (leading to the formation of the Zn-OH nucleophile). Next, the zinc-bound hydroxide attacks the electrophilic amide carbon (Fig. 1.9 B). The zinc metal ion also operates as a Lewis acid catalyst which stabilizes the build-up of negative charge by carbonyl oxygen coordination along with electrostatic stabilization by the positively charged Arg. The 'tetrahedral intermediate' is formed and subsequently Glu-270 acts as a general acid stabilising the leaving amino group by proton transfer (Fig. 1.9 C). The products of the reactions are then released (Fig. 1.9 D) and after that a new water molecule and substrate approach and the cycle starts again.

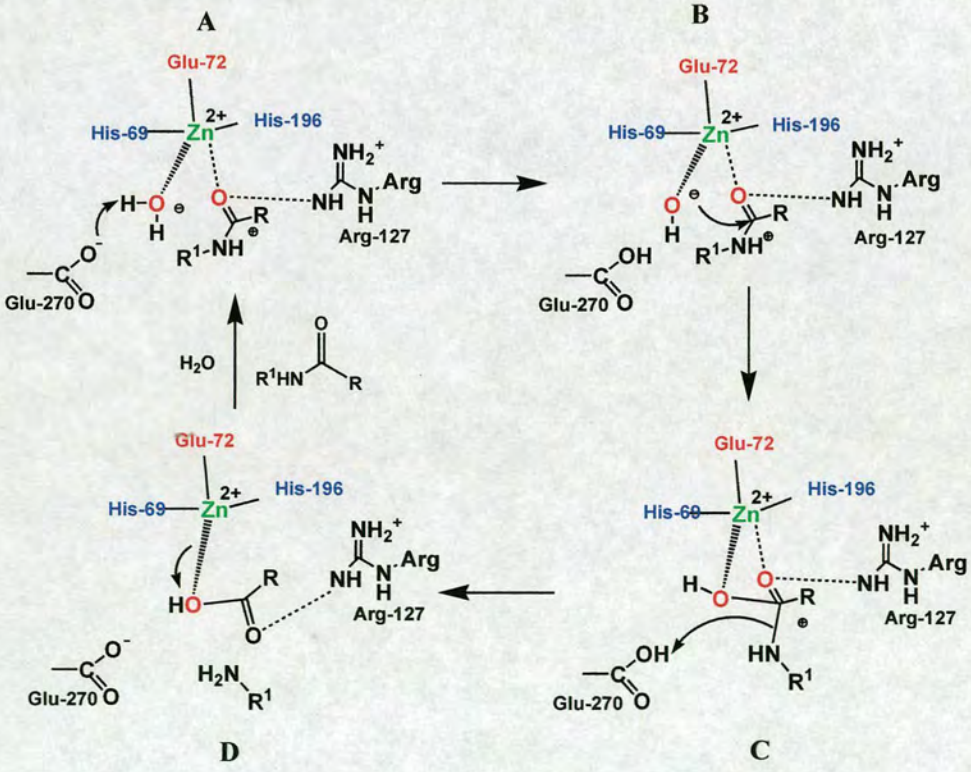

Fig. 1.9 Hydrolysis mechanism for carboxypeptidase A *via* Zn-OH nucleophile.

1.5 Current Peptide Cleavage Agents and Artificial Peptidases

1.5.1 Peptide Cleavage Agents

Analytical biochemistry and molecular biology need cleavage methods for several studies concerning proteins, such as determination of amino acid sequences, studies of protein association, analysis of protein domains and synthesis of new drugs. The peptide bond is extremely unreactive and its cleavage is generally achieved by proteolitic enzymes. These enzymes are used to achieve selective and catalytic cleavage of peptides and proteins under mild conditions, but unfortunately, there are only few of them and at the same time they present several shortcomings as cleavage agents. Several of these enzymes are active only at specific conditions, such as narrow range of pH and temperature, which are often incompatible with the proteins or processes of interest. In addition, proteins are usually denatured before undergoing proteolytic digestion, therefore, the pattern of cleavage gives often little information about the actual structure and function of the protein under investigation. Besides, the inhomogeneous distribution of the cleavage sites in the natural peptidases often gives too large fragments for sequencing. On the other hand, the commonly used chemical peptide cleavage agent, cyanogene bromide, is both toxic and volatile, requires harsh conditions, must be applied in large excess over the substrate, gives several side reactions producing protein fragments that are irreversibly modified and often cleavage is incomplete.[26]

Therefore, new artificial cleavage agents are needed. Developing synthetic metallo-peptidases is helpful for a better understanding of biochemistry and molecular biology and the role(s) of metal ion(s) in natural hydrolases. Synthetic models of enzymes have

the potential to elucidate and quantify the effect of specific interactions or groups in enzyme catalysis. As such, synthetic modelling chemistry is an important discipline of bioinorganic chemistry.

1.5.2 Synthetic Peptidases

Smaller synthetic peptidases, more robust and more readily available than the natural enzymes could then be designed for specific applications. Firstly, artificial peptidases could be useful in the elucidation of large protein sequence.[26] Secondly, artificial peptidases are potential conformational probes as alternatives to commonly used techniques NMR and X-ray. Indeed, the former may give useful information, but often not easy to interpret, and the latter necessitates crystals that may be difficult to grow. In addition, both techniques require large amounts of material. As a result, it is often hard to characterise the features of the enzymes and establish their mechanism of action.

Peptidase-like models have been an excellent tool to elucidate the role of the metal ion in natural peptidases. To design artificial peptidases we have to take into account the following aspects for the hydrolysis of amide bonds. The enzyme readily forms a complex with the substrate, which in turns rapidly undergoes to chemical transformations. This task is achieved by the enzyme *via* (i) bringing reactants in close proximity, (ii) providing functional groups for acid or basic catalysis, (iii) binding the transition state more strongly than the reactants or products and (iv) supplying attacking groups. A strategy to afford synthetic models with similar features is to incorporate metals in organic compounds. Metal ions could promote the hydrolysis by providing (i) a rigid scaffold, (ii) coordination of the carbonyl oxygen with subsequent activation of

the amide carbonyl bond, (iii) a charge neutralization to facilitate nucleophilic attack, (iv) stabilization of the charge build-up in the transition state and of the leaving group and (v) a nucleophile at neutral pH, (vi) metal-bound water molecules acting as general acids for the expulsion of amines.[1,2]

1.5.3 Examples of artificial peptidases

Over the years many model systems have been studied and developed to gain an insight into the hydrolysis of peptides. Early model systems failed to provide a substantial rate enhancement[27] and exhaustive information for the metal-mediated cleavage of amide bonds. Meriwhether and Westheimer, for instance, achieved peptide hydrolysis through metal systems generated *in situ,* but it was not possible to determine the structure of the complexes, or to postulate any mechanism for the hydrolytic reactions.[27a] In order to mimic certain features of carboxypeptidase A (CPA), Breslow *et al.* synthesised a cobalt(III) complex with a ligand coordinated through an amide oxygen and providing simultaneously a phenolic hydroxyl group in close proximity to the amide.[28] This model represents a noteworthy case where a metal ion and an acidic functional group assist amide hydrolysis (Fig. 1.10). The cobalt (III) ion coordinates the carbonyl oxygen, thus strongly activating the amide carbon; this in turn undergoes nucleophilic attack by an external hydroxide ion. When the phenolic hydroxyl group was replaced by OMe, the rate of the cleavage decreased of a factor of 100 at pH ranging from 7.5 and 9 in water–DMSO mixtures. This result suggested that the phenol–OH possibly promotes protonation of the amine nitrogen, thus facilitating the release of the leaving group.

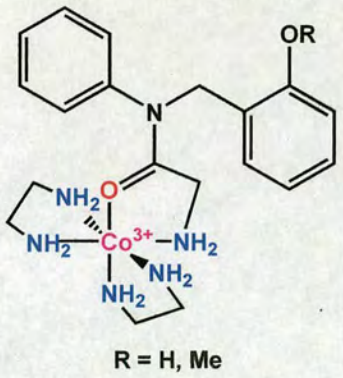

Fig. 1.10 Example of a model system for CPA .

Another important system that shows cooperation of a divalent metal ion and a carboxylate nucleophile in amide and ester hydrolysis was investigated by Suh and coworkers.[29] In this copper(II) complex (Fig 1.11) hydrolysis of the amide bond takes place with a half life of 10 min at 50°C in a DMSO:water (95:5) medium, which is ca. 300-fold rate enhancement compared with the background reaction in the absence of metal ion and carboxylate. Remarkably, these models show how cooperation of metals and functional groups, acidic and nucleophilic, can significantly affect the cleavage of peptide bonds.

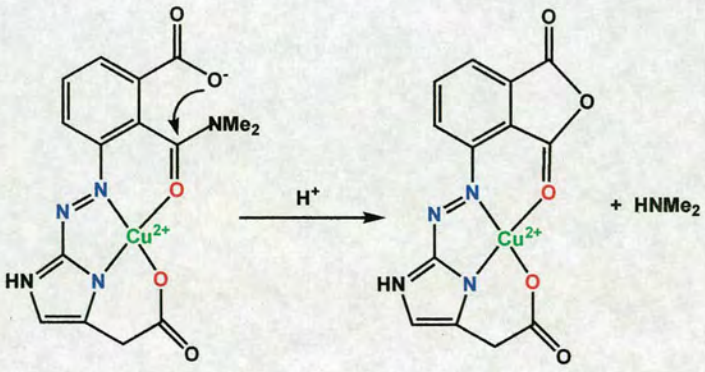

Fig. 1.11 Peptidase model system showing cooperation of metal ion and nucleophile.

Kostić *et al.* carried out several studies involving Pt(II) diamine and $[PtCl_4]^{2-}$ complexes for regioselective acidic hydrolysis of short peptides containing cysteine or

methionine.[30] These two amino acids provide a sulphur atom as metal binding site and the hydrolysed peptide bond is the one involving the carboxyl group of the amino acid to which the complex is bound (Fig. 1.12). Initially the metal coordinates to the sulphur, next follows coordination of the amide oxygen that displaces one of the metal bound amine ligands or chloride ion.

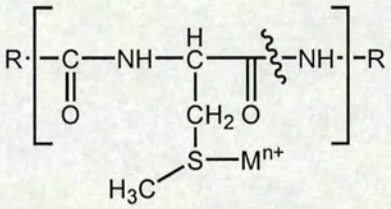

Fig. 1.12 Model systems containing Pt(II) and Pd(II) for regioselective hydrolysis of peptides.

The activated amide bond undergoes nucleophilic attack by either an external or a metal-bound water molecule (Fig 1.13).

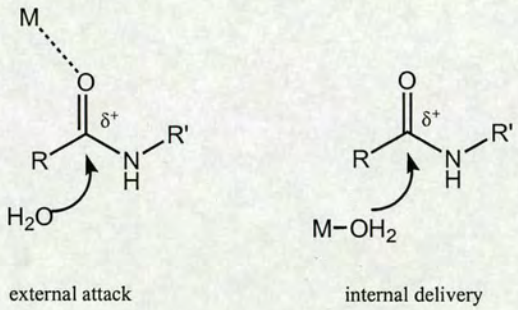

Fig. 1.13 Possible modes of attack of a water molecule for hydrolysis of peptides containing Pt(II) and Pd(II).

Similar studies for selective hydrolysis of peptides were carried out using the same cysteine, methionine containing polypeptides and various Pd(II) complexes (Fig. 1.12). Some aspects, concerning ligands substitution at metal site during the cleavage process, were elucidated by using the more labile Pd(II) ion. The acidic conditions used and the

trans labilising effect of sulphur allow water to replace the amine chelating ligands, thus affording always the same active hydrolysed species (Fig. 1.14), regardless of whether the starting material was $[PdCl_4]^{2-}$, $[Pd(en)(H_2O)_2]^{2+}$, or $[Pd(H_2O)^3(OH)]^+$.[31]

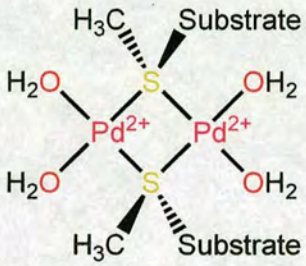

Fig 1.14 The proposed active hydrolised species of Pd(II) complexes for the cleavage of sulphur-containing peptides.

Interestingly, when the ligands used were sulphur atoms, which are not displaceable, the rate of the amide cleavage decreased as the number of sulphur atoms increased from zero to two. This suggests that the nucleophilic species is likely to be an intramolecular metal-bound water molecule rather than an external one.

More recent studies, where Pd(II) is anchored to a methionine or a hystidine residue, showed that these complexes promote regioselective hydrolysis of synthetic and natural oligopeptides.[32] All the N-terminus peptides were acetylated to prevent unwanted binding of Pd(II) complexes, and the anchoring sites are preceded by two glycines and followed by an alanine residue. The reaction takes place in acidic aqueous solution to avoid formation of insoluble hydroxo-bridged Pd(II) species and when pH is kept at 1.5 or higher cleavage of the peptide bond occurs only at the second peptide bond upstream from the anchor site (Fig. 1.15), which is the amide bond of the amino acid residue before the histidine or methionine side chain in the sequence.

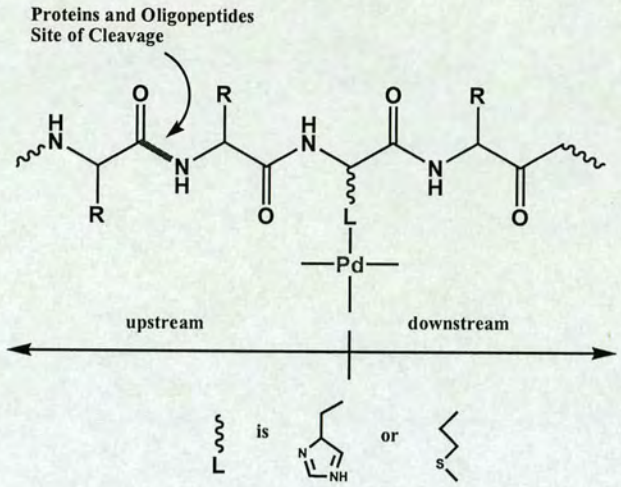

Fig 1.15 Pd(II) complexes of oligopeptides and site of cleavage..

1.6 Our Approach to Model Peptidases

1.6.1 Difficulties and Strategies

Since enzyme catalysis occurs at the active site, which is a small region of the enzyme, small synthetic models are primarily designed to resemble the active site. This requires a great deal of ligand design and knowledge of the chemistry involved. There are several problems associated with modelling zinc-containing active sites. The first difficulty has to do with mimicking the number of metal sites. For the case of monometallic zinc enzymes this means that ligand systems must be capable of preventing oligomerisation. A common strategy involves the attachment of bulky groups. Also, the same properties of zinc beneficial for catalysis, such as fast ligand exchange and flexible geometries, are an inconvenient for the syntheses of stable complexes. The stability problem can be minimised with the use of polydentate ligands. Because of the flexible geometry of the zinc ion, more difficulties are associated with the reproduction of the tetrahedral geometry found in the active sites of zinc enzymes.

Finally and even more challenging is to mimic the role of second sphere residues. In this case, the positioning of 'second sphere' groups in model systems needs to be very precise for them to exert the desired role.

1.6.2 Ligand Framework

As mentioned above, modelling the first co-ordination sphere of zinc(II) in active site requires ligands able to provide various coordination environments. An appropriate ligand framework for this purpose is (6-R^1-2-pyridylmethyl)-R (Fig. 1.16). This framework can easily incorporate functional groups that supply different numbers and types of metal binding sites and at the same time satisfy the requirements discussed above:

-presence of bulky groups (R), in order to prevent oligomerization.

-polydentate ligands, to afford relatively stable zinc-complexes.

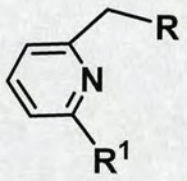

Fig 1.16 The ligand framework (6-R^1-2-pyridylmethyl)-R.

Exploiting this motif as a building block, a new set of ligands with N_2 and N_4 metal supporting sites, along with a previously reported ligand with a mixed nitrogen/sulfur (N_2S_2) coordination environment[33] have been synthesised. Each of the ligands provides different kind of interactions at the zinc site. The number and the types of the metal binding atoms affect electronically the bound zinc(II) ion particularly its Lewis acidity.

Another important feature of this ligand unit is that R^1 can be turned into a functional group carrying an intramolecular amide oxygen which can act as an additional binding site for metal coordination (Fig. 1.17). This represents a suitable feature for models of peptidases as amide oxygen to metal binding is considered to be one of the key steps in the chemistry of the enzyme.

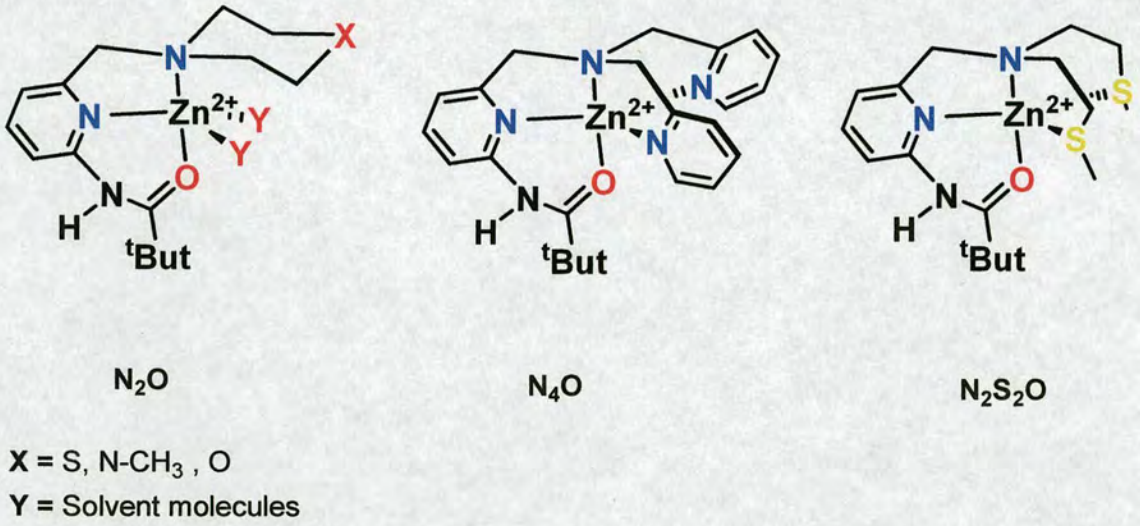

Fig 1.17 Model zinc(II) complexes with an intramolecular amide to metal bond.

1.6.3 Second Sphere Features

It was previously mentioned, another important centre of attention in peptidase chemistry must be the second co-ordination sphere of the zinc(II) centre, as these groups seem to have an important role in catalysis. These roles may apply into both the ground and transition state species. The pyridine unit in the ligand framework can be functionalised in such a way as to have R' providing hydrogen-bonding groups that resemble the second sphere amino acid functionalities in peptidase (Fig 1.18). Thus, the role exerted by these groups in both ground state and transition state species can be elucidated and quantified.

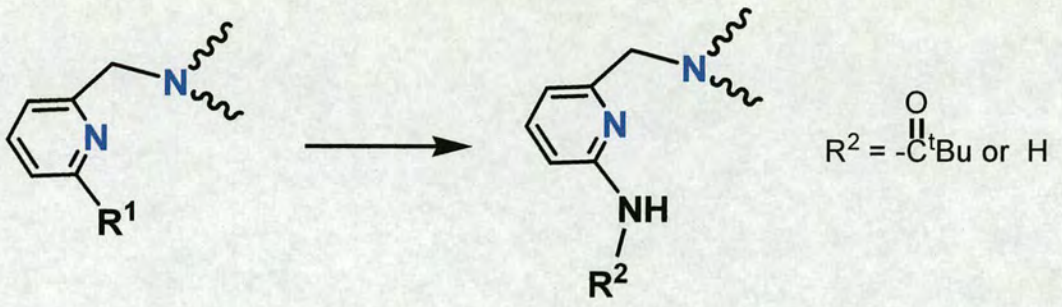

Fig 1.18 Functionalities at the ligand framework providing H-bonds.

1.6.4 Selected Ligands

The ligands selected to investigate the effect of second sphere residues are shown in Fig. 1.19.

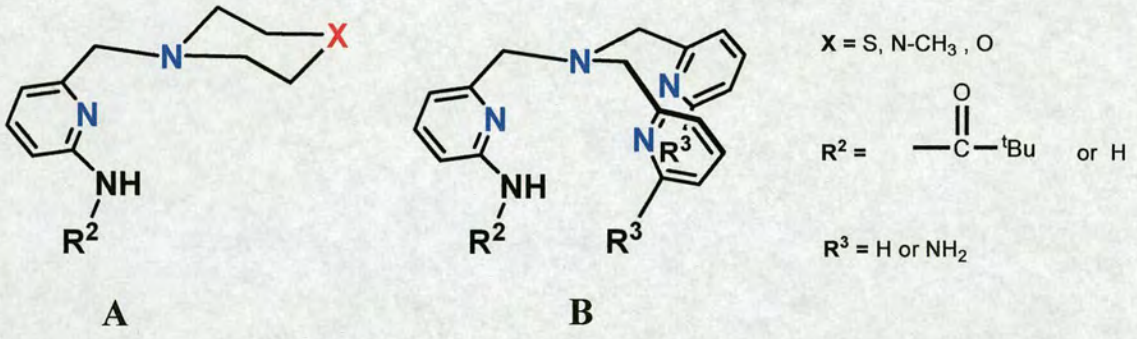

Figure 1.19 Schematic illustration of the ligands selected to model second coordination sphere.

These systems provide different metal binding sites and offer an amide NH or/and an amine group able to hydrogen bond other metal bound ligands, such as a substrate and/or a solvent molecule (Fig 1.20). Such interactions may contribute with the metal towards nucleophilic activation, and aid in the event of recognition, positioning and binding of substrates. Ligands of the type **A**, supply an N_3 or N_2O coordination environment, thus forming metal complexes that leave open available vacant positions at the metal site accessible for approaching substrate molecules. For instance, they can

bind other external ligands with hydrogen bond functionalities capable of hydrogen bonding the intramolecular metal bound amide oxygen. Alternatively, they can also bind exogenous substrates such as peptides. Ligands of the type **B** provide N4 or N4O metal binding motives, leading to more stable metal complexes, and more hindered metal sites. However, they give the opportunity to supply simultaneously an amide bond and amine group(s) as H-bond donor(s). In these systems, metal coordination and hydrogen bonding interactions at the amide oxygen could, in principle, cooperate in order to render the amide carbon atom more electrophilic, hence more prone to nucleophilic attack.

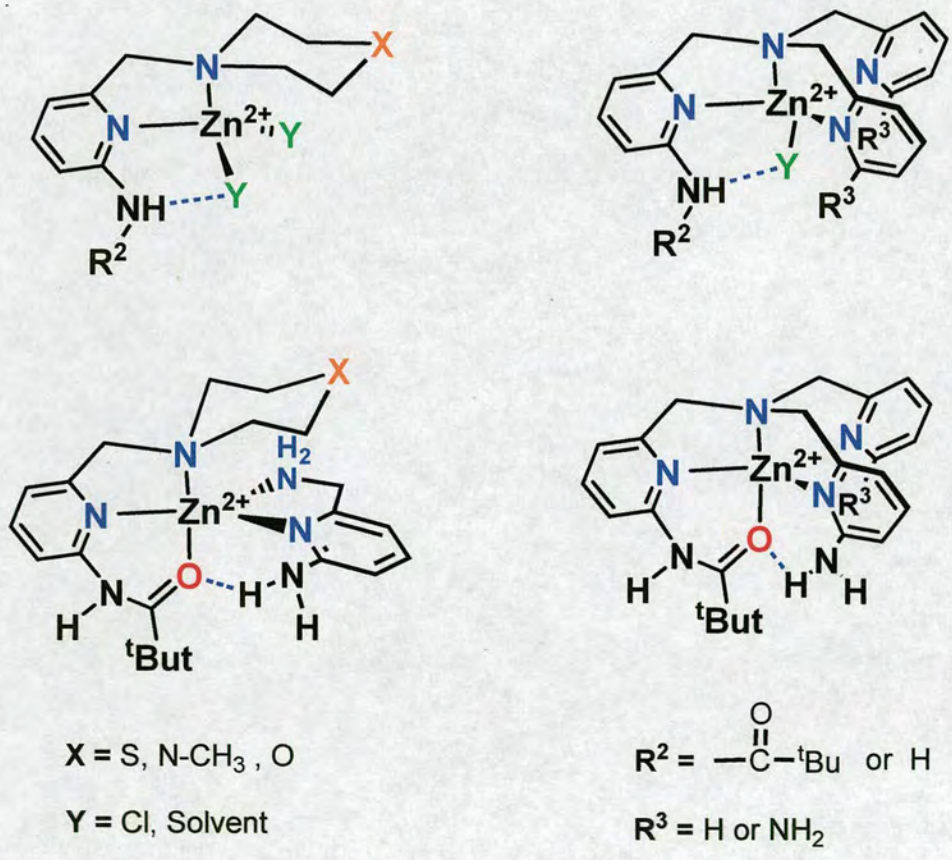

Fig. 1.20 Illustration of H-bond interactions occurring at the zinc(II) complexes.

All these features have been investigated and will be discussed in the next chapters in the following order:

Chapter 2 illustrates how adjustments of the first coordination sphere influence the strength of coordination of an intramolecular amide bond and its cleavage. The following section investigates hydrogen bonding to the metal-bound ligands and examines possible strategies to induce and manipulate the strength of these interactions (chapter 3). Next, studies on modification of the second coordination sphere show changes in the stability of the intramolecular amide bond towards cleavage reaction (chapter 4). The last part of the thesis describes how one of these model systems can bind and hydrolyse an exogenous unactivated peptide (glycylglycine) at a site that closely resembles the active site of aminopeptidase A (chapter 5).

References

[1] E. L. Hegg and J. N. Burstyn, *Coord. Chem. Rev.*, 1998, **173**, 133.

[2] R. Krämer, *Coord. Chem. Rev.*, 1999, **182**, 243.

[3] L. Stryer, *Biochimica*, Zanichelli, Bologna, 1996.

[4] R. Wolfenden and M. J. Snider, *Acc. Chem. Res.*, 2001, **34**, 938.

[5] D. L. Nelson and M. M. Cox, *'Principles of Biochemistry'*, Worth Publishers, New York, 2000.

[6] A. J. Kirby, *Angew. Chem. Int. Ed.*, 1996, **35**, 707

[7] G. A. Jeffrey and W. Saenger, *'Hydrogen Bonding in Biological Structures'*, Springer, 1991.

[8] G. Hummer, S. Garde, A. E. Garcia, A. Pohorille and L. R. Pratt, *Proc. Natl. Acad. Sci. U.S.A.*, 1996, **93**, 8951.

[9] A. Pohorille and L. R. Pratt, *J. Am. Chem. Soc.*, 1990, **112**, 5066.

[10] S. J. Lippard and J. M. Berg, *'Principles of Bioinorganic chemistry'*, University Science Books, Mill Valley, CA, 1994.

[11] E. Ochiai, *J. Chem. Educ.*, 1998, **64**, 943.

[12] W. N. Lipscomb and N. Sträter, *Chem. Rev.*, 1996, **96**, 2375.

[13] T. G. Spiro, *'Zinc Enzymes'*; ed. J. W. Sons, John Wiley & Sons, 1983.

[14] (*a*) B. L. Vallee and D. S. Auld, *Proc. Natl. Acad. Sci. U. S. A.*, 1990, **87**, 220; (*b*) B. L. Vallee and D. S. Auld, *Biochemistry*, 1990, **29**, 5647; (*c*) C. F. Mills, *'Zinc in human biology'*, Springer-Verlag, New York, 1989; (*e*) D. H. Nies, *Appl. Microbiol. Biotechnol.*, 1999, **31**, 730.

[15] H. Vahrenkamp, *Acc. Chem. Res.*, 1999, **32**, 589.

[16] R. G. Pearson, *J. Am. Chem. Soc.*, 1963, **85**, 3533.

[17] L. M. Sayre, *J. Am. Chem. Soc.*, 1986, **108**, 1632.

[18] X. Iturrioz, R. Rozenfeld, A. Michaud, P. Corvol and C. Llorens-Cortes, *Biochemistry*, 2001, **40**, 14440.

[19] M. K. Chan, W. Gong, P. T. Rajagopalan, Bing Hao, C. M. Tsai and D. Pei, *Biochemistry*, 1997, **36**, 13904.

[20] H. R. Sigel and B. Martin, *Chem. Rev.*, 1982, **82**, 385.

[21] D. Kahne and W. C. Still, *J. Am. Chem. Soc.*, 1988, **110**, 7529.

[22] A. Radzicka and R. Wolfenden, *J. Am. Chem. Soc.*, 1996, **118**, 6105.

[23] T. Yamana, Y. Mizukami, A. Tsuji, Y. Yasuda and K. Masuda, *Chem. Pharm. Bull*,. 1972, **20**, 881.

[24] D. W. Christianson and W. N Lipscomb, *Acc. Chem. Res.*, 1989, **22**, 62.

[25] (*a*) B. M. Britt and W. L. Peticolas, *J. Am. Chem. Soc.*, 1992, **114**, 5259.; (*b*) J. Suh, W. Cho, S. Chung, *J. Am. Chem. Soc.*, 1985, **118**, 4530.

[26] (*a*) T. N. Parac and N. M Kostić, *J. Am. Chem. Soc.*, 1996, **118**, 51; (*b*) G. B. Karet and N. M Kostić, *Inorg.Chem.*, 1998, **37**, 1021; (*c*) T. N. Parac and N. M Kostić, *Inorg.Chem.*, 1998, **37**, 2141; (*d*) T. N. Parac , G. M. Ullman and N. M Kostić, *J. Am. Chem. Soc.*, 1999, **121**, 3127.

[27] (*a*) L. Meriwhether and F. H. Westheimer, *J. Am. Chem. Soc.*, 1956, **78**, 5119; (*b*) A. Nakahara, K. Hamada, Y. Nakao and T. Higashiyama, *Coord. Chem. Rev.*, 1968, **3**, 207; (*c*) D. A. Long, T. G. Truscott, J. R. Cronin and R. G. Lee, *Trans. Faraday Soc.*, 1971, **67**, 1094.

[28] A. Schepartz and R. Breslow, *J. Am. Chem. Soc.* 1987, **109**, 1814.

[29](*a*) J. Suh, *Acc. Chem. Res.*, 1992, **25**, 273; (*b*) J. Suh, T. H. Park and B. K. Hwang, *J. Am. Chem. Soc.*, 1992, **114**, 5141; (*c*) J. Suh, *Bioorg. Chem.*, 1990, **18**, 345; (*d*) J. Suh, B. K. Hwang and Y. H. Koh, *Bioorg. Chem.*, 1990, **18**, 207.

[30] I. E. Burgeson and N. M Kostić, *Inorg.Chem.*, 1991, **20**, 4299.

[31] L. Zhu and N. M Kostić, *J. Am. Chem. Soc.*, 1993, **117**, 4566.

[32] N. Milović and N. M Kostić, *J. Am. Chem. Soc.*, 2002, **124**, 4759.

[33] (*a*) L. M. Berreau, R. A. Allred, M. M. Makowska-Grzyska and A. M. Arif, *Chem. Commun.*, 2000, 1423; (*b*) L. M. Berreau, M. M. Makowska-Grzyska and A. M. Arif, *Inorganic Chemistry*, 2000, **39**, 4390; (*c*) L. M. Berreau, M. M. Makowska-Grzyska and A. M. Arif, *Inorg. Chem.*, 2001, **40**, 2212; (*d*) D. K. Garner, R. A. Allred; K. J. Tubbs, A. M. Arif and L. M. Berrau, *Inorg. Chem*,. 2002, **41**, 3533.

Chapter 2

Zinc(II) complexes with intramolecular amide oxygen coordination as models of metalloamidases

2.1 Introduction

Peptidases are enzymes that catalyse the hydrolysis of peptide bonds of polypeptides and proteins. They commonly require a single metal ion, typically zinc(II), as essential co-factor. The zinc(II) ion is in a coordination environment in which three binding sites are taken by protein residues with a binding frequency of His ≫ Glu >Asp = Cys.[1] The fourth or even additional sites can be occupied by water and/or the peptide substrate, and as a result, these sites are utilised for promoting amide hydrolysis. It has been proposed that metal ions can promote the hydrolysis of peptide bonds in one of the following ways (see chapter1);[2] (1) by activating the carbonyl bond (electrophile activation); (2) by providing a nucleophile (OH) at neutral pH and (3) by providing a way to activate simultaneously the carbonyl bond and to generate the nucleophile at neutral pH.

Despite the considerable current interest in developing synthetic peptidases, the precise roles of the metal ions and the mechanisms of hydrolysis of peptide bonds in peptidases are not well understood.[3] Understanding the basic principles of peptide hydrolysis by peptidases, however, is necessary for the rational design of synthetic peptidases, for which important applications in biotechnology have been envisioned.[4]

2.1.1 Amide Coordination Sites

Amide bonds are planar and present a double bond character that is almost equally delocalised between the C-N and the C-O bond (Fig. 2.1).[5] They can provide two possible

binding sites to Lewis acids, the oxygen and the nitrogen. Although the amide bond is essentially neutral, it undergoes deprotonation and protonation at different pH values.

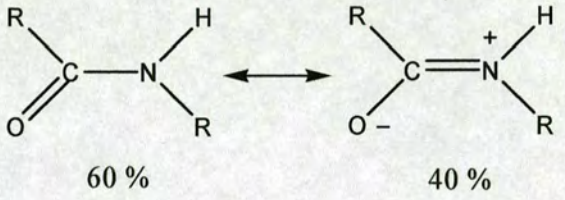

Fig. 2.1 General resonance structure for an amide bond

A good outline of the possible protonic equilibria was well summarized by Sigel[5] (Fig. 2.2).

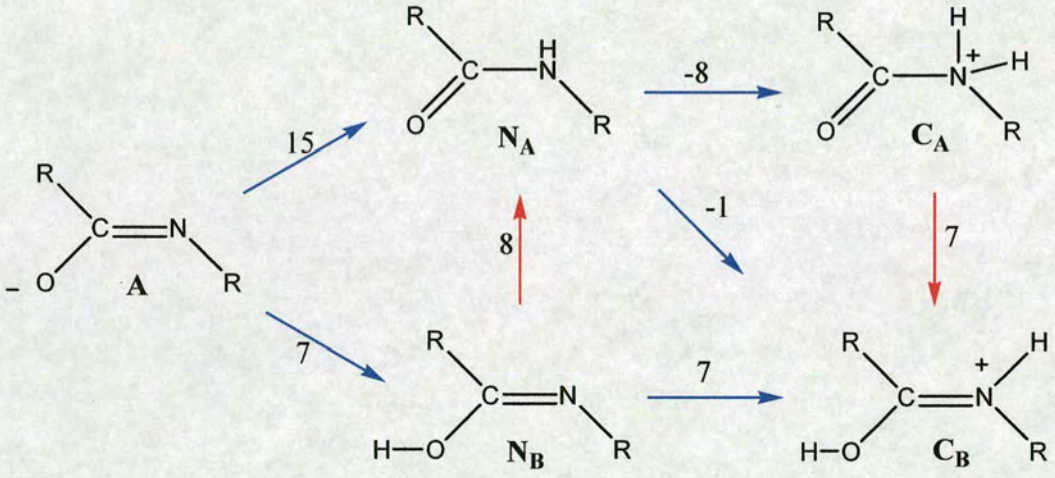

Fig. 2.2 General protonic and tautomeric equilibria of amides. The horizontal and diagonal arrows (blue) represent protonic equilibiria and vertical arrows (red) symbolise tautomeric equilibria, the displayed values are the constant equilibrium in logarithmic units.

Starting from basic solution, the deprotonated amide anion (**A**, far left) can be easily converted to the neutral amide (log K_a = 15), which will exist in a dynamic equilibrium (concentration of $\mathbf{N_A}$ is 10^8 higher than $\mathbf{N_B}$). In acid solution, two sites are available for

protonation, the nitrogen and the oxygen. Protonation at the oxygen occurs with a much greater constant (log K_a = -1) than protonation at the nitrogen (log K_a = -8), therefore, the O-protonated amide cation ($\mathbf{C_B}$) will be present at a concentration 10^7 times higher than the N-protonated amide cation ($\mathbf{C_A}$).

This trend parallels the tendency of amide metallation; the amide anion will bind metal ions at the amide nitrogen, whereas a neutral peptide bond will coordinate metals mainly at the amide oxygen. Metal substitution for a hydrogen at an amide nitrogen reduces the polarizability of the peptide bond, hence decreasing the electrophilicity of the amide carbon and its reactivity towards nucleophilic attack. In this case, peptide cleavage is inhibited.[5]

Metallation at an amide oxygen enhances the double bond character along the C-N bond. Since hydrolysis of peptide bonds involves a very poor leaving group (RNH^-), in principle, strengthening the C-N bond may slow down the reaction. On the other hand, metal coordination at the amide oxygen adds a positive charge at the peptide bond, thus polarising the C-O bond. As a result, the amide carbon will be more electro-positive and, therefore, more prone to undergo nucleophilic attack.

In designing new model systems that promote amide cleavage these observations should be taken into account. Good criteria that a model must include were given by Sayre:[2] "(1) that the metal remain stoichiometrically coordinated throughout the hydrolysis reaction and (2) that the metal does not interact with the leaving nitrogen, where the nitrogen has developed

full basic character, since this would inhibit the required protonation (RNH-M cannot be nearly as good leaving group as RNH_2)". The models investigated in this study promote amide oxygen coordination, and amide nitrogen coordination cannot occur for steric reasons.

2.1.2 Previous Models

Several metal complexes have been used as synthetic models for peptidases in order to explore mechanistic aspects of hydrolysis of peptide bonds.[3d] Groves *et al.,* carried out studies by investigating complexes that limit the modes of interaction between the metal and the amide bond.[6] These models were specifically designed to prevent coordination of the amide bond in order to promote intramolecular attack of a metal bound hydroxide. Inert (Co(III)), and labile (Cu(II) and Zn(II)) metal complexes of this type (Fig. 2.3) demonstrated that a significant rate acceleration in amide hydrolysis could be achieved (10^4- to 10^6-fold rate acceleration).

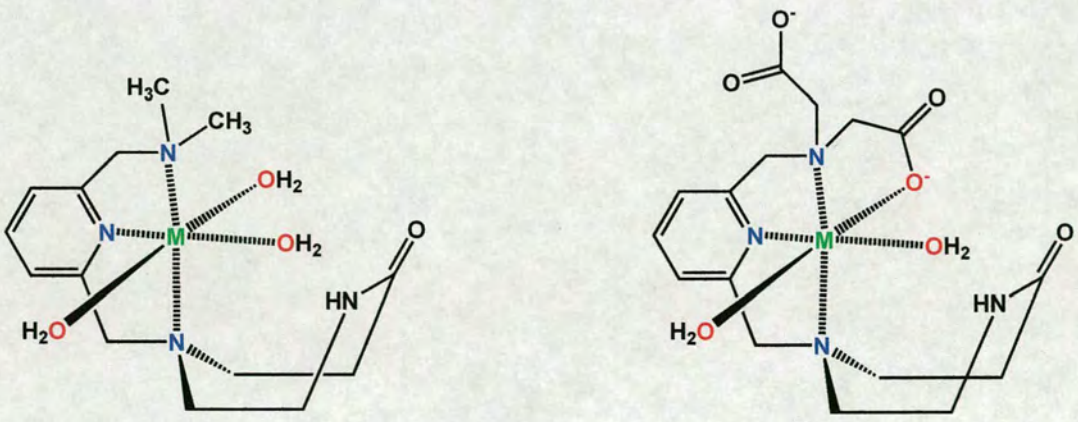

Fig. 2.3 Model metal complexes promoting metal-hydroxide attack for hydrolysis of an intramolecular amide bond.

In most of these studies, however, the simultaneous activation of nucleophile and electrophile species through metal coordination was not possible due to the nature of the complex formed. Studies by Chin and coworkers, using a *cis*-diaqua Cu(II) complex (**A**) and a monoaqua Cu(II) complex (**B**) (Fig 2.4), showed **A** to be over two orders of magnitude more effective than **B** at promoting the hydrolysis of peptide bonds.[7] The fact that complex **A** offers two available binding sites, whereas complex **B** only one, suggests that a more effective mechanism for metal ion promoted amide hydrolysis may involve combined activation of nucleophile (metal-hydroxide) and electrophile (metal-bound amide).

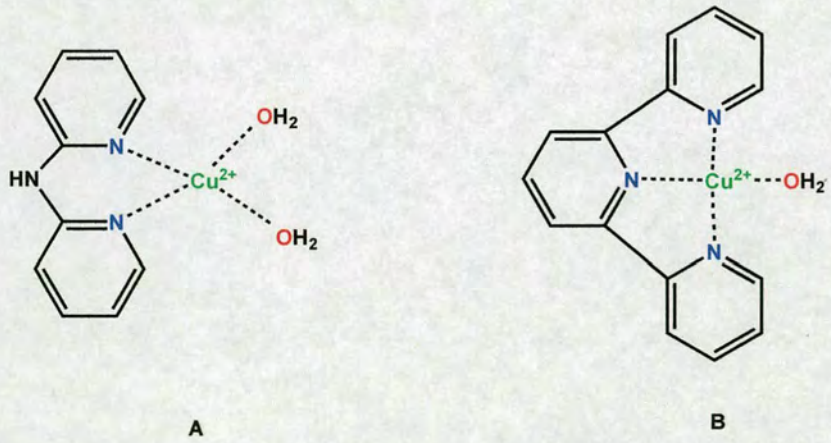

Fig. 2.4 Model metal complexes promoting metal-hydroxide attack for hydrolysis of amide bond.

Moreover, peptide bond hydrolysis catalysed by hydroxide ions involves two tetrahedral intermediates (**T**). Addition of the hydroxide to the amide bond forms the first intermediate

T1, then migration of the hydroxide proton gives rise to the second intermediate **T2,** thus favouring the expulsion of the amine group (Scheme 2.1).

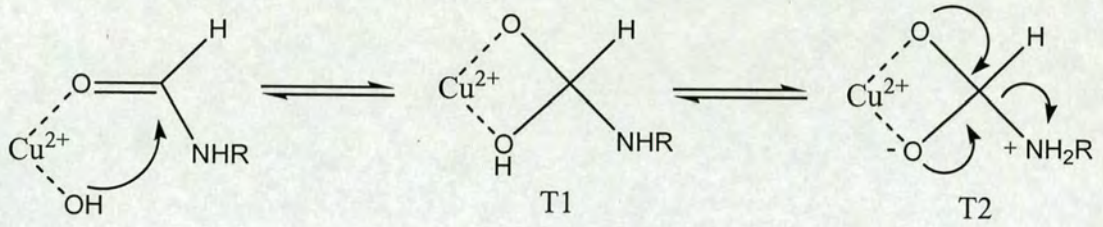

Scheme 2.1

Complex **A** offers also the possibility to chelate and stabilise the tetrahedral intermediates of the reactions, hence making the reaction more favourable.

In conclusion, these are only a few examples of synthetic models of peptidases with biologically relevant and substitutionally labile metal ions such as Cu(II) and Zn(II),[6b,8] and as a result, there is little mechanistic information available on labile metal-promoted amide hydrolysis. Thus, additional investigations on amide hydrolysis promoted by synthetic metal comlplexes are needed. The study herein exploits the use of the ligand unit (6-pivaloylamido-2-pyridylmethyl)amine as a way to induce an N_2O coordination environment for zinc(II) ions, in which oxygen coordination is provided by an intramolecular amide carbonyl group (Fig. 2.5). This ligand moiety as part of three polydentate ligands with and without additional coordinating groups allows the formation of zinc(II) complexes with different coordination environments.

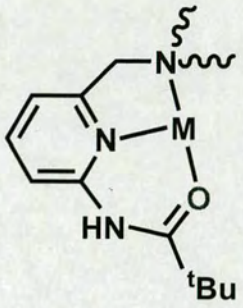

Fig 2.5 The ligand unit (6-pivaloylamido-2-pyridylmethyl)amine.

The structures and amide oxygen binding strength of the three zinc(II) complexes in the solid state and in solution are compared. Amide cleavage reactions of these ligands and their zinc(II) complexes are investigated. Zinc(II)-promoted amide cleavage in methanol is observed in two of the complexes. The rate of amide cleavage appears to be correlated with the strength of amide coordination and Lewis acidity of the zinc(II) centre determined by X-ray, NMR and IR studies.

2.2 Results and Discussion

2.2.1 Design and Synthesis

The ligand unit (6-pivaloylamido-2-pyridylmethyl)amine (Fig. 2.5) ideally positions an amide oxygen for intramolecular metal coordination. This fragment can be incorporated into a variety of polydendate ligands thus allowing the formation of metal complexes with different coordination environments and amide oxygen coordination as models for peptidases. In this work we show that ligands $\mathbf{L}^{2.1}$, $\mathbf{L}^{2.2}$ and $\mathbf{L}^{2.3}$ provide N_4O, N_2S_2O and N_2O coordination for zinc when reacted with a suitable zinc precursor (Scheme 2.2).

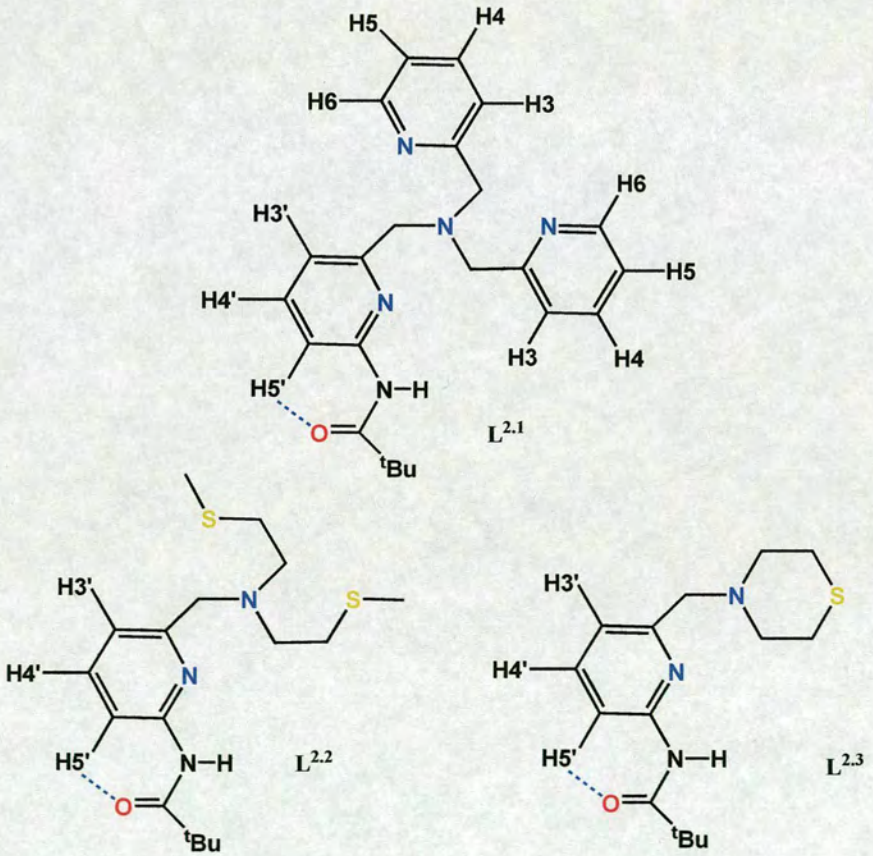

Scheme 2.2

The reaction of $\mathbf{L}^{2.1,\ 2.3}$ with equimolar amounts of $ZnCl_2$ affords complexes which exhibit internal N–H···Cl–Zn hydrogen bonding (Scheme 2.3 A).[9] The reaction (Scheme 2.3 B) of $\mathbf{L}^{2.1,\ 2.2}$ with $[Zn(NCCH_3)_4](PF_6)_2$ or $Zn(ClO_4)_2{\cdot}6H_2O$, however, affords trigonal bipyramidal $[(\mathbf{L}^{2.1,\ 2.2})Zn]^{2+}$ cations in which the carbonyl oxygen of the pivaloylamido group is coordinated axially.[9,10] Similarly, the reaction of equimolar amounts of $Zn(ClO_4)_2{\cdot}6H_2O$ and $\mathbf{L}^{2.3}$ (Scheme 2.3 C) affords a complex with amide oxygen coordination that, in addition, can accommodate a variety of additional ligands including water. Thus, $\mathbf{L}^{2.3}$ allows the simultaneous coordination of an amide oxygen and a water molecule to a zinc(II) ion, a structural motif relevant to postulated mechanisms of zinc-promoted hydrolysis of peptide bonds in peptidases.[2,3]

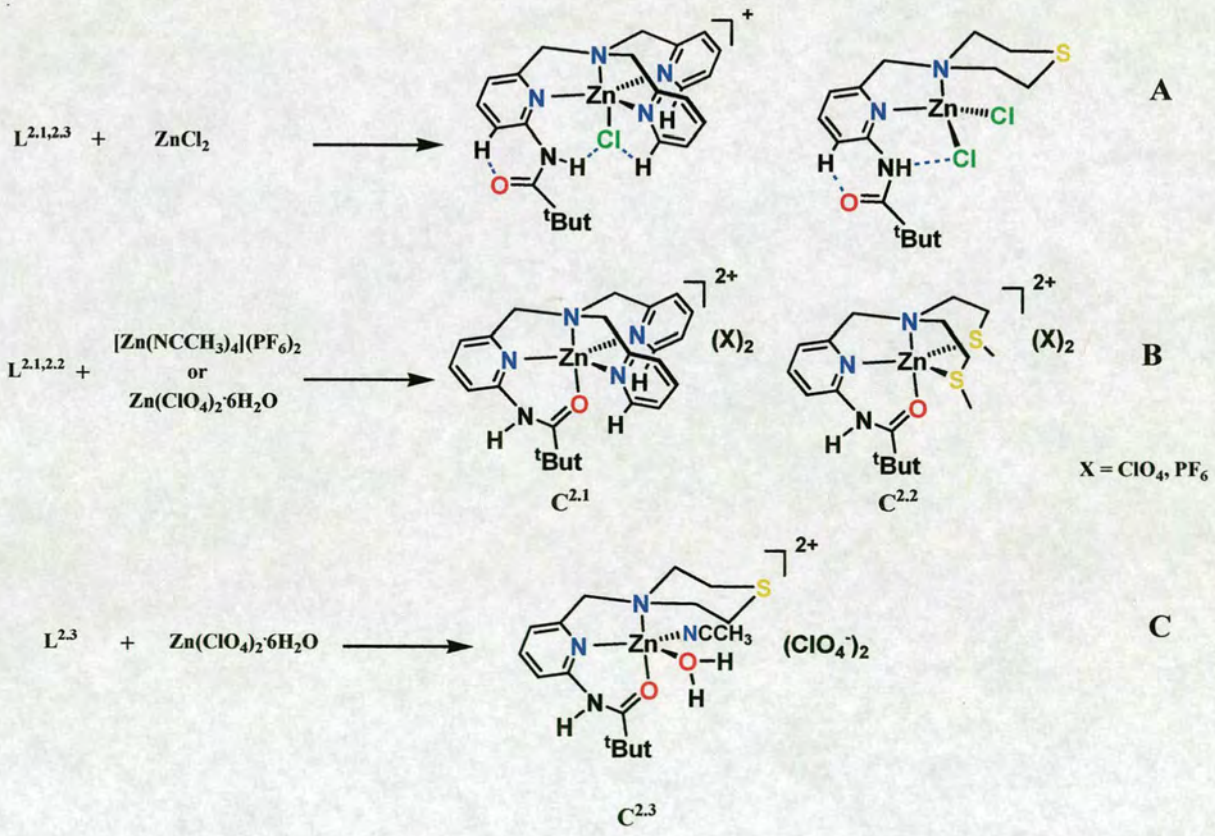

Scheme 2.4

2.2.2 X-Ray Crystallography

2.2.2.1 Structure of $[(L^{2.3})Zn(OH_2)(CH_3CN)](ClO_4)_2$ $C^{2.3}$

Single crystals of $C^{2.3}$ suitable for X-ray diffraction were grown by slow evaporation of acetonitrile solutions. A thermal ellipsoid plot of the molecular structure of $C^{2.3}$ is shown in Fig. 2.6 and a list with selected distances and angles is given in Table 2.1. The zinc(II) centre is in a square pyramidal environment in which the base of the pyramid is formed by the pyridine and amine units, the amide oxygen and the water molecule. The acetonitrile molecule completes the pyramid by occupying the apical position.

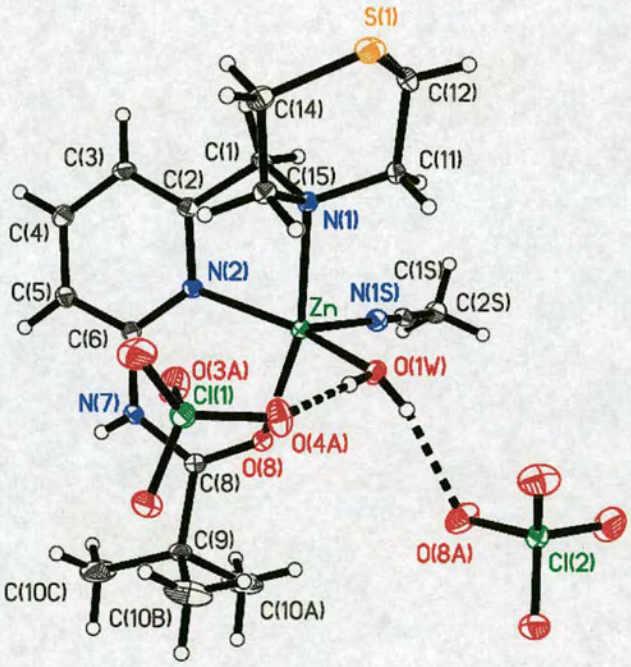

Fig. 2.6 Thermal ellipsoid plot drawn with 30% probability ellipsoids of the molecular structure of the $[(L^{2.3})Zn(H_2O)(CH_3CN)](ClO_4)_2$ $C^{2.3}$.

The square pyramidal geometry, however, is quite distorted (O(1W)–Zn–N(1S) 103.1(10)°, O(1W)–Zn–N(2) 151.17(9)°, N(2)–Zn–N(1S) 105.65(9)°) leaving a readily accessible coordination site adjacent to the amide oxygen, which in the crystal structure is weakly occupied by a ClO_4^- anion (O(3A)···C(8) 3.181(3) Å, Zn–O(3A) 2.955(3) Å, O(3A)–Zn–N(1S) 166.43(8)°, O(3A)–Zn–O(1W) 77.5(8)°). The Zn–O(8) distance, 2.0306(19) Å, is slightly longer than in $\mathbf{C}^{2.1}$ [9a] (2.0005(16) Å) and $\mathbf{C}^{2.2}$ [10] (2.006(3) Å).

Table 2.1 Selected bond lengths (Å) and angles (°) for $\mathbf{C}^{2.3}$

Distances		Angles	
Zn–O(1W)	2.001(2)	O(1W)–Zn–N(1S)	103.1(10)
Zn–O(8)	2.0306(19)	O(1W)–Zn–N(2)	151.17(9)
Zn–N(1)	2.169(2)	N(2)–Zn–N(1S)	105.65(9)
Zn–N(2)	2.049(2)	O(1W)–Zn–O(8)	93.39(8)
Zn–N(1S)	2.056(2)	O(1W)–Zn–N(1)	92.67(8)
		O(8)–Zn–N(1S)	93.89(8)
N(7)–C(6)	1.402(3)	N(1S)–Zn–N(1)	98.79(9)
N(7)–C(8)	1.350(3)	N(2)–Zn–O(8)	86.91(8)
C(8)–O(8)	1.234(3)	N(2)–Zn–N(1)	80.85(8)
C(8)–C(9)	1.529(4)	O(8)–Zn–N(1)	164.33(8)
		C(8)–N(7)–C(6)	130.1(2)
		N(7)–C(8)–C(9)	117.5(2)
		O(8)–C(8)–N(7)	123.5(2)
		O(8)–C(8)–C(9)	119.0(2)

This structural feature suggests that the amide oxygen binds somewhat more weakly to the zinc(II) centre of $\mathbf{C}^{2.3}$ than to that of $\mathbf{C}^{2.1}$ or $\mathbf{C}^{2.2}$. The angle N(1)–Zn–O(8) of 164.33(8)° is smaller than in $\mathbf{C}^{2.1}$ (167.75(6)°) and $\mathbf{C}^{2.2}$ (167.5(2)°), *i.e.* it deviates even further from linearity. An important difference between the coordination environment of $\mathbf{C}^{2.3}$ compared

to $\mathbf{C}^{2.1}$ or $\mathbf{C}^{2.2}$ is the simultaneous coordination of the amide oxygen and a water molecule (Zn–O(1W), 2.001(2) Å). The simultaneous binding of an amide oxygen and water molecule is a structural feature proposed for the double activation mechanism exerted by the Lewis acidic zinc(II) centre in peptidases and proteases. The zinc-bound water (O(1W)) is 4.041 Å away from the carbon of the amide group (C(8)) and doubly hydrogen bonded to the two ClO_4^- counter ions (O(1W)···O(4A) 2.700(3) Å, O(1W)···O(8A) 2.740(3) Å).

2.2.3 NMR and IR studies

2.2.3.1 Solution Structures

Zinc(II) complexes $\mathbf{C}^{2.1}$–$\mathbf{C}^{2.3}$ in acetonitrile solutions are all characterized by ^{1}H NMR resonances shifted downfield relative to the corresponding 'free' ligand ($\mathbf{L}^{2.1–2.3}$), a feature consistent with metal binding (Fig. 2.7, Table 2.2).

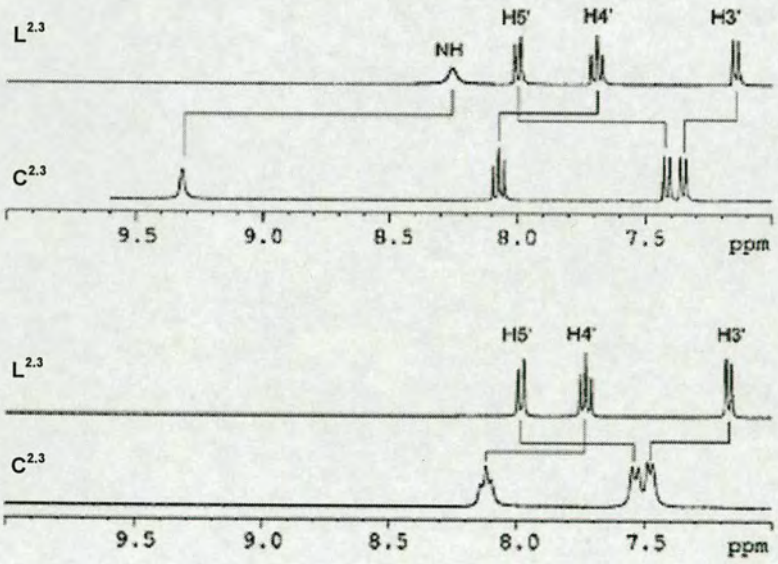

Fig. 2.7 Aromatic and NH region of the ^{1}H NMR (360.1 MHz, 293 K) of $\mathbf{L}^{2.3}$(in CD_3CN), $\mathbf{C}^{2.3}$ (in CD_3CN), $\mathbf{L}^{2.3}$ (in CD_3OD) and $\mathbf{C}^{2.3}$ (in CD_3OD). See Table 2.3 for chemical shift values and Scheme 2.2 for labelling explanation.

This downfield shift is more prominent for the amide N–H resonance, which is shifted by 1.38, 1.15 and 1.06 ppm in $\mathbf{C}^{2.1}$, $\mathbf{C}^{2.2}$ and $\mathbf{C}^{2.3}$, respectively, suggesting that the strength of amide oxygen coordination to the zinc(II) centre follows the order $\mathbf{C}^{2.1} > \mathbf{C}^{2.2} > \mathbf{C}^{2.3}$.

Table 2.2 Summary of selected ^{1}H NMR (360 MHz, CD_3CN, 293 K) chemical shift data for $\mathbf{L}^{2.1–2.3}$ and $\mathbf{C}^{2.1}$–$\mathbf{C}^{2.3}$[a] (see Scheme 2.2 for atom labelling).

		$\mathbf{L}^{2.1, 2.2}$	$\mathbf{C}^{2.1}$, $\mathbf{C}^{2.2}$
^{t}Bu	H10	1.26, 1.26	1.55 (+0.29), 1.38 (+0.12)
NH	H7	8.16, 8.24	9.54 (+1.38), 9.39 (+1.15)
PyCH_2N	H1′$_{A,B}$	3.71, 3.68	4.33 (+0.62), 4.21 (+0.53)
Py (aromatic)	H3′	7.32, 7.24	7.39 (+0.07), 7.42 (+0.18)
	H4′	7.67, 7.70	8.10 (+0.43), 8.15 (+0.45)
	H5′	7.98, 8.00	7.51 (–0.53), 7.49 (–0.51)

[a]Chemical shifts are in ppm relative to CH_3CN at 1.94 ppm. Values in parentheses denote chemical shifts downfield (positive) or upfield (negative) *vs.* values in previous column. The symbol ′ refers to the 2-pyridylmethyl with the 6-pivaloylamido group.

		$\mathbf{L}^{2.3}$	$\mathbf{C}^{2.3}$
^{t}Bu	H10	1.26	1.36 (+ 0.10)
NH	H7	8.26	9.32 (+1.06)
PyCH_2N	H1′$_{A,B}$	3.50	4.09 (+0.59)
Py (aromatic)	H3′	7.14	7.35 (+0.21)
	H4′	7.69	8.10 (+0.41)
	H5′	8.00	7.41 (–0.59)

The feature of the ^{1}H NMR spectra of $\mathbf{L}^{2.1–2.3}$ and $\mathbf{C}^{2.1}$–$\mathbf{C}^{2.3}$ that is most informative of the structure adopted, however, is the chemical shift of H5′ (see Scheme 2.2 for atom labelling), as it gives information of the orientation of the amide group. In $\mathbf{L}^{2.1–2.3}$ the H5′ resonance appears considerably downfield of the other aromatic resonances due to the close proximity of H5′ and the amide oxygen.[9] Thus, in $\mathbf{C}^{2.1}$–$\mathbf{C}^{2.3}$ only the H5′ resonance undergoes a large upfield shift (0.55–0.59 ppm) relative to the corresponding ligand, something that is consistent with breaking a C–H5′···O=C interaction, thus allowing amide

oxygen binding to the zinc(II) centre. Very similar ^{1}H NMR spectra were obtained in methanol, which suggests that $\mathbf{L}^{2.1\text{-}2.3}$ and $\mathbf{C}^{2.1}$–$\mathbf{C}^{2.3}$ adopt very similar structures in acetonitrile and methanol solutions (Fig. 2.7). ^{13}C NMR studies provided an additional diagnostic parameter of the adopted structures and strength of amide oxygen binding in $\mathbf{C}^{2.1}$–$\mathbf{C}^{2.3}$. Thus, the position of the carbonyl resonances in the ^{13}C NMR spectra of $\mathbf{C}^{2.1}$, $\mathbf{C}^{2.2}$ and $\mathbf{C}^{2.3}$ in acetonitrile of 187.1, 185.7 and 184.1 ppm, respectively, compared to 176.9 ppm for $\mathbf{L}^{2.1}$, 177.9 ppm for $\mathbf{L}^{2.2}$ and 177.9 ppm for $\mathbf{L}^{2.3}$ provides further evidence of carbonyl binding in $\mathbf{C}^{2.1}$–$\mathbf{C}^{2.3}$. The magnitude of the downfield shift experienced by the carbonyl resonance of 10.2 ppm for $\mathbf{C}^{2.1}$ relative to free $\mathbf{L}^{2.1}$, 7.8 ppm for $\mathbf{C}^{2.2}$ relative to $\mathbf{L}^{2.2}$ and 6.2 ppm for $\mathbf{C}^{2.3}$ relative to $\mathbf{L}^{2.3}$ reinforces that the strength of amide oxygen binding to the zinc(II) centre follows the order $\mathbf{C}^{2.1} > \mathbf{C}^{2.2} > \mathbf{C}^{2.3}$. IR studies are in total agreement with all the conclusions derived from the NMR and X-ray data regarding the strength of amide oxygen coordination to the zinc(II) centre in $\mathbf{C}^{2.1}$–$\mathbf{C}^{2.3}$. Thus, the IR spectra of $\mathbf{C}^{2.1}$, $\mathbf{C}^{2.2}$ and $\mathbf{C}^{2.3}$ in acetonitrile show $\nu_{C=O}$ bands shifted to lower wavenumbers relative to the corresponding free ligand by 40 ± 4, 41 ± 4 and 30 ± 4 cm^{-1}, respectively (Table 2.3).

Table 2.3 Selected infrared and vibrational data of $\mathbf{L}^{2.1\text{–}2.3}$ and $\mathbf{C}^{2.1}$–$\mathbf{C}^{2.3}$ in acetonitrile

	ν_{N-H}[a]/cm^{-1}	$\nu_{C=O}$[a]/cm^{-1}
$\mathbf{L}^{2.1}$	3439	1687
$\mathbf{C}^{2.1}$	3320	1647
$\mathbf{L}^{2.2}$	3438	1683
$\mathbf{C}^{2.2}$	3333	1642
$\mathbf{L}^{2.3}$	3439	1686
$\mathbf{C}^{2.3}$	3361	1656

[a] ± 4 cm^{-1}.

The strength of amide oxygen coordination is also reflected in the extent by which the ν_{N-H} is shifted to lower wavenumbers, 119 ± 4 cm^{-1} for $\mathbf{C}^{2.1}$ relative to $\mathbf{L}^{2.1}$, 105 ± 4 cm^{-1} for $\mathbf{C}^{2.2}$ relative to $\mathbf{L}^{2.2}$ and 78 ± 4 cm^{-1} for $\mathbf{C}^{2.3}$ relative to $\mathbf{L}^{2.C2.3}$. Both parameters are indicative of amide oxygen coordination being strongest in $\mathbf{C}^{2.1}$ and weakest in $\mathbf{C}^{2.3}$.

2.2.3.2 Reactions with $Me_4NOH{\cdot}5H_2O$

Recently, it was reported that addition of $Me_4NOH{\cdot}5H_2O$ (1 equiv.) to $\mathbf{C}^{2.2}$ in methanol at 50(1) °C results in cleavage of the *tert*-butylamide to yield quantitatively the product of methanolysis methyl trimethylacetate.[10]

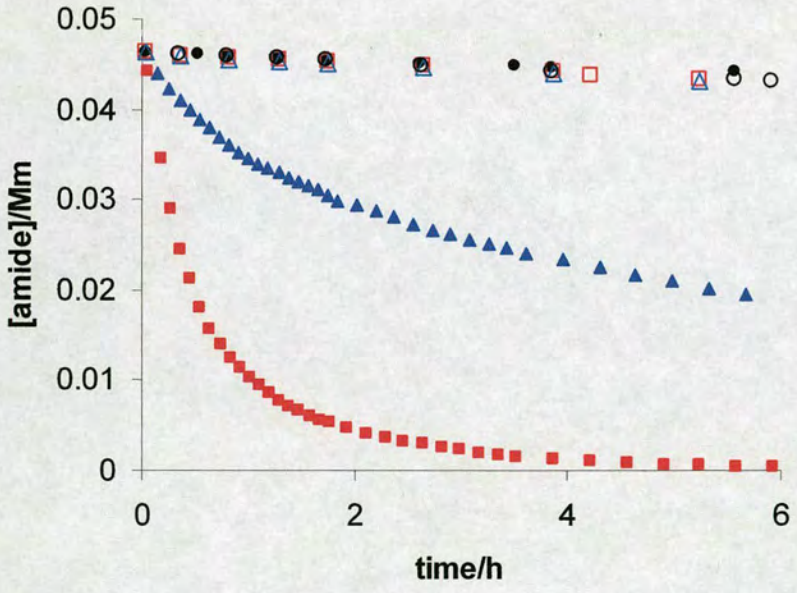

Fig. 2.8 Representative time courses for the reaction of $\mathbf{C}^{2.1}$(■),$\mathbf{C}^{2.2}$(▲), $\mathbf{C}^{2.3}$(●), $\mathbf{L}^{2.1}$(□), $\mathbf{L}^{2.2}$(△) and $\mathbf{L}^{2.3}$(○) (0.046 M) with $Me_4NOH{\cdot}5H_2O$ (1 equiv.) in methanol at 50 °C.

It was also reported that under the same experimental conditions $\mathbf{L}^{2.2}$ does not undergo amide cleavage after 140 h, which suggested that the amide methanolysis reaction was mediated by the zinc(II) ion. In an attempt to gain insights into the mechanism and chemical basis of why zinc(II) ions promote amide cleavage reactions we have compared the ability of $\mathbf{L}^{2.1-2.3}$ and $\mathbf{C}^{2.1}$–$\mathbf{C}^{2.3}$ to undergo amide methanolysis. It was found that $\mathbf{L}^{2.1-2.3}$ and $\mathbf{C}^{2.1}$–$\mathbf{C}^{2.3}$ all undergo amide cleavage in methanol upon addition of $Me_4NOH{\cdot}5H_2O$ (1 equiv.) at 50(1) °C (Scheme 2.4, Figs. 2.8 and 2.9).

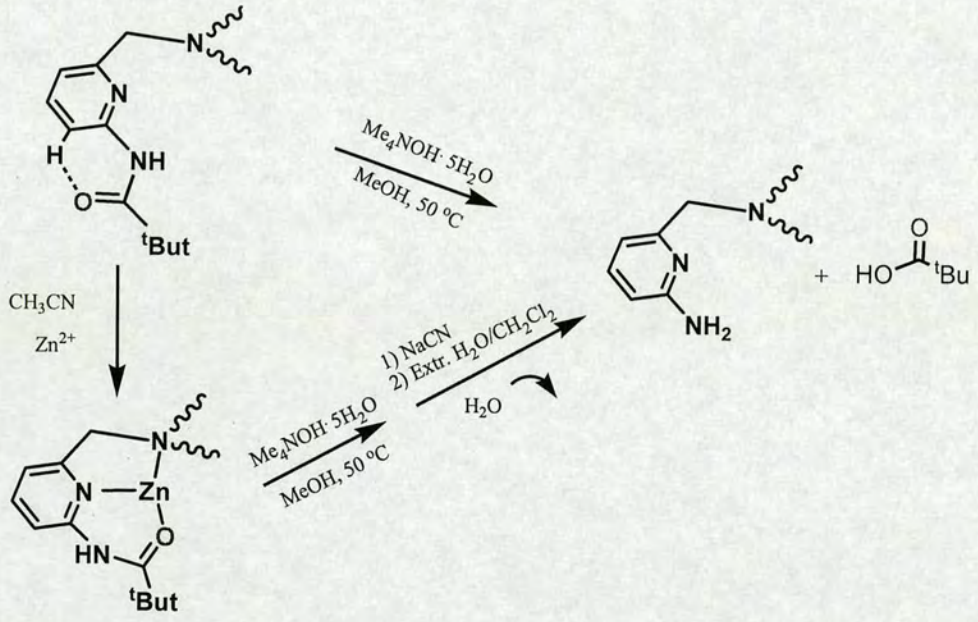

Scheme 2.4

In each case the reaction was monitored by ^{1}H NMR. After the addition of $Me_4NOH{\cdot}5H_2O$ the *tert*-butyl resonance of the amide appears at 1.47 ppm for $\mathbf{C}^{2.1}$, 1.43 ppm for $\mathbf{C}^{2.2}$, 1.37 ppm for $\mathbf{C}^{2.3}$ and 1.31 ppm for $\mathbf{L}^{2.1-2.3}$, which presumably reflects the different degrees of

activation of the amide group for nucleophilic attack. Over time the amide resonance

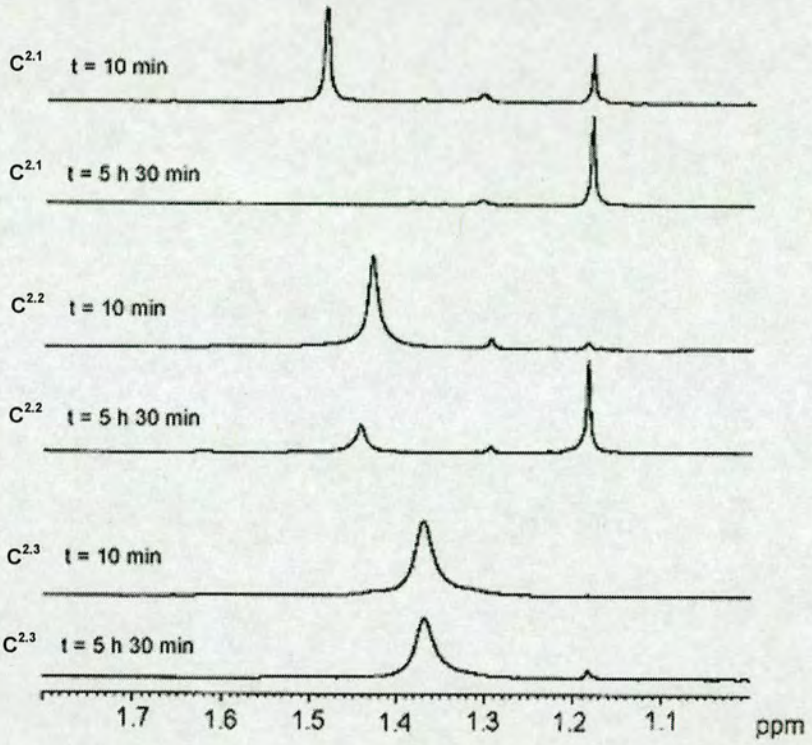

Fig. 2.9 ^{1}H NMR spectra of the reaction of $\mathbf{C}^{2.1}$–$\mathbf{C}^{2.3}$ with $Me_4NOH{\cdot}5H_2O$ (1 equiv.) in d_4-MeOH at 50 °C showing in each case the resonance of the *tert*-butyl group of the starting amide (downfield signal) and the methyl trimethylacetate product (upfield signal) at t= 10 min and t= 5.5 h.

progressively disappears and a resonance at 1.18 ppm appears, which corresponds to methyl trimethylacetate (Fig. 2.9). To confirm the identity of the product(s) of the amide cleavage reactions of $\mathbf{L}^{2.1\text{-}2.3}$ and $\mathbf{C}^{2.1}$- $\mathbf{C}^{2.3}$, the ^{1}H NMR spectra of the reaction mixtures were compared with those of methyl trimethylacetate (Aldrich) or trimethylacetic acid (Aldrich) added to an NMR tube containing the corresponding amino ligands 6-amino-2-pyridylmethyl)-R $\mathbf{L}^{2.1'\text{-}2.3'}$ (R = bis(2-pyridylmethyl)amine $\mathbf{L}^{2.1'}$, bis(2-

(methylthio)ethyl)amine $\mathbf{L}^{2.2'}$ and $N(CH_2CH_2)_2S$ $\mathbf{L}^{2.3'}$) (or equimolar amounts of $\mathbf{L}^{2.1'-2.3'}$ and $Zn(ClO_4)_2{\cdot}6H_2O$) in CD_3OD (0.045 M) (Scheme 2.5).

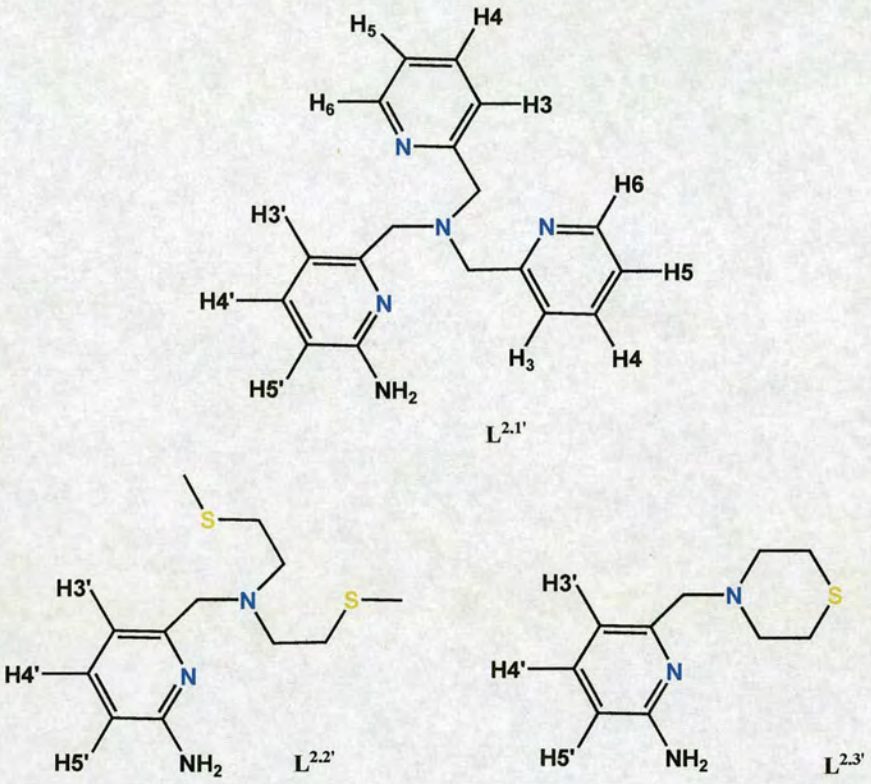

Scheme 2.5

Given that the position of ^{1}H NMR resonance of the methyl trimethylacetate product is in all cases 1.18 ppm it is reasonable to suggest that this does not bind to the product zinc(II) complexes. In fact, over much longer periods of time, trimethylacetic acid is also formed at similar rates for $\mathbf{C}^{2.1}$–$\mathbf{C}^{2.3}$ and $\mathbf{L}^{2.1-2.3}$, which is also consistent with the lack of binding of methyl trimethylacetate to a Zn^{2+} ion. Trimethylacetic acid, however, binds to the product zinc(II) complexes as judged by the position of the *tert*-butyl proton resonance, 1.39, 1.31, 1.25 and 1.13 ppm for $\mathbf{C}^{2.1}$, $\mathbf{C}^{2.2}$, $\mathbf{C}^{2.3}$ and $\mathbf{L}^{2.1-2.3}$, respectively.

The half-life ($t_{1/2}$) of the amide bond was found to be 0.41 h for $\mathbf{C}^{2.1}$, 3.95 h for $\mathbf{C}^{2.2}$, 125 h for $\mathbf{C}^{2.3}$, 55 h for $\mathbf{L}^{2.1}$, 60.1 h for $\mathbf{L}^{2.2}$ and 63.9 h for $\mathbf{L}^{2.3}$. Thus, amide cleavage of $\mathbf{C}^{2.1}$ *vs.* $\mathbf{L}^{2.1}$, $\mathbf{C}^{2.2}$ *vs.* $\mathbf{L}^{2.2}$ and $\mathbf{C}^{2.3}$ *vs.* $\mathbf{L}^{2.3}$ is accelerated by a factor of *ca.* 133, 15 and 0.5, respectively. The rate of amide cleavage correlates remarkably well with the X-ray, ^{1}H and ^{13}C NMR and IR data which suggested that the strength of the interaction between the zinc(II) centre and amide carbonyl group was $\mathbf{C}^{2.1} > \mathbf{C}^{2.2} > \mathbf{C}^{2.3}$. Catalytic zinc sites possess a predominantly N-donating ligand[3a-b] environment and only very rarely N/S ligation.[11]

The rare occurrence of cysteine ligation in a few mononuclear and dinuclear catalytic zinc(II) active sites has prompted considerable research efforts toward the generation of zinc(II) complexes with mixed N/S coordination environments.[12] It is interesting to observe that the N_4 ligation of $\mathbf{C}^{2.1}$ is more efficient than the N_2S_2 coordination environment of $\mathbf{C}^{2.2}$ in promoting the amide cleavage reaction. The simultaneous binding of the amide group and water has been proposed as an event in one of the possible mechanisms of amide bond hydrolysis in metallopeptidases, which may be particularly efficient as it involves the zinc(II) centre bringing in close proximity and activating both nucleophile (water) and substrate (peptide) species. In $\mathbf{C}^{2.3}$, however, despite the simultaneous amide/oxygen binding, amide cleavage is not accelerated relative to in the 'free' ligand, which is a significant finding.

2.3 Conclusion

This study has explored fundamental chemical and structural features of zinc-mediated amide cleavage reactions. The approach consisted of using the ligand unit (6-pivaloylamido-2-pyridylmethyl)amine as a method to induce intramolecular amide oxygen coordination to a zinc(II) centre. The three ligands used, $\mathbf{L}^{2.1-2.3}$, formed mononuclear zinc(II) complexes with amide oxygen coordination to a zinc(II) centre with different coordination environments, $\mathbf{C}^{2.1}$–$\mathbf{C}^{2.3}$. The simultaneous binding of a water molecule and amide was observed in $\mathbf{C}^{2.3}$. This arrangement resembles the motif that has been proposed to be involved in the double nucleophile/substrate Lewis acidic activation and positioning mechanism of amide bond hydrolysis in metallopeptidases.

A clear correlation was found between the information extracted from solid state and solution structural studies and that of functional studies. Thus, X-ray, ^{1}H and ^{13}C NMR and IR data suggest that the strength of amide oxygen binding follows the trend $\mathbf{C}^{2.1} > \mathbf{C}^{2.2} > \mathbf{C}^{2.3}$, which would be consistent with the notion that the Lewis acidity of the zinc(II) centre follows the same order. We have found that $\mathbf{C}^{2.1}$–$\mathbf{C}^{2.3}$ and $\mathbf{L}^{2.1-2.3}$ all undergo amide cleavage reactions in methanol upon addition of an equimolar amount of $Me_4NOH{\cdot}5H_2O$, and that the rate of the amide cleavage reaction follows the trend $\mathbf{C}^{2.1} > \mathbf{C}^{2.2} > \mathbf{C}^{2.3}$, $\mathbf{L}^{2.1-2.3}$.

Thus the observed trend in rate of amide methanolysis is identical to that of the strength of amide oxygen binding. Despite the simultaneous amide/water binding in $\mathbf{C}^{2.3}$, its amide cleavage reaction is not accelerated relative to that of the free ligand $\mathbf{L}^{2.3}$. In contrast, this

work showed that amide oxygen coordination is a key event in zinc-mediated amide cleavage reactions and that it is greatly influenced by the primary coordination sphere of the zinc(II) centre. From this work it appears that nitrogen is more efficient than mixed nitrogen/sulfur coordination, which would explain the binding frequency His ≫Glu > Asp = Cys found for catalytic zinc sites in Nature.

2.4 Experimental

2.4.1 General

Reagents were obtained from commercial sources and used as received unless otherwise noted. Solvents were dried and purified under N_2 by using standard methods[13] and were distilled immediately before use. All compounds were prepared under N_2 unless otherwise mentioned. $\mathbf{L}^{2.1}$, $\mathbf{L}^{2.2}$, $\mathbf{L}^{2.1'}$, $\mathbf{L}^{2.2'}$ and $\mathbf{C}^{2.2}$ were synthesized according to recently reported procedures.[9,10] The NMR spectra were obtained using a Bruker DPX 360 at 20 °C in CD_3CN unless otherwise noted. ^{13}C and ^{1}H chemical shifts are referenced with respect to the carbon (δ_C 1.32 and 118.26 ppm) and residual proton (δ_H 1.94 ppm) solvent peaks. Peak assignments are done with the aid of 2-D NMR spectroscopy. Sample concentrations for the NMR studies were 0.02–0.04 M. Mass spectra were performed on a micromass Platform II system operating in Flow Injection Analysis mode with the electrospray method. Elemental analyses were carried out by the microanalyses service provided by the School of Chemistry at the University of Edinburgh. Infrared spectra were recorded with a JASCO FTIR-410 spectrometer between 4000 and 250 cm^{-1} as KBr pellets (solid state) or as acetonitrile solutions in KBr cells.

2.4.2 Synthesis

$L^{2.3}$. Thiomorpholine (14.75 mmol, 1.5 cm^3) and Na_2CO_3 (145 mmol, 17.5 g) were dissolved in CH_3CN (~150 cm^3). This solution was then treated with 2-(pivaloylamido)-6-

(bromomethyl)pyridine[14] (14.75 mmol, 4 g) and the resulting mixture was stirred for 24 h at 80 °C. The solution was cooled to room temperature, and then poured in 1 M $NaOH_{(aq)}$ (200 cm^3). The product was extracted with CH_2Cl_2 (3 × 150 cm^3). The organic phase was collected, dried over Na_2SO_4, and concentrated under reduced pressure to afford a yellow oil. This crude material was purified by flash chromatography (silica gel, EtOAc–hexanes (2 :1)) to give the pure product (2.4 g, 55%) (Found: C, 61.61; H, 7.80; N, 14.27. for Calc. for $C_{15}H_{23}N_3OS$: C, 61.40; H, 7.90; N, 14.32%).

^1H NMR (CD_3CN, 360.1 MHz): δ_H 8.26 (br s, 1H, py′-N*H*), 8.00 (d, J = 8.3 Hz, 1H, py′-H5), 7.69 (t, J = 7.9 Hz, 1H, py′-H4), 7.14 (d, J = 7.3 Hz, 1H, py′-H3), 3.50 (s, 2H, NCH_2-py′), 2.70–2.60 (m, 8H, $N(CH_2CH_2)_2S$), 1.26 (s, 9H, $C(CH_3)_3$). ^{13}C NMR (CD_3CN, 90.5 MHz): δ_C 177.9 (C=O), 158.3 (py′-C2), 152.2 (py′-C6), 139.5 (py′-C3), 119.3 (py-C4′), 112.6 (py′-C5), 65.3 (NCH_2-py′), 55.8 and 28.5 ($N(CH_2CH_2)_2S$), 40.3 ($C(CH_3)_3$), 27.4 ($C(CH_3)_3$). ESI-MS (+ion): found *m/z* 294.2 (100%), calc. 294.16 (100%) for $[(\mathbf{L}^{2.3})H]^+$, and matches theoretical isotope distribution.

$\mathbf{L}^{2.3'}.\mathbf{L}^{2.3}$ (2.39 mmol, 0.7 g) was dissolved in 2 M HCl (50 cm^3). The resulting solution was heated at reflux overnight. The solution was allowed to cool to room temperature, after which, 1 M NaOH was added until pH ~13. The product was extracted with CH_2Cl_2 (3 × 100 cm^3). The combined organic phases were dried over Na_2SO_4 and evaporated to dryness under reduced pressure to afford the ligand as a yellow solid, which was recrystallised from diethyl ether (0.410 g, 82%) (Found: C, 57.19; H, 7.36; N, 18.85. Calc. for $C_{10}H_{15}N_3S{\cdot}0.14(CH_3CH_2)_2O$: C, 57.74; H, 7.53; N, 19.11%).

^{1}H NMR (CD_3CN, 360.1 MHz): δ_H 7.37 (t, J = 7.9 Hz, 1H, py′-H4), 6.64 (d, J = 7.2 Hz, 1H, py′-H3), 6.35 (d, J = 7.9 Hz, 1H, py′-H5), 4.8 (br, 2H, py′-NH_2), 3.40 (s, 2H, NCH_2-py′), 2.69–2.60 (m, 4H and 4H, N(CH_2CH_2)$_2$S). ^{13}C NMR (CD_3CN, 90.5 MHz): δ_C 159.9 and 157.9 (py′-C2 and py′-C6), 138.6 (py′-C3), 112.7 and 107.2 (py′-C4 and py′-C5), 65.7 (NCH_2-py′), 55.9 and 28.5 (N(CH_2CH_2)$_2$S). ESI-MS (+ion): found *m/z* 209.7 (100%), calc. 210.11 (100%) for [(**L**$^{2.3•}$)H]$^+$, and matches theoretical isotope distribution.

[(L$^{2.1}$)Zn](ClO$_4$)$_2$ C$^{2.1}$. $Zn(ClO_4)_2 \cdot 6H_2O$ (94 mg, 0.25 mmol) and **L**$^{2.1}$ (73 mg, 0.25 mmol) were dissolved in acetonitrile (5 cm^3) and the solution was stirred for 1 h at room temperature. The solution was filtered through Celite and the solvent evaporated under vacuum to yield the pure product as a yellow solid in quantitative yield (Found: C, 39.79; H, 4.19; N, 10.53. Calc. for $C_{23}H_{27}Cl_2N_5O_9Zn \cdot 2H_2O$: C, 40.05; H, 4.53; N, 10.15%).

^{1}H NMR (CD_3CN, 360.1 MHz): δ_H 9.54 (br s, 1H, NH), 8.58 (d, J = 5.4 Hz, 2H, py-H6), 8.14 (td, J = 7.6, 1.5 Hz, 2H, py-H4), 8.10 (t, J = 7.9 Hz, 1H, py′-H4), 7.66 (t, J = 5.9 Hz, 2H, py-H5), 7.61 (d, J = 7.9 Hz, 2H, py-H3), 7.51 (d, J = 8.3 Hz, 1H, py′-H5), 7.39 (d, J = 7.6 Hz, 1H, py′-H3), 4.57 (s, 4H, NCH_2-py), 4.33 (s, 2H, NCH_2-py′), 1.55 (s, 9H, C(CH_3)$_3$). ^{13}C NMR (CD_3CN, 90.5 MHz, 298 K): δ_C 187.1 (C=O) 156.0 (py-C2) 153.6 and 152.4 (py′-C2 and py′-C6), 149.3 (py-C6), 144.5 (py′-C3), 142.9 (py-C3), 126.4 and 125.8 (py-C4 and py-C5), 122.1 and 115.1 (py′-C4 and py′-C5), 58.2 (NCH_2-py), 57.9 (NCH_2-py′), 42.6 (C(CH_3)$_3$), 27.1 (C(CH_3)$_3$). ESI-MS (+ion) found *m/z* 226.6 (100%), calc. 226.57 for [(**L**$^{2.1}$)Zn]$^{2+}$, and matches theoretical isotope distribution.

[(L$^{2.3}$)Zn(H$_2$O)(CH$_3$CN)](ClO$_4$)$_2$ C$^{2.3}$. $Zn(ClO_4)_2 \cdot 6H_2O$ (149 mg, 0.4 mmol) and **L**$^{2.3}$ (117 mg, 0.4 mmol) were dissolved in acetonitrile (15 cm^3) and the solution was stirred for

1 h at room temperature. The solvent was evaporated under vacuum to yield the pure product as a yellow solid in quantitative yield (Found: C, 32.69; H, 4.48; N, 8.84. Calc. for $C_{17}H_{28}Cl_2N_4O_{10}SZn$: C, 33.10; H, 4.58; N, 9.08%).

^{1}H NMR (CD_3CN, 360.1 MHz): δ_H 9.32 (br s, 1H, NH), 8.10 (dd, J = 8.6, 7.9 Hz, 1H, py′-H4), 7.42 (d, J = 8.3 Hz, 1H, py′-H5), 7.35 (d, J = 7.6 Hz, 1H, py′-H3), 4.09 (s, 2H, NCH_2-py), 3.35–2.53 (m, 8H, N(CH_2CH_2)$_2$S) 1.37 (s, 9H, C(CH_3)$_3$). ^{13}C NMR (CD_3CN, 90.5 MHz, 298 K): δ_C 184.1 (C=O) 152.4 and 151.9 (py′-C2 and py′-C6), 143.9 (py′-C3), 121.8 and 116.7 (py′-C4 and py′-C5), 56.5 (NCH_2-py′), 54.7 and 22.1 (N(CH_2CH_2S)$_2$), 41.7 (C(CH_3)$_3$), 26.9 (C(CH_3)$_3$).

2.4.3 X-Ray crystallography

Crystal data for [($\mathbf{L}^{2,3}$)Zn(OH_2)(NCCH_3)](ClO_4)$_2$: $C_{17}H_{28}N_4O_{10}Cl_2SZn$, M = 616.76, orthorhombic, space group *Pbca*, a = 17.5901(18), b = 15.6105(16), c = 18.4076(19), U = 5054.5(9) Å^3, Z = 8, T = 150(2) K, λ(Mo-Kα) = 0.71073, D_c = 1.621, μ = 1.324 mm^{-1}, 30143 reflections measured, 6288 unique, R_{int} = 0.0551 (all data), R_1 = 0.0628 (all data), wR_2 = 0.1299 (all data), S = 1.069 (all data), largest difference peak, hole 1.04, –0.65 e$^-$Å^{-3}.

Crystals suitable for X-ray diffraction studies were grown by slow evaporation of acetonitrile solutions at room temperature.

Intensity data for [($\mathbf{L}^{2,3}$)Zn(OH_2)(NCCH_3)](ClO_4)$_2$ were collected at 150 K using a Bruker (formerly Siemens) AXS SMART APEX area detector diffractometer with graphite-monochromated Mo-Kα radiation (λ = 0.71073 Å). The structures were solved by

direct methods and refined to convergence against F^2 data using the SHELXTL suite of programs.[15] Data were corrected for absorption applying empirical methods using the program SADABS,[16] and the structures were checked for higher symmetry using the program PLATON.[17] All non-hydrogen atoms were refined anisotropically unless otherwise noted. Hydrogen atoms were placed in idealized positions and refined using a riding model with fixed isotropic displacement parameters. The N-H hydrogens were located in the difference map and refined isotropically.

References

[1] B. L. Valle and D. S. Auld, *Proc. Natl. Acad. Sci. USA*, 1990, **87**, 220.

[2] L. M. Sayre, *J. Am. Chem. Soc.*, 1986, **108**, 1632.

[3] (*a*) W. N. Lipscomb and N. Straeter, *Chem. Rev.*, 1996, **96**, 2375; (*b*) E. L. Hegg and J. N. Burstyn, *Coord. Chem. Rev.*, 1998, **173**, 133; (*c*) D. W. Christianson and W. N. Lipscomb, *Acc. Chem. Res.*, 1989, **22**, 62; (*d*) H. Kim and W. N. Lipscomb, *Biochemistry*, 1991, **30**, 8171.

[4] (*a*) T. N. Parac and N. M. Kostic, *J. Am. Chem. Soc.*, 1996, **118**, 51; (*b*) T. M. Rana and C. F. Meares, *Proc. Natl. Acad. Sci. USA*, 1991, **88**, 10578; (*c*) T. M. Rana and C. F. Meares, *J. Am. Chem.Soc.*, 1991, **113**, 1859.

[5] H. Sigel and R. Martin, *Chem. Rev.*, 1982, **82**, 385.

[6] (*a*) J. T. Groves and L. A. Baron, *J. Am. Chem. Soc.*, 1989, **111**, 5442; (*b*) J. T. Groves, R. Rife and R. Chambers, Jr., *J. Am. Chem. Soc.*, 1984, **106**, 630.

[7] J. Chin, V. Jubian and K. Mrejen, *Chem. Commun.*, 1990, 1326.

[8] (*a*) T. H. Fife and T. J. Przystas, *J. Am. Chem. Soc.*, 1986, **108**, 4631; (*b*) L. M. Sayre, K. V. Reddy, A. R. Jacobson and W. Tang, *Inorg. Chem.*, 1992, **31**, 935; (*c*) E. L. Hegg and J. N. Burstyn, *J. Am. Chem. Soc.*, 1995, **117**, 7015; (*d*) X. S. Tan, Y. Fujii, T. Sato, Y. Nakano and M. Yashiro, *Chem. Commun.*, 1999, 881.

[9] (*a*) J. C. Mareque-Rivas, R. Torres-Martín-de-Rosales and S. Parsons, *Dalton Trans.*, 2003, 2156; (*b*) J. C. Mareque-Rivas, E. Salvagni, R. Torres-Martín-de-Rosales and S. Parsons, *Dalton Trans.*, 2003, 3339.

[10] L. M. Berreau, M. M. Makowska-Grzyska and A. M. Arif, *Inorg. Chem.*, 2000, **39**, 4390

[11] (*a*) H. Eklund and C. I. Brändén, *Zinc Enzymes*, T. G. Spiro, John Wiley and Sons, New York, 1983; (*b*) M. K. Chan, W. Gong, P. T. R. Rajagopalan, B. Hao, C. M. Tsai and D. Pei, *Biochemistry*, 1997, **36**, 13904; (*c*) L. Betts, S. Xiang, S. A. Short, R. Wolfenden and C. W. Carter, Jr., *J. Mol. Biol.*, 1994, **235**, 635; (*d*) M. H. Bracey, J. Christiansen, P. Tovar, S. P. Cramer and S. G. Bartlett, *Biochemistry*, 1994, **33**, 12126; (*e*) Z. Wang, W. Fast, A. M. Valentine and S. J. Benkovic, *Current Opinion in Chemical Biology*, 1999, **3**, 614.

[12] (*a*) L. M. Berreau, R. A. Allred, M. M. Makowska-Grzyska and A. M. Arif, *Chem. Commun.*, 2000, 1423; (*b*) D. K. Garner, S. B. Fitch, L. H. McAlexander, L. M. Bezold, A. M. Arif and L. M. Berreau, *J. Am. Chem. Soc.*, 2002, **124**, 9970; (*c*) D. K. Garner, R. A. Allred, K. J. Tubbs, A. M. Arif and L. M. Berreau, *Inorg. Chem.*, 2002, **41**, 3533; (*d*) L. M. Berreau, M. M. Makowska-Grzyska and A. M. Arif, *Inorg. Chem.*, 2001, **40**, 2212 .

[13] W. L. F. Armarego and D. D. Perrin *Purification of Laboratory Chemicals*, Butterworth-Heinemann, Oxford, 1997

[14] L. M. Berreau, S. Mahapatra, J. A. Halfen, V. G. Young, Jr. and W. B. Tolman, *Inorg. Chem.*, 1996, **35**, 6339.

[15] G. M. Sheldrick *SHELXS and SHELXL 97*, University of Göttingen, 1997

[16] (*a*) G. M. Sheldrick, *Empirical absorption correction program*, University of Göttingen, based upon the method of Blessing, 1995; (*b*) R. H. Blessing, *Acta Crystallogr., Sect. A*, 1995, **51**, 33.

[17] A. L. Spek, *Acta Crystallogr., Sect. A.*, 1990, **46**, C34.

Chapter 3

Internal hydrogen bonding in tetrahedral and trigonal bipyramidal zinc(II) complexes of pyridine-based ligands

3.1 Introduction

3.1.1 Hydrogen Bonding: General

Conventionally, the hydrogen bond (H-bond) is defined as a weak electrostatic interaction where a hydrogen atom is bonded covalently to a strongly electronegative donor atom (D) and interacting with a lone pair of electrons associated with a strongly electronegative atom called the acceptor (A). In the covalent D-H bond the electron on the hydrogen atom has its centre of mass displaced towards the centre of the covalent bond. In other words, the hydrogen atom is deshielded generating a dipole with a positive charge localised on the proton of the D-H bond. The Columbic interaction of the positive charge of this dipole with any significant accumulation of electrons of the acceptor atom gives rise to the hydrogen bond (Fig. 3.1).[1,2]

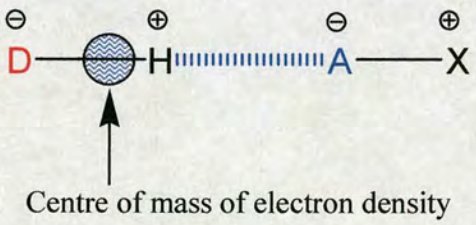

Fig 3.1 Displacement of the centre of mass of the electron associated with the proton.

The degree of deshielding of the hydrogen atom is a function of the electronegativity of the donor atom: the more electronegative the donor atom, the more descreened the proton and the stronger the hydrogen bond. Thus, traditionally only electronegative atoms were believed to act as hydrogen bond donors and acceptors. However, with time many hydrogen bond donor and acceptor sites that do not fall within this classification have been

discovered. A typical example is given by the C-H· · ·O=C interaction,[2,3] especially present in biomolecules, where the donor carbon atom is not electronegative.

Where, therefore, can we set a limit for the definition of hydrogen bond interaction? A good clarification that did not set a limit, but extended it, was given by Pimentel and McClellan: "a hydrogen bond between a functional group A-H and an atom or group of atoms B is said to exist when (a) there is evidence of a bond formation and (b) there is evidence that this bond linking A-H and B specifically involves the hydrogen atom already bonded to A".[1]

The energy of the hydrogen bonds generally ranges from 8 to 22 kJ. mol^{-1}, which indicates that their strength can vary from moderately strong to very weak. Usually the strength is related to the distance between the proton and the acceptor (H· · ·A), which ranges from about 1.5 Å (strong) to about 3.0 Å (weak). In addition, hydrogen bond has directional preferences in that the D-H· · ·A angle tends to be linear, *ca.* 165°.[2]

To determine hydrogen bond structural features the most accurate technique is single crystal neutron diffraction, but these analyses are relatively few. For that reason, hydrogen bond structural data come mainly from X-ray crystallography, which is the most reliable technique to determine interatomic geometries in the solid state accurately. However, since X-ray scattering is proportional to the square of the atomic number, it is difficult to locate the exact position of hydrogen atoms on electron density maps generated by X-ray diffraction. Therefore, in order to establish the presence of hydrogen bonds from X-ray

crystallographic data one has to rely on the use of D···A distance cutoffs. An early criterion was given by Hamilton and Ibers that said that a hydrogen bond occurs when the separation between the donor and the acceptor is shorter than the sum of the van der Waals contact radii.[2] This definition is, however, not correct, since it is based on the assumption that hydrogen bond at long distances are due to van der Waals interactions. The energy of van der Waals forces follows the potential energy curve of Lennard-Jones, which is proportional to $1/r^6$ (r = radius), thus decreasing very rapidly with the distance. Columbic interactions, instead, vary more slowly, depending on 1/r. Since electrostatic Columbic interactions predominate at longer ranges in hydrogen bonds, they exist at distances that are greater than van der Waals contacts. Therefore, they can still occur at distances that go beyond the sum of van de Waals radii of the donor and the acceptor, and/or the proton and the acceptor.

Even if X-ray crystallographic data suggests the presence of a D-H···A hydrogen bonding from the D···A distance and D-H···A angle, it is important to demonstrate its existence using other techniques. Moreover, since hydrogen bonds are relatively weak interactions, it is possible that they exist in the solid state, but may break in solution.

Hence, whenever possible, it is also important to compare solution and solid state data. In this study, structural features, including hydrogen bonding interactions found in the solid state by X-ray diffraction analysis, are contrasted and correlated with NMR and/or IR studies in solution.

3.1.2 Important Aspects of Hydrogen Bonding in Nature and Research

The great importance of hydrogen bonding has been widely recognised and studied for many years. The increasing interest on this subject is illustrated in Fig. 3.2, which shows the number of papers published each year containing the concept of "hydrogen bonding" since 1970 (the search was carried out with Scifinder). The trend suggests that there are currently about 20000 publications a year on the subject of hydrogen bonding.

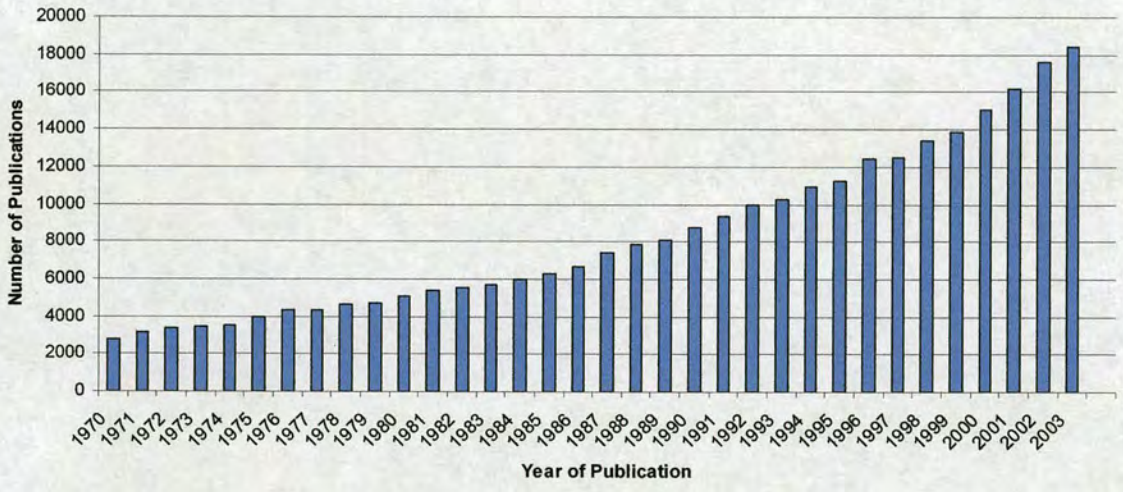

Fig. 3.2 Number of papers containing the concept of "Hydrogen Bonding" versus the year of publication.

Hydrogen bonds play a vital role in life. For instance they stabilise the secondary structures of proteins, they represent the main feature of the base-pair DNA double helix, and they are essential for many biological transformations. Why has this weak interaction been so exploited by nature? The energy of an individual hydrogen bond may be not sufficient to accomplish the needs of biological functions and it is almost negligible if compared for instance with covalent bond energies lying usually around 300 kJ mol^{-1}. However, the mutual cooperativity of hydrogen bond donors and acceptors results in an augmented and

additive global strength. Moreover, hydrogen bond interactions can be easily switched on and off at life temperature, fundamental event in the biological processes of fast inter-molecular recognition and reaction.[2,3] In addition, hydrogen bonding to metal-coordinated molecules seems to play a supporting role in metallo enzyme's catalysis. Consequently, another aspect that has received inner current attention is the study of hydrogen bonding in metal complexes.[4,5,6,7]

3.1.3 H-bond in Metal Complexes

There is a vast choice of hydrogen bonding interactions involving metal complexes. Metal complexes can be involved in external (or intermolecular) hydrogen bonding when the hydrogen bond donor or acceptor is part of an external molecule or ion, or it is part of another metal complex. These interactions are particularly relevant to supramolecular chemistry aspects. If the interacting hydrogen bond donor and acceptor are part of metal-bound ligands of the same metal complex then the metal complex typically exhibits intramolecular (or internal) hydrogen bonding. These interactions are of significance because they can affect the molecular structure and the chemistry of metal complexes.

The different hydrogen bonds in metal complexes can be well described referring to a domain model proposed by Dance.[8] This consists of three domains: the *metal domain*, the *ligand domain* and the *periphery domain* (Fig. 3.3). The *metal domain* is the core of the molecule, namely a region containing the central metal atom, or metal atoms for a dinuclear or metal cluster complex. The *ligand domain* is the area delimited by the ligand atoms at the immediate surrounding of the metal domain, these ligand atoms are directly

bound to the metal centre or exert a strong electronic interaction with the metal. The *periphery domain* consists of peripheral atoms or functional groups of the metal-bound ligands that are far from and weakly interact with the metal centre. Around the periphery domain there is the *environment* that is made of solvent molecules in solution, neighbouring molecules in the solid state and may be absent in the gas phase.

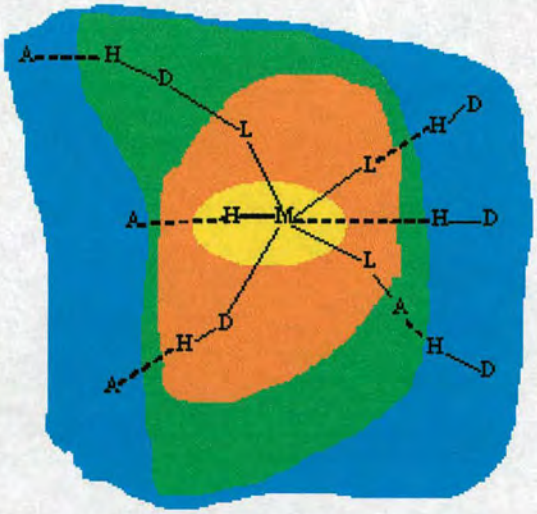

Fig. 3.3 Illustration of the domain model for hydrogen bonding interactions involving metal complexes. Metal domain (yellow), ligand domain (orange), periphery domain (green), environment (blue).[8]

Hydrogen bonding interactions in metal complexes can occur in each of these domains. It is also relevant for this study to note that the metal centre (M) can influence hydrogen bonding in two modes: *directly* or *indirectly*. The metal is *directly* involved when it acts as a hydrogen bond donor, M–H···A, or acceptor, D–H···M, these interactions operate in the metal domain. Instead, the metal influence is *indirect* in the ligand domain; hydrogen bonds in the ligand domain involve a hydrogen bond donor and/or acceptor that it is part of a metal –bound ligand and they are local to the metal. The metal is coordinated to a donor, M–D, or acceptor, M–A, and affect their electronic properties through electron donation/back donation. This may change the polarity or the acidity of the hydrogen bond

donor, M–D–H···A, or may influence the availability of the acceptor lone pair, D–H···A–M, in both cases, the hydrogen bond interactions may be strengthened.[4b] Lastly, the metal can also exert an *indirect* influence, but in less extent, on the hydrogen bonds of the periphery domain, which are those affecting the metal second coordination sphere.

This work is mainly concerned with H-bonds in the metal and ligand domains and another aspect relevant to this study is the ability of metals to increase the capability of certain ligands to take part in hydrogen bonding; an example of considerable current interest is halogens, which, when metal-bound are very effective hydrogen bond acceptors but bound to carbon atoms are not.[4f,5]

3.1.4 H-bond in Hydrolytic Zinc Enzymes

There is a growing awareness that hydrogen bonding to metal-coordinated molecules may be able to play key supporting roles in zinc enzymes (see chapter 1).[6b-e] Thus, carboxypeptidase A,[9] aminopeptidase A,[10] the lethal anthrax factor (LF),[11] thermolysin[12] and pseudomonas aeruginosa alkaline protease[13] are just a few examples of zinc peptidases, amidases and nucleases in which XH groups (X = N, O) of arginine, lysine, histidine, tyrosine and/or serine residues are hydrogen bonded to zinc(II)-bound water and/or substrate groups. In these enzymes the cooperation between metals and non-coordinating active-site residues could be involved in the activation, recognition and/or stabilization mechanisms displayed by these important enzymes. In fact, several very interesting recent results have shown the importance of incorporating second sphere elements in synthetic

models of several types of zinc(II) enzymes including lyases,[14] nucleases,[6g] phosphoryl transferases[15] and oxidoreductases.[6f,16]

Despite the great potential of exploiting and modelling second-sphere hydrogen bonding features of metal centres, very few studies have investigated factors affecting their strength. Strategies to induce and manipulate the strength of hydrogen bonding to metal-bound ligands, however, is a key aspect for any research concerned with exploiting or modelling the effects of these interactions.[17]

This study examines strategies and principles to induce and manipulate hydrogen bonding interactions in metal complexes. We investigate the strength of internal N–H···Cl–Zn hydrogen bonding in tetrahedral and trigonal bipyramidal geometries as model interactions. Factors that affect the strength of the internal N–H···Cl–Zn hydrogen bond and how these changes are expressed spectroscopically are also discussed.

3.2 Results and Discussion

3.2.1 Design and Synthesis

The ligand fragment (6-R^1-2-pyridylmethyl)amine (R^1 = NHCOR or NH_2) (Fig. 3.4) has a suitable stereochemistry for an N–H group to participate in an internal hydrogen bond to an adjacent metal-bound ligand.

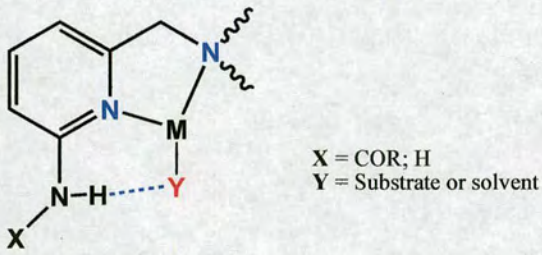

Fig. 3.4 Metal binding mode of the ligand fragment (6-R1-2-pyridylmethyl)amine.

This fragment can be incorporated into a variety of polydentate ligands thus allowing the systematic investigation and exploitation of internal hydrogen bonding in metal complexes of different geometries and chemistry.

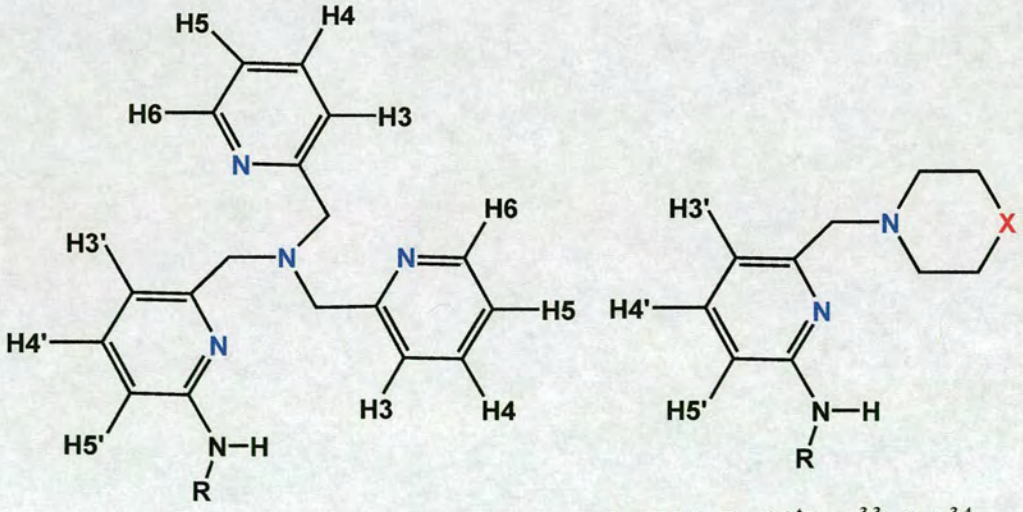

R = CO^{t}Bu ($L^{3.1}$); H ($L^{3.2}$)

X = N-Me; R = CO^{t}Bu ($L^{3.3}$); H ($L^{3.4}$)
X = O; R = CO^{t}Bu ($L^{3.5}$); H ($L^{3.6}$)

Scheme 3.1

Thus, the bis-(2-pyridylmethyl)amine-based ligands $\mathbf{L}^{3.1}$ and $\mathbf{L}^{3.2}$ (Scheme 3.1) provide a good ligand platform for investigating how the nature of the hydrogen bonding group affects the strength of hydrogen bonding to metal bound ligands in trigonal bipyramidal and octahedral coordination environments. The N-methylpiperazine and morpholine based ligands $\mathbf{L}^{3.3\,-\,3.6}$ (Scheme 3.1) offer the opportunity of investigating the same effects in tetrahedral and trigonal bipyramidal ligand environments. As a group, these ligands can be used to assess and compare the strength of internal hydrogen bonding at these metal geometries. In addition, amine and amide groups differ in terms of hydrogen bonding, steric and electronic properties. The synthesis of $\mathbf{L}^{3.3\,-\,3.4}$ can be accomplished in 3–6 steps using 2-(pivaloylamido)-6-(bromomethyl)pyridine[18] ($\mathbf{L}^{3.0}$) as common reagent (Scheme 3.2).

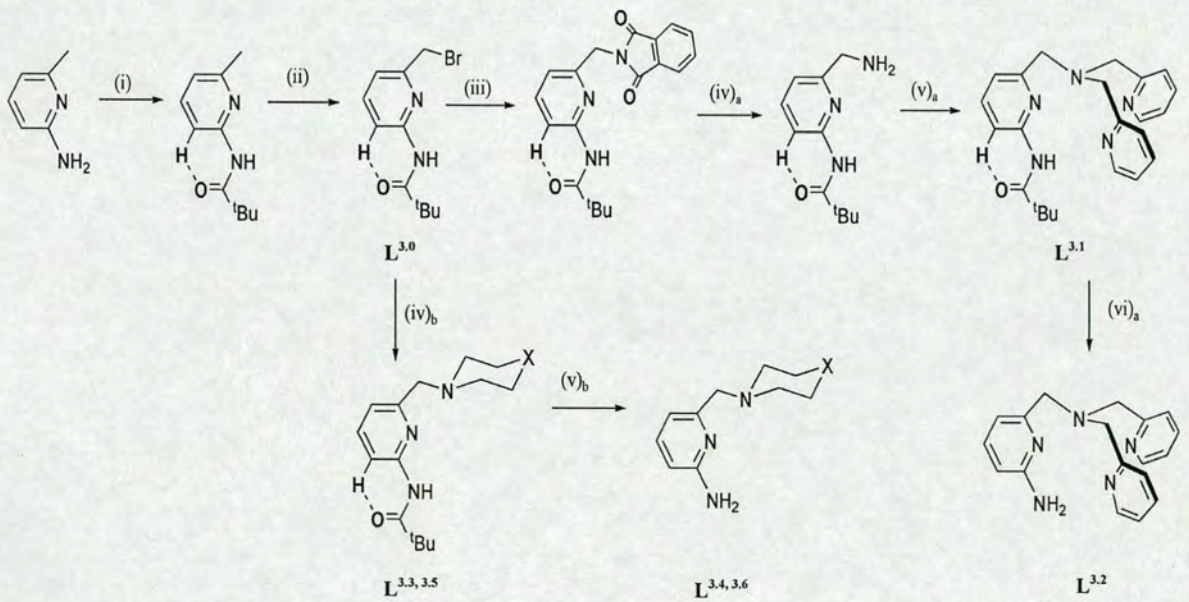

Scheme 3.2 Reagents and conditions used for the synthesis of $\mathbf{L}^{3.0\,-\,3.6}$; (i) ^{t}BuCOCl (1.5 equiv.), CH_2Cl_2, NEt_3, 22 h; (ii) NBS (1.5 equiv.) AIBN (0.1 equiv.), CCl_4, 80 °C, 3.5 h; (iii) potassium phthalamide (1 equiv.), DMF, 120 °C, 3 h; (iv)$_a$ $N_2H_4{\cdot}H_2O$ (1 equiv.), EtOH, 60 °C, 3 h; (v)$_a$ and (iv)b $PyCH_2Cl$ (2 equiv.) or $HN(CH_2CH_2)_2X$ (1 equiv.), Na_2CO_3, CH_3CN, 60 °C, 20–48 h (vi)$_a$; (v)$_b$ 2 M $HCl_{(aq)}$,, 70 °C, 24–40 h.

The reaction of the N-methyl-piperazine and morpholine based ligands $\mathbf{L^{3.3-3.6}}$ with $ZnCl_2$ affords neutral $[(\mathbf{L^{3.3-3.5}})Zn(Cl)_2]$ complexes ($\mathbf{L^{3.3}}$, $\mathbf{C^{3.3}}$; $\mathbf{L^{3.4}}$, $\mathbf{C^{3.4}}$; $\mathbf{L^{3.5}}$, $\mathbf{C^{3.5}}$; $\mathbf{L^{3.6}}$, $\mathbf{C^{3.6}}$), in which the zinc(II) center is tetrahedrally N_2Cl_2 ligated. It was recently reported that reaction of $\mathbf{L^{3.1}}$ with $ZnCl_2$ gives $[(\mathbf{L^{3.1}})Zn(Cl)](Cl)$ $\mathbf{C^{3.1'}}$, which then combined with $NaBPh_4$ afforded the $[(L^{3.1})Zn(Cl)](BPh_4)$ salt ($\mathbf{L^{3.1}}$, $\mathbf{C^{3.1}}$), in which the zinc(II) centre was in a trigonal bipyramidal N_4Cl ligand environment with the Cl ligand occupying one of the axial positions.[19] An identical behaviour was observed for $\mathbf{L^{3.2}}$, from which the $[(\mathbf{L^{3.2}})Zn(Cl)](BPh_4)$ salt ($\mathbf{L^{3.2}}$, $\mathbf{C^{3.2}}$) was prepared (Scheme 3.3).

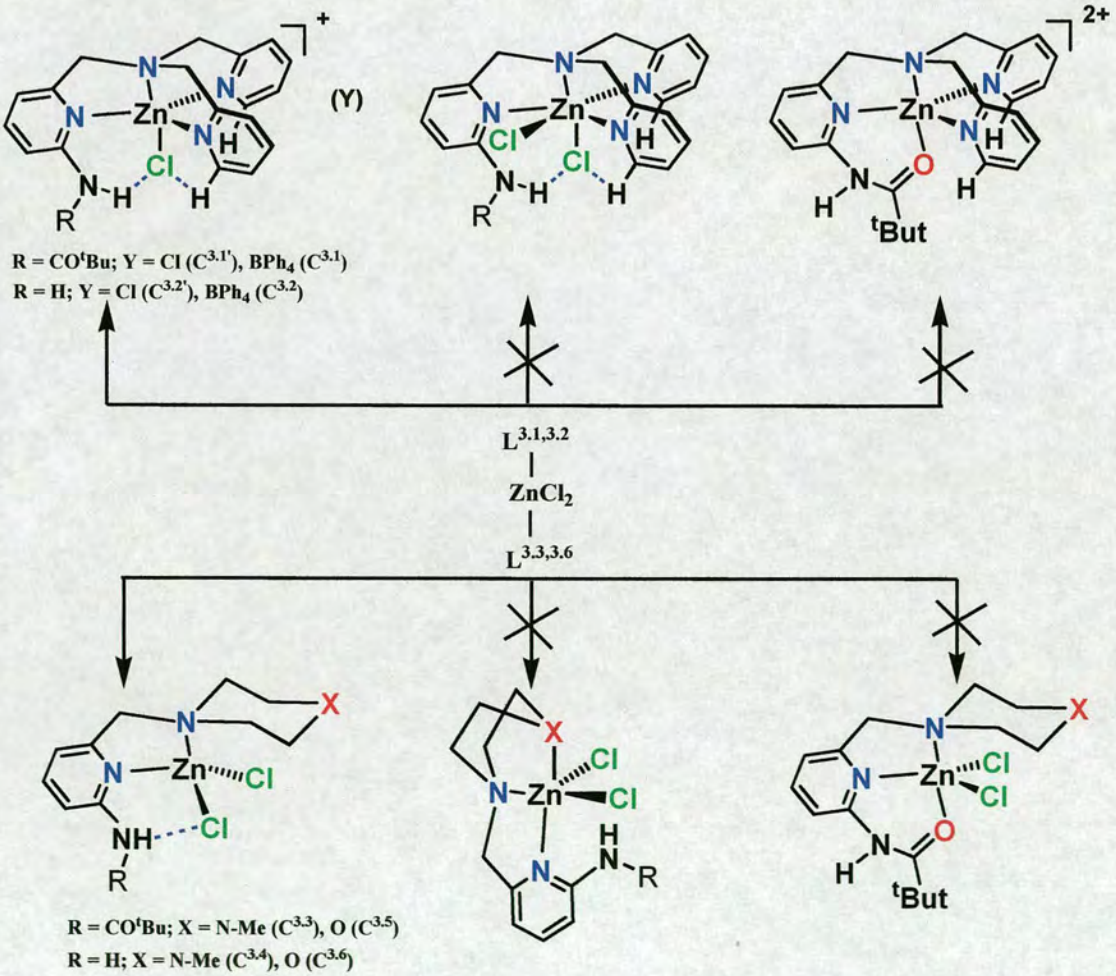

Scheme 3.3

This result suggests that, in the presence of Cl ligand(s) zinc(II) complexes of $\mathbf{L}^{3.1,3.2}$, the trigonal bipyramidal $[(\mathbf{L}^{3.1,3.2})Zn(Cl)]^+$ cation is preferred over trigonal bipyramidal $[(\mathbf{L}^{3.1,3.2})Zn](Cl)_2$, octahedral $[(\mathbf{L}^{3.1,3.2})Zn(Cl)]^+$ and octahedral $[(\mathbf{L}^{3.1,3.2})Zn(Cl)_2]$ coordination environments. Interestingly, in the $[(\mathbf{L}^{3.3-3.5})Zn(Cl)_2]$ complexes the zinc(II) ion prefers tetrahedral N_2Cl_2 ligation over trigonal bipyramidal N_2Cl_2O and N_3Cl_2 (or N_2OCl_2) coordination environments (Scheme 3.3), despite the fact that chelate effects and the possibility of coordinating an additional group to the zinc(II) centre could be considered sources of stability.

3.2.2 X-Ray Crystallography

Crystal data for $[(\mathbf{L}^{3.3})Zn(Cl)_2]$ $\mathbf{C}^{3.3}\cdot CH_3CN$, $[(\mathbf{L}^{3.4})Zn(Cl)_2]$ $\mathbf{C}^{3.4}$, $[(\mathbf{L}^{3.5})Zn(Cl)_2]$ $\mathbf{C}^{3.5}$ and $[(\mathbf{L}^{3.6})Zn(Cl)_2]$ $\mathbf{C}^{3.6}$, is listed in Table 3.1. Single crystals suitable for X-ray diffraction were grown by slow evaporation of acetonitrile or acetonitrile/water solutions.

Table 3.1 Crystallographic data and structure refinement details for, $\mathbf{C}^{3.3}\cdot CH_3CN$, $\mathbf{C}^{3.4}$, $\mathbf{C}^{3.5}$ and $\mathbf{C}^{3.6}$

	$\mathbf{C}^{3.3}\cdot CH_3CN$	$\mathbf{C}^{3.4}$	$\mathbf{C}^{3.5}$	$\mathbf{C}^{3.6}$
mpirical Formula	$C_{18}H_{29}Cl_2N_5OZn$	$C_{11}H_{18}Cl_2N_4Zn$	$C_{15}H_{23}Cl_2N_3O_2Zn$	$C_{10}H_{15}Cl_2N_3OZn$
ormula	467.73	342.56	413.63	329.52
K	150(2)	150(2)	150(2)	150(2)
rystal system	Triclinic	Orthorhombic	Orthorhombic	Monoclinic
pace group	$P\bar{1}$	$P2_12_12_1$	$Pbca$	$P2_1/n$
rystal size/mm	0.81×0.76×0.20	0.54×0.32×0.20	0.35 × 0.21× 0.14	0.6×0.17 ×0.13
Å	7.9950(13)	9.0138(7)	10.9906(7)	7.3993(4)
Å	10.2286(16)	11.1924(9)	16.3898(10)	10.5846(6)
Å	14.220(3)	14.6243(11)	20.4387(12)	17.0626(10)
/°	101.773(2)	90	90	90
/°	100.503(2)	90	90	96.1520(10)
°	92.944(2)	90	90	90
Å^3	1114.6(3)	1475.4(2)	3681.7(4)	1328.62(13)
	2	4	8	4
/g cm^{-3}	1.394	1.542	1.492	1.647
mm^{-1}	1.359	2.015	1.635	2.237
eflections	9678, 5113	9124, 3556	22085, 4586	8041, 3169
easured, unique				
nt	0.0229	0.0284	0.0499	0.02
$(F)^a$	0.0363	0.0246	0.0691	0.0283
$R_2(F^2)^a$ (all data)	0.0874	0.0554	0.1183	0.0664
$F^2)^a$ (all data)	1.057	1.024	1.218	1.062
rgest difference	0.745, –0.334	0.382, –0.355	0.585, –0.561	0.372, –0.301
ak, hole/e Å^3				

$^a R_1(F) = \Sigma(||F_o| - |F_c||)/\Sigma(|F_o|$; $wR_2(F^2) = [\Sigma w(F_o^2 - F_c^2)^2/\Sigma wF_o^4]^{1/2}$; $S(F^2) = [\Sigma w\,(F_o^2 - F_c^2)^2/(n-p)]^{1/2}$.

3.2.2.1 Structures of $[(L^{3.3})Zn(Cl)_2]$ $C^{3.3}\cdot CH_3CN$ and $[(L^{3.5})Zn(Cl)_2)]$ $C^{3.5}$

Thermal ellipsoid plots for $C^{3.3}$ and $C^{3.5}$ are shown in Fig. 3.5 and selected distances and angles are given in Table 3.2.

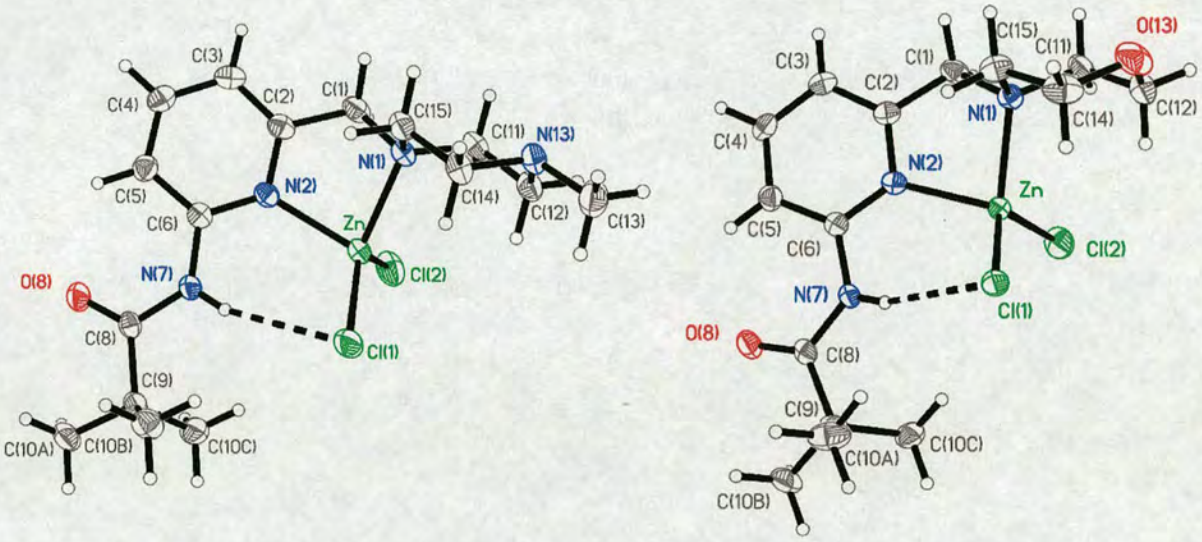

Fig. 3.5 Thermal ellipsoid plot drawn with 50% probability ellipsoids of the molecular structure of $[(L^{3.3})Zn(Cl)_2]$ $C^{3.3}$ (left) and $[(L^{3.5})Zn(Cl)_2]$ $C^{3.5}$ (right).

Table 3.2 Selected bond lengths (Å) and angles (°) for zinc(II) complexes $C^{3.3}\cdot CH_3CN$ and $C^{3.4-3.6}$

	$C^{3.3}\cdot CH_3CN$	$C^{3.4}$	$C^{3.5}$	$C^{3.6}$
Zn–Cl(1)	2.2016(6)	2.2122(5)	2.2338(9)	2.2053(5)
Zn–Cl(2)	2.2238(6)	2.2311(5)	2.1924(9)	2.2066(5)
Zn–N(1)	2.0830(14)	2.0854(16)	2.071(3)	2.1018(14)
Zn–N(2)	2.0823(14)	2.0450(15)	2.091(3)	2.0403(14)
N(2)–Zn–N(1)	82.90(6)	83.55(6)	83.06(10)	82.90(5)
N(2)–Zn–Cl(1)	108.21(4)	108.51(5)	103.22(7)	113.71(4)
N(1)–Zn–Cl(1)	125.43(4)	124.96(4)	118.62(8)	118.44(4)
N(2)–Zn–Cl(2)	109.86(4)	116.60(5)	117.82(7)	112.32(4)
N(1) –Zn–Cl(2)	104.00(4)	106.93(4)	111.12(8)	107.03(4)
Cl(1) –Zn–Cl(2)	119.91(3)	113.40(2)	117.93(4)	117.473(19)

In both compounds the zinc(II) centre is in a tetrahedral N_2Cl_2 environment. The position of the amide group in $\mathbf{C}^{3.3}\cdot CH_3CN$ and $\mathbf{C}^{3.5}$ is such that allows the N–H group to form internal N–H···Cl hydrogen bonds (N(7)···Cl(1) 3.3580(15) Å; H(7N)···Cl(1) 2.38 Å; N(7)–H(7N)···Cl(1) 162.1° for $\mathbf{C}^{3.3}\cdot CH_3CN$ and N(7)···Cl(1) 3.277(3) Å; H(7N)···Cl(1) 2.30 Å; N(7)–H(7N) ···Cl(1) 161.6° for $\mathbf{C}^{3.5}$). The small angle between the pyridine (N2C2C3C4C5C6) and amide planes (N7C8O8), 16.2° for $\mathbf{3}\cdot CH_3CN$ and 15.2° for $\mathbf{C}^{3.5}$, seems optimum for the interaction of the amide oxygen (O8) with the hydrogen in the adjacent position of the pyridine ring (H(5A)) (C(5)O(8) 2.823(2) Å; H(5A)···O(8) 2.25 Å; C(5)–H(5A)···O(8) 117.8° for $\mathbf{C}^{3.3}\cdot CH_3CN$ C(5)···O(8) 2.842(4) Å; H(5A)···O(8) 2.27 Å; C(5)–H(5A)···O(8) 118.2° for $\mathbf{C}^{3.5}$).

The chloride in $\mathbf{C}^{3.3}$ and $\mathbf{C}^{3.5}$ is therefore positioned so that the amide plane can be oriented simultaneously to optimise N–H···Cl–Zn and C–H···OC interactions. In contrast, in the trigonal bipyramidal complex $\mathbf{C}^{3.1}$ the angle between amide and pyridine planes is 31.5°, which presumably optimises the N–H···Cl–Zn hydrogen bonding at expense of weakening the C–H···OC interaction. Internal N–H···Cl–Zn hydrogen bonding in the tetrahedral zinc(II) complexes $\mathbf{C}^{3.3}$ and $\mathbf{C}^{3.5}$, however, is significantly longer (weaker) than in $\mathbf{C}^{3.1}\cdot CH_3CN$. Rozenberg *et al.* proposed a useful equation (Eq. 1) to determine hydrogen bond energies from the D-H···A distance of hydrogen bond interactions found in X-ray crystal structures.[20]

$$-\Delta H = 0.134(\boldsymbol{r})^{-3.05} \qquad (1)$$

This equation, where $-\Delta H$ is in kJ·mol^{-1} and r is the D-H···A distance in nm, is based on empirical data and allows to estimate crystal hydrogen bond energies. Hence, by substituting the appropriate distances in Eq. 1, the H-bond energies can be approximately quantified and compared. The internal N–H···Cl–Zn hydrogen bonding distances (Table 3.3) for $\mathbf{C}^{3.1}$, $\mathbf{C}^{3.3}$ and $\mathbf{C}^{3.5}$ are 0.220 nm, 0.238 nm, 0.230 nm, respectively and the corresponding H-bond energies are 13.6 , 10.7 and 11.9 kJ·mol^{-1}.

Table 3.3 Geometric features of internal hydrogen bonding interactions in $\mathbf{C}^{3.1}\cdot CH_3CN$, $\mathbf{C}^{3.2}\cdot 0.5CH_3CN$, $\mathbf{C}^{3.3}\cdot CH_3CN$, $\mathbf{C}^{3.4}$, $\mathbf{C}^{3.5}$ and $\mathbf{C}^{3.6}$.

	Interaction	N–H[a]/Å	N···Cl/Å	H···Cl/Å	N–H···Cl/°	Ref.
Trigonal bipyramidal						
$\mathbf{C}^{3.1}\cdot CH_3CN$	N(7) –H(7N)···Cl	1.01[a]	3.2127(19)	2.22	167.7	19
$\mathbf{C}^{3.2}\cdot 0.5CH_3C$	N(7) –H(7NA)···Cl	1.01	3.213(3)	2.24	160.4	21
Tetrahedral						
$\mathbf{C}^{3.3}\cdot CH_3CN$	N(7)–H(7N)···Cl(1)	1.01[a]	3.3580(15)	2.38	162.1	21
$\mathbf{C}^{3.4}$	N(7)–H(7NA)···Cl(1)	1.01[a]	3.402(2)	2.44	158.3	21
$\mathbf{C}^{3.5}$	N(7)–H(7N)···Cl(1)	1.01[a]	3.277(3)	2.30	161.6	21
$\mathbf{C}^{3.6}$	N(7)–H(7NA)···Cl(1)	1.01[a]	3.6342(18)	2.71	152.6	21

[a]Extended distance.

3.2.2.2 Structures of $[(L^{3.4})Zn(Cl)_2]$ $C^{3.4}$ and $[(L^{3.6})Zn(Cl)_2)]$ $C^{3.6}$

Thermal ellipsoid plots of the molecular structures of $\mathbf{C}^{3.4}$ and $\mathbf{C}^{3.6}$ are shown in Fig. 3.6 and a list with selected distances and angles is given in Table 3.3. As in $\mathbf{C}^{3.3}$ and $\mathbf{C}^{3.5}$, the zinc(II) centre is in a N_2Cl_2 tetrahedral environment. The Zn–N_{py} distances in $\mathbf{C}^{3.4}$ and $\mathbf{C}^{3.6}$ are slightly shorter than in $\mathbf{C}^{3.3}\cdot CH_3CN$ and $\mathbf{C}^{3.5}$ presumably reflecting the electron donating and electron withdrawing nature of the amine and amide units, respectively.

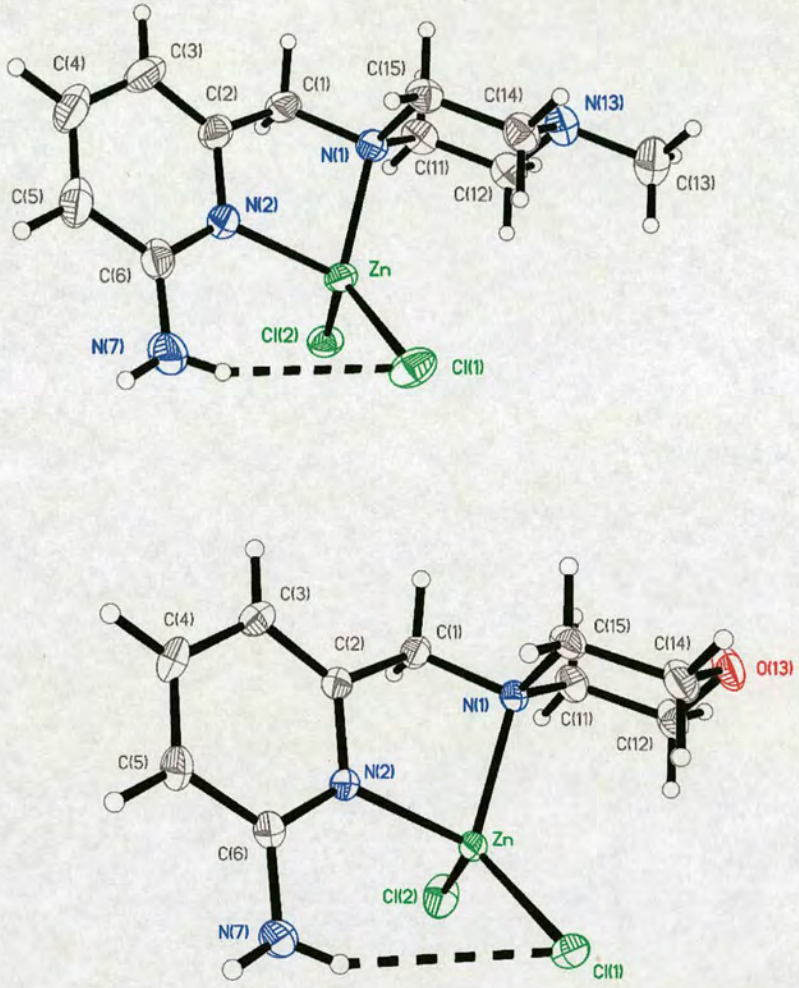

Fig. 3.6 Thermal ellipsoid plot drawn with 50% probability thermal ellipsoids of the molecular structure of $[(\mathbf{L}^{3.4})Zn(Cl)_2]$ $\mathbf{C}^{3.4}$ (*top*) and $[(\mathbf{L}^{3.6})Zn(Cl)_2]$ $\mathbf{C}^{3.6}$ (*bottom*).

The amine N–H groups are involved in internal (intramolecular) and external (intermolecular) hydrogen bonding to chloride ligands (Fig. 3.7). Internal N–H···Cl hydrogen bonding in $\mathbf{C}^{3.4}$ is only slightly longer than in $\mathbf{C}^{3.3}\cdot CH_3CN$ even though the latter contains a substantially stronger hydrogen bond donor, and significantly shorter than in $\mathbf{C}^{3.6}$. The internal N–H···Cl–Zn hydrogen bonding energies have been estimated using Eq. 1 and distances reported in Table 3.3 and they are 9.90 and 7.10 $kJ\cdot mol^{-1}$ for $\mathbf{C}^{3.4}$ and $\mathbf{C}^{3.6}$ respectively.

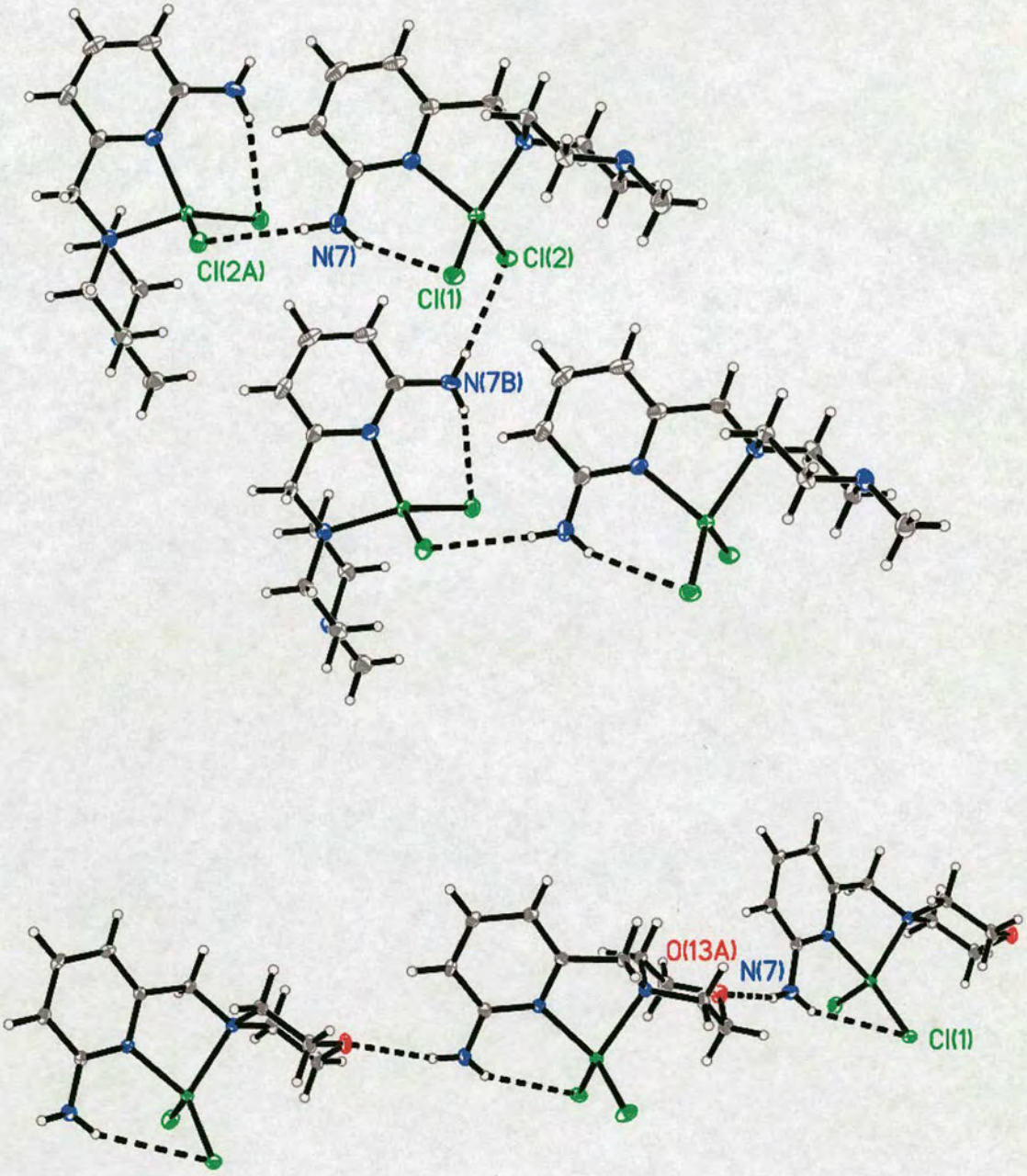

Fig. 3.7 Thermal ellipsoid plots drawn with 30% probability ellipsoids showing the involvement of the external amine NH of $\mathbf{C}^{3.4}$ in intermolecular N–H···Cl hydrogen bonding (top) and $\mathbf{C}^{3.6}$ in intermolecular N–H···O hydrogen bonding (bottom).

The external N–H of $\mathbf{C}^{3.4}$ is involved in intermolecular N–H···Cl(2)–Zn hydrogen bonding (N(7)···Cl(2) 3.34 Å; H(7NB)···Cl(2) 2.35 Å; N(7)–H(7NB)···Cl(2) 169°), in $\mathbf{C}^{3.6}$, it forms

an intermolecular N–H···O(13) hydrogen bond (N(7)···O(13) 3.01 Å; H(7NB)···O(13) 2.02 Å; N(7)–H(7NB)···O(13) 164°). The different preference of the external N–H for intermolecular hydrogen bonding may be partly due to the different steric effects of the N(13)–CH_3 ($\mathbf{C}^{3.4}$) and O(13) ($\mathbf{C}^{3.6}$) and could affect the strength of the internal N–H···Cl–Zn hydrogen bonds in the solid state.

3.2.2.3 Comparison of Structures ($C^{3.1\text{-}3.6}$)

Trigonal bipyramidal N_4ClZn structures have slightly longer Zn–$N_{py'}$ distances (py' = pyridine carrying the N–H hydrogen bond donor), ca. 2.07 Å in $\mathbf{C}^{3.2}$ and 2.13 Å in $\mathbf{C}^{3.1}$, than the tetrahedral N_2Cl_2Zn structures $\mathbf{C}^{3.3\text{-}3.6}$ (2.04–2.08 Å). In principle this structural feature should favour a slightly shorter (stronger) internal N–H···Cl–Zn hydrogen bond in $\mathbf{C}^{3.3\text{-}3.6}$, as it would bring the hydrogen bond donor and acceptor closer. In addition, the zinc(II) centre in $\mathbf{C}^{3.3\text{-}3.6}$ should be more strongly Lewis acidic than in $\mathbf{C}^{3.1}$, $\mathbf{C}^{3.2}$ as a result of having a lower coordination number, a feature which would make the N–H groups stronger hydrogen bond donors. This study shows that internal hydrogen bonding is stronger in the trigonal bipyramidal zinc(II) complexes $\mathbf{C}^{3.1}$ and $\mathbf{C}^{3.2}$ than in the tetrahedral $\mathbf{C}^{3.3\text{-}3.6}$. In idealised tetrahedral and trigonal bipyramidal geometries the Cl$ZnN_{py'}$ angle would be around 109° and 90°, respectively. This structural feature would force the N–H groups (hydrogen bond donor) and Cl ligand (hydrogen bond acceptor) to be further apart in tetrahedral ligand environments and could be a priori interpreted as the plausible reason for the observed weaker internal N–H···Cl–Zn hydrogen bonding in the tetrahedral structures. This X-ray crystallographic study, however, shows that the Cl$ZnN_{py'}$ angle in the trigonal bipyramidal complexes $\mathbf{C}^{3.1}$ and $\mathbf{C}^{3.2}$ are in the 106–110° range, compared to

103–114° in the tetrahedral complexes $\mathbf{C}^{3.3\text{-}3.6}$. Thus, the main reason for the stronger internal N–H···Cl–Zn hydrogen bonding in the trigonal bipyramidal structures appears to be in fact the smaller angle between the ZnN(2)C(6)N(7) and ZnN(2)Cl planes (ZnN(2)Cl(1) for $\mathbf{C}^{3.3\text{-}3.6}$), which is 25.1° in $\mathbf{C}^{3.1}$ and 20.6° in $\mathbf{C}^{3.2}$ compared to 34.5° in $\mathbf{C}^{3.3}$, 39.4° in 4, 44.0° in $\mathbf{C}^{3.5}$ and 43.9° in $\mathbf{C}^{3.6}$. This crystallographic analysis also shows that the geometric features of the internal N–H···Cl–Zn hydrogen bond in $\mathbf{C}^{3.1}$ and $\mathbf{C}^{3.2}$ are approximately the same despite amide N–H groups being presumably better hydrogen bond donors. One structural feature that may partly account for this somewhat unexpected result is the shorter $Zn–N_{py'}$ distance of $\mathbf{C}^{3.2}$ compared to $\mathbf{C}^{3.1}$ due to the electron donating and withdrawing effect of the amine pivaloylamido groups on the pyridine ring, respectively. A similar effect was found in the tetrahedral structures of $\mathbf{C}^{3.3}$ and $\mathbf{C}^{3.5}$. This could be a potentially important result in that it implies that even a poor hydrogen bond donor, if brought sufficiently close to the hydrogen bond acceptor as the result of short (strong) metal–ligand binding, should result in a short (strong) internal hydrogen bond to another ligand. Moreover, it could suggest that the same effect (the electron withdrawing nature) that makes the amide a better hydrogen bond donor than an amine, when part of a ligand, can cause it to be further away from the metal-bound hydrogen bond acceptor. Thus, it appears to us that an alternative strategy to induce strong internal hydrogen bonding in coordination complexes could be to attach the hydrogen bonding group to a ligand that induces short metal–ligand distances.

3.2.3 NMR and IR Studies

NMR and IR studies were used to probe the solution structures of $\mathbf{L}^{3.1-3.6}$ and the zinc(II) complexes $\mathbf{C}^{3.1-3.6}$ in acetonitrile and to correlate these with the X-ray crystal structures.

3.2.3.1 6-Pivaloylamido-2-pyridylmethyl Derivatives

The arrangement of the amide group of the metal-free ligands $\mathbf{L}^{3.1}$, $\mathbf{L}^{3.3}$ and $\mathbf{L}^{3.5}$ is such that allows the intramolecular interaction of H5' with the amide oxygen. This deduction is consistent with the X-ray crystal structure of $\mathbf{L}^{3.1}$ and the observed downfield position of the H5 resonance (Fig. 3.8, Table 3.4).[19]

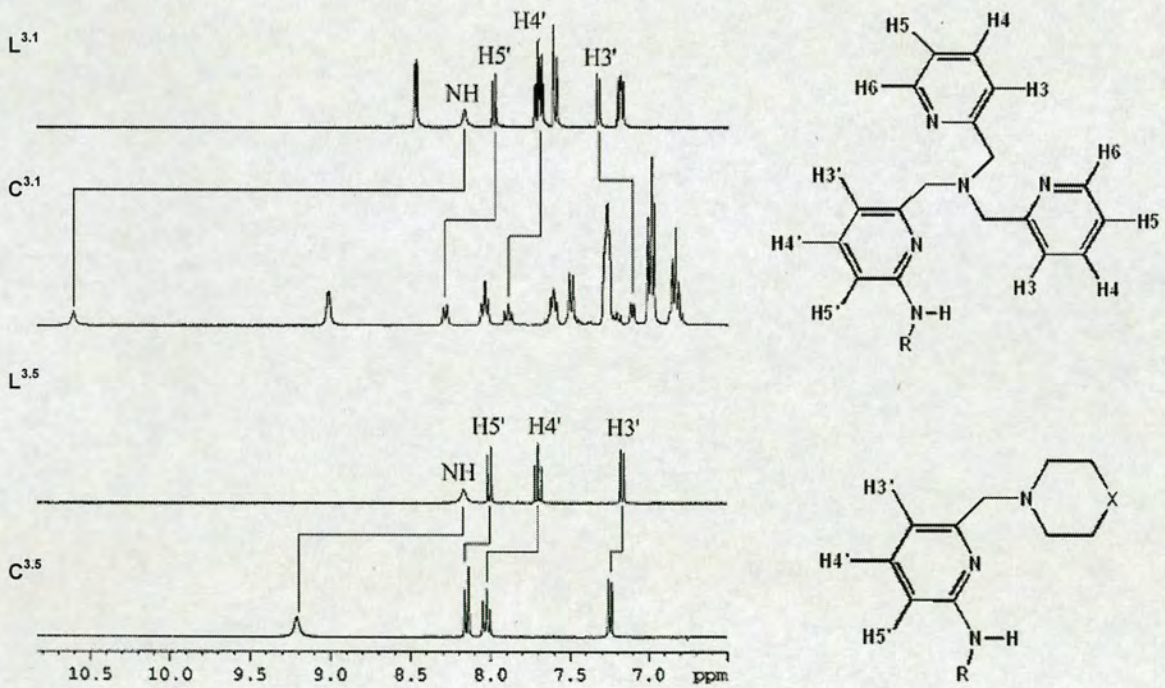

Fig. 3.8 Aromatic and NH region of the ^{1}H NMR (360.1 MHz, CD_3CN, 293 K) of $\mathbf{L}^{3.1}$, $[(\mathbf{L}^{3.1})Zn(Cl)](BPh_4)$ $\mathbf{C}^{3.1}$, $\mathbf{L}^{3.3}$ and $[(\mathbf{L}^{3.3})Zn(Cl)_2]$ $\mathbf{C}^{3.3}$. See Table 2.5 for chemical shift values and Scheme 3.1 for labelling explanation.

Table 3.4 Summary of selected 1H NMR (360 MHz, CD3CN, 293 K) chemical shift data for $\mathbf{L}^{3.3\text{ -}3.6}$ and $\mathbf{C}^{3.3\text{ -}3.6}$

	$\mathbf{L}^{3.3}$, $\mathbf{L}^{3.5}$	$\mathbf{C}^{3.3}$, $\mathbf{C}^{3.5}$	$\mathbf{L}^{3.4}$, $\mathbf{L}^{3.6}$	$\mathbf{C}^{3.4}$, $\mathbf{C}^{3.6}$
^{t}Bu				
H10	1.26, 1.27	1.33 (+0.07), 1.32 (+ 0.05)		
NH				
H7	8.17, 8.17	9.32 (+1.15), 9.21 (+ 1.04)	4.9, 4.8	5.89 (+0.99), 5.87 (+ 1.07)
PyCH_2N				
H1′$_{A,B}$	3.48, 3.49	4.00 (+0.52), 4.00 (+0.51)	3.42, 3.35	3.82 (+0.40), 3.80 (+0.45)
Py (aromatic)				
H3′	7.14,7.17	7.21 (+0.07), 7.24 (+0.07)	6.63, 6.65	6.69 (+0.06), 6.69 (+ 0.04)
H4′	7.69,7.70	8.00 (+0.31), 8.02 (+0.32)	7.37, 7.37	7.61 (+0.24), 7.63 (+0.26)
H5′	7.97, 8.00	8.22 (+0.25), 8.14 (+ 0.14)	6.35, 6.36	6.69 (+0.34), 6.69 (+0.33)

[a] Chemical shifts are in ppm relative to CH_3CN at 1.94 ppm. Values in parentheses denote chemical shifts downfield (positive) or upfield (negative) *versus* values in the corresponding ligand. The symbol ′ refers to the 2-pyridylmethyl with the 6-pivaloylamido or amino group.

In the zinc(II) chloride complexes $\mathbf{C}^{3.1}$, $\mathbf{C}^{3.3}$ and $\mathbf{C}^{3.5}$, proton resonances of 6-pivaloylamido-2-pyridylmethyl unit (py'CH2–) are shifted downfield by 0.2–0.3 ppm relative to the corresponding ligand ($\mathbf{L}^{3.1}$, $\mathbf{L}^{3.3}$ or $\mathbf{L}^{3.5}$), a feature consistent with metal binding (Fig. 3.9, Table 3.5). That the NH proton resonance undergoes significantly more prominent downfield shifts of ca. 1.05–1.15 ppm in the tetrahedral complexes $\mathbf{C}^{3.3}$ and $\mathbf{C}^{3.5}$ and of *ca.* 2.5 ppm in $\mathbf{C}^{3.1}$ provides good evidence that internal N–H···Cl–Zn hydrogen bonding is retained in solution. The same data clearly suggest that these hydrogen bonds are weaker in the tetrahedral complexes $\mathbf{C}^{3.3}$ and $\mathbf{C}^{3.5}$ than in the trigonal bipyramidal complex $\mathbf{C}^{3.1}$, in agreement with the X-ray crystal structures. The strength of the N–H···Cl–Zn hydrogen bonding can be approximately quantified from the positions of the N–H stretching vibration, N–H, using Iogansen's equation (Eq. 2):[22]

$$-\Delta H = 1.3(\Delta \nu)^{1/2} \qquad (2)$$

Where $-\Delta H$ is in kJ·mol^{-1} and $\Delta \nu$ is in cm^{-1}. This equation has been *empirically* determined and it allows to establish the energy of the hydrogen bond ($-\Delta H$) through the shift of the D–H stretching vibration ($\Delta \nu_{D\text{-}H}$), where D represents hydrogen bond donor. This equation has been widely used and it is applicable to shifts larger than 100 cm^{-1}.[23,24] Thus, N–H band of the trigonal bipyramidal complex $\mathbf{C}^{3.1}$ is shifted to lower energy values by 173 ± 4 cm^{-1} relative to $\mathbf{L}^{3.1}$ (Table 3.5), which corresponds to a hydrogen bond energy of 16.8 ± 0.6 kJ mol^{-1}. In tetrahedral complexes $\mathbf{C}^{3.3}$ and $\mathbf{C}^{3.5}$ the N–H vibration is weakened by 124 and 110 cm^{-1} relative to in the corresponding ligand, respectively,

which corresponds in this case to hydrogen bond energies of 13.4 and 14.2 ± 0.6 kJ mol^{-1}.

Hence, the strength of internal hydrogen bond energy determined using Iogansen´s equation can be approximately correlated with the values calculated using Rozenberg's equation (Eq. 1) from X-ray crystal structure distances (see 3.2.2.1). However, these values appear to differ slightly (*ca.* 3 kJ·mol^{-1}), which could be due to the inductive effect of the metal. In actual fact, Rozenberg's equation (Eq. 1) has been derived from Iogansen's equation (Eq. 2) and empirical data from organic compounds, as a result the inductive effect of the metal is largely omitted.

Table 3.5 Selected infrared vibrational data of $\mathbf{L}^{3.1,\ 3.3,\ 3.5}$ and $\mathbf{C}^{3.1}$, $\mathbf{C}^{3.3}$ and $\mathbf{C}^{3.5}$ in acetonitrile solution.

	$\nu_{N\text{-}H}$[a]/cm^{-1}
$\mathbf{L}^{3.1}$	3438
$[(\mathbf{L}^{3.1})Zn(Cl)](BPh_4)$ $\mathbf{C}^{3.1}$	3264
(difference)	(+174)
$\mathbf{L}^{3.3}$	3439
$[(\mathbf{L}^{3.3})Zn(Cl)_2]$ $\mathbf{C}^{3.3}$	3315
(difference)	(+124)
$\mathbf{L}^{3.5}$	3440
$[(\mathbf{L}^{3.5})Zn(Cl)_2]$ $\mathbf{C}^{3.5}$	3330.0
(difference)	(+110)

[a] Â±4 cm^{-1}

3.2.3.2 6-Amino-2-pyridylmethyl Derivatives

In the tetrahedral complexes $\mathbf{C}^{3.4}$ and $\mathbf{C}^{3.6}$ the NH_2 protons appear as a broad singlet at 5.9 ppm compared to 4.9 ppm in $\mathbf{L}^{3.4}$ and 4.8 ppm in $\mathbf{L}^{3.6}$ (Fig. 3.10, Table 3.5). The fact that the downfield shifts of the amine protons are very similar for $\mathbf{C}^{3.4}$ and $\mathbf{C}^{3.6}$ and to the chemical shift changes experienced by the amide NH proton of $\mathbf{C}^{3.3}$ relative to $\mathbf{L}^{3.3}$ (1.15 ppm) and of $\mathbf{C}^{5}$ relative to $\mathbf{L}^{3.5}$ (1.04 ppm) can be taken as indicative that internal N–H···Cl–Zn hydrogen bonding in $\mathbf{C}^{3.3\text{ - }3.6}$ is of similar strength, in good agreement with the X-ray crystal structures of $\mathbf{C}^{3.3}$, $\mathbf{C}^{3.4}$ and $\mathbf{C}^{3.5}$. This result also suggests that the longer internal N–H···Cl–Zn hydrogen bond in the crystal structure of $\mathbf{C}^{3.6}$ may be due to close packing effects. The larger downfield shift experienced by the amine proton resonance of $\mathbf{C}^{3.2}$ or $\mathbf{C}^{3.2'}$ relative to $\mathbf{L}^{3.2}$ of ca. 2.2 ppm in solution is consistent also with internal hydrogen bonding in the tetrahedral complexes $\mathbf{C}^{3.4}$ and $\mathbf{C}^{3.6}$ being weaker than in the trigonal bypiramidal complex $\mathbf{C}^{3.2}$ as implied by the X-ray crystal structures.

3.3 Conclusion

This study has explored the use N–H groups of the ligand unit (6-X-2-pyridylmethyl)amine (X = NHCOR or NH_2) as a strategy to induce internal hydrogen bonding to an adjacent metal-bound ligand in different coordination geometries. Three ligands with a pivaloylamido group, $\mathbf{L}^{3.1,\ 3.3,\ 3.5}$ and three ligands with an amino group, $\mathbf{L}^{3.2,\ 3.4,\ 3.6}$ were examined in this study. Ligands with the pivaloylamido group form zinc(II) complexes $\mathbf{C}^{3.1}$, $\mathbf{C}^{3.3}$ and $\mathbf{C}^{3.5}$ with internal N–H···Cl–Zn hydrogen bonding. Ligands with the amino group also form zinc(II) complexes $\mathbf{C}^{3.2}$, $\mathbf{C}^{3.2'}$, $\mathbf{C}^{3.4}$ and $\mathbf{C}^{3.6}$ with internal H···Cl–Zn hydrogen bonding and a variety of external hydrogen bonding. The X-

ray crystal structures of a trigonal bipyramidal zinc(II) complexes with N_4Cl coordination environment, $\mathbf{C}^{3.1}$,[19] $\mathbf{C}^{3.2}$, and four tetrahedral (N_2Cl_2), $\mathbf{C}^{3.3-3.6}$, were compared.[21] These five X-ray crystal structures together show that the geometry of the internal N–H···Cl–Zn hydrogen bond is relatively insensitive to the nature of the hydrogen bond donor. These structures show also that internal N–H···Cl–Zn hydrogen bonding is significantly shorter (stronger) in the trigonal bipyramidal complexes. We propose that a variety of structural parameters determine the geometry of the internal N–H···Cl–Zn hydrogen bond, including the Zn–$N_{py'}$ distance and the angle between the plane containing the hydrogen bond donor and Zn–Cl vector of the hydrogen bond acceptor. Thus, metal–ligand effects and geometry are clear examples of the inorganic factors that affect the strength of hydrogen bonding interactions involving coordination complexes. The main objective of this study was to correlate the information extracted from X-ray studies with structural and spectroscopic studies in solution. Thus, the studies reported herein provide very good evidence that the structural features found in the solid state structures, are retained in solution and are clearly expressed in the ^{1}H, ^{13}C NMR and IR spectra of these compounds. This study also provides an upper limit of the strength of the internal N–H··· Cl–Zn hydrogen bonding in acetonitrile solution using IR, which is 13–14 kJ mol^{-1} in the tetrahedral complexes ($\mathbf{C}^{3.3-3.6}$) , lower than the trigonal bipyramidal complexes $\mathbf{C}^{3.1}$, $\mathbf{C}^{3.2}$ and $\mathbf{C}^{3.2'}$ (16–17 kJ mol^{-1}). The magnitude of changes in the ^{1}H NMR spectra of $\mathbf{C}^{3.1-3.6}$ can be correlated with the strength of the hydrogen bond in acetonitrile solutions and corroborates the conclusions derived from the X-ray crystallographic studies.

There is considerable current interest in elucidating the role(s) of second-sphere hydrogen bonding to metal-bound species in metallohydrolases, oxidases and peroxidases using small-molecule models.[6f-k] This important chemistry requires metal centres such as Zn(II), Cu(I/II) and Fe(II/III). Based on this work it is reasonable to suggest that strong internal hydrogen bonding in models of these metalloenzymes could be effectively pursued with ligands that induce short metal–L distances (L = ligand carrying the hydrogen bonding group).

In addition, this work shows that hydrogen bonding in tetrahedral complexes, which is the most common geometry in metallohydrolases, can be weaker than in trigonal bipyrimidal complexes.

3.4 Experimental

3.4.1 General

Reagents were obtained from commercial sources and used as received unless otherwise noted. Solvents were dried and purified under N_2 by using standard methods[12] and were distilled immediately before use. All compounds were prepared under N_2 unless otherwise mentioned. The NMR spectra were obtained using a Bruker ARX 250 or Bruker DPX 360 at 20 °C in CD_3CN unless otherwise noted. ^{13}C and ^1H chemical shifts are referenced with respect to the carbon (δ_C 1.32 and 118.26 ppm) and residual proton (δ_H 1.94 ppm) solvent peaks. Peak assignments are done with the aid of 2-D NMR spectroscopy. Sample concentrations for the NMR studies were 1.4–28 mM. Mass spectra were performed on a micromass Platform II system operating in Flow Injection Analysis mode with the electrospray method. Elemental analyses were carried out by the microanalyses service provided by the School of Chemistry at the University of Edinburgh. Infrared spectra were recorded with a JASCO FTIR-410 spectrometer between 4000 and 250 cm^{-1} as KBr pellets (solid state) or as acetonitrile solutions in KBr cells. The strength of N–H···Cl–Zn hydrogen bonding was estimated using solid-state and solution FTIR studies applying Iogansen's equation[9a] and/or variable temperature NMR coalescence methods.[9b] The variable temperature ^1H NMR studies were repeated twice on freshly prepared samples and gave reproducible results.

3.4.2 Synthesis of Ligands

$L^{3.3}$. *N*-Methylpiperazine (0.23 cm^3, 2 mmol) and Na_2CO_3 (2.12 g, 20 mmol) were dissolved in CH_3CN (~15 cm^3). This solution was then treated with 2-(pivaloylamido)-6-(bromomethyl)pyridine[18] (**$L^{3.0}$**) (0.542 g, 2 mmol) and the resulting mixture was stirred for 24 h at 80 °C. The solution was cooled to room temperature, and then poured in 1 M $NaOH_{(aq)}$ (20 cm^3). The product was extracted with CH_2Cl_2 (3 × 50 cm^3). The combined organic phases were dried over Na_2SO_4, and concentrated under reduced pressure to afford an orange oil. This oil was treated with diethyl ether and the white precipitate removed by filtration. The filtrate was evaporated under vacuum to afford the pure compound (0.389 g, 67%) (Found: C, 65.82; H, 8.91; N, 19.00. Calc. for $C_{16}H_{26}N_4O$: C, 66.17; H, 9.02; N, 19.29%).

^{1}H NMR (CD_3CN, 360.1 MHz): δ_H (ppm) 8.17 (br s, 1H, py′-NH), 7.97 (d, J = 7.9 Hz, 1H, py′-H5), 7.69 (t, J = 7.8 Hz, 1H, py′-H4), 7.14 (d, J = 7.6 Hz, 1H, py′-H3), 3.48 (s, 2H, NCH_2-py′), 2.50–2.30 (m, 8H, $N(CH_2CH_2)_2NCH_3$), 2.12 (s, 3H, NCH_3), 1.26 (s, 9H, $C(CH_3)_3$).^{13}C NMR (CD_3CN, 90.5 MHz): δ_C (ppm) 178.5 (C=O). 159.2 (py′-C2), 152.9 (py′-C6), 140.0 (py′-C3), 120.1 and 113.2 (py′-C4 and py′-C5), 65.4 (NCH_2-py′), 56.9 and 54.7 ($N(CH_2CH_2)_2NCH_3$), 46.9 (NCH_3) 41.0 ($C(CH_3)_3$), 28.1 ($C(CH_3)_3$). ESI-MS (+ ion): Found 291.2 (100%). Calc. 291.22 (100%) for $[(\mathbf{L^{3.3}})H]^+$, and matches theoretical isotope distribution.

$L^{3.4}$. L^3 (8.8 mmol, 2.55 g) was dissolved in 2 M HCl (145 cm^3). The resulting yellow solution was heated at reflux overnight. The solution was allowed to cool to room

temperature, after which, 1 M NaOH was added until ~pH 14. The product was extracted with CH_2Cl_2 (3 × 100 cm^3). The combined organic phases were dried over Na_2SO_4 and dried to dryness under reduced pressure to afford the ligand as a yellow solid (1.36 g, 75%) (Found: C, 63.12; H, 8.51; N, 26.22. Calc. for $C_{11}H_{18}N_4 \cdot 0.2H_2O$: C, 62.95; H, 8.84; N, 26.69%).

^{1}H NMR (CD_3CN, 360.1 MHz): δ_H (ppm) 7.37 (dd, J = 7.9, 7.3 Hz, 1H, py′-H4), 6.63 (d, J = 7.3 Hz, 1H, py′-H3), 6.35 (d, J = 7.9 Hz, 1H, py′-H5), 4.9 (br, 2H, py′-NH_2) 3.42 (s, 2H, NCH_2-py′), 2.41–2.30 (m, 8H, N(CH_2CH_2)$_2$NCH$_3$), 2.17 (s, 3H, NCH_3). ^{13}C NMR (CD_3CN, 90.5 MHz): δ_C (ppm) 159.9 and 158.0 (py′-C2 and py′-C6), 138.6 (py′-C3), 112.9 and 107.2 (py′-C4 and py′-C5), 65.1 (NCH_2-py′), 55.9 and 54.1 (N(CH_2CH_2)$_2$NCH$_3$), 46.3 (NCH_3). ESI-MS (+ ion): Found 207.2 (100%). Calc. 207.16 (100%) for $[(\mathbf{L}^{3.4})H]^+$, and matches theoretical isotope distribution.

$L^{3.5}$. This ligand was prepared in the same way as $\mathbf{L}^{3.3}$ using morpholine (2 mmol, 0.17 cm^3) (0.480 g, 87%) (Found: C, 64.45; H, 8.25; N, 14.77. Calc. for $C_{15}H_{23}N_3O_2$: C, 64.95; H, 8.36; N, 15.15%).

^{1}H NMR (CD_3CN, 360.1 MHz): δ_H (ppm) 8.17 (br s, 1H, py′-NH), 8.00 (d, J = 8.2 Hz, 1H, py′-H5), 7.70 (t, J = 7.6 Hz, 1H, py′-H4), 7.17 (d, J = 7.6 Hz, 1H, py′-H3), 3.49 (s, 2H, NCH_2-py′), 3.62, 2.43 (m, 4H and 4H, N(CH_2CH_2)$_2$O), 1.27 (s, 9H, C(CH_3)$_3$).^{13}C NMR (CD_3CN, 90.5 MHz): δ_C (ppm) 177.9 (C=O). 158.1 and 152.2 (py′-C2 and py′-C6), 139.4 (py′-C3), 119.5 and 112.7 (py′-C4 and py′-C5), 65.1 (NCH_2-py′), 67.4 and 54.5 (N(CH_2CH_2)$_2$O), 40.3 (C(CH_3)$_3$), 27.4 (C(CH_3)$_3$). ESI-MS (+ ion): Found 277.8 (100%), Calc. 278.19 (100%) for $[(\mathbf{L}^{3.5})H]^+$, and matches theoretical isotope distribution.

$L^{3.6}$. This ligand was prepared by acid hydrolysis of **$L^{3.5}$** (0.400 g, 1.44 mmol) in the same way as **$L^{3.4}$** (0.210 g, 75%) (Found: C, 61.78; H, 7.75; N, 21.47. Calc. for $C_{10}H_{15}N_3O$: C, 62.15; H, 7.82; N, 21.74%).

^{1}H NMR (CD_3CN, 360.1 MHz): δ_H (ppm) 7.37 (t, J = 7.6 Hz, 1H, py′-H4), 6.65 (d, J = 7.6 Hz, 1H, py′-H3), 6.36 (d, J = 7.9 Hz, 1H, py′-H5), 4.8 (br, 2H, py′-NH_2), 3.35 (s, 2H, NCH_2-py′), 3.61 and 2.41 (m, 4H and 4H, N(CH_2CH_2)$_2$O). ^{13}C NMR (CD_3CN, 90.5 MHz): δ_C (ppm) 159.9 and 157.5 (py′-C2 and py′-C6), 138.6 (py′-C3), 112.9 and 107.2 (py′-C4 and py′-C5), 65.5 (NCH_2-py′), 67.5 and 54.6 (N(CH_2CH_2)$_2$O). ESI-MS (+ ion). Found 194.0 (100%), Calc. 194.13 (100%) for [(**$L^{3.6}$**)H]$^+$, and matches theoretical isotope distribution.

3.4.3 Synthesis of Zinc(II) Complexes

[($L^{3.3}$)Zn($Cl)_2$] $C^{3.3}$. $ZnCl_2$ (55 mg, 0.4 mmol) and **$L^{3.3}$** (116 mg, 0.4 mmol) were dissolved in dry CH_3CN (20 cm^3) and the reaction mixture was stirred at room temperature for 1 h. The solution was then filtered through Celite and the solvent removed under vacuum to afford the pure compound as a yellow solid (yield >90%) (Found: C, 44.14; H, 5.7; N, 12.69. Calc. for $C_{16}H_{26}Cl_2N_4OZn{\cdot}0.5H_2O$: C, 44.11; H, 6.25; N, 12.86%).

^{1}H NMR (CD_3CN, 360.1 MHz): δ_H (ppm) 9.32 (s, 1H, NH), 8.22 (d, J = 8.2 1H, py′-H5), 8.00 (t, J = 7.9 Hz, 1H, py′-H4), 7.21 (d, J = 7.8 Hz, 1H, py′-H3), 4.00 (s, 2H, NCH_2-py′), 3.16 and 2.8–2.60 (m, 2H and 6H, N(CH_2CH_2)$_2$NCH_3), 2.28 (s, 3H, NCH_3),

1.33 (s, 9H, $C(CH_3)_3$).). ^{13}C NMR (CD_3CN, 62.9 MHz, 298 K): δ_C (ppm) 178.5 (C=O). 152.8 and 152.6 (py'-C2 and py'-C6), 143.7 (py'-C3), 120.1 (py-C4'), 117.3 (py'-C5), 62.2 (NCH_2-py'), 54.7 and 54.0 ($N(CH_2CH_2)_2NCH_3$), 45.5 (NCH_3), 40.9 ($C(CH_3)_3$), 27.3 ($C(CH_3)_3$). ESI-MS (+ ion): Found 389.3 (100%), Calc. 389.11 $\{(\mathbf{L}^{3.3})ZnCl\}^+$. Found 427.3 (100%), Calc. 427.08 $[(\mathbf{L}^{3.3})Zn(Cl)_2]H^+$ (10% intensity relative to $\{(\mathbf{L}^{3.3})ZnCl\}^+$), and matches theoretical isotope distribution.

$[(\mathbf{L}^{3.4})Zn(Cl)_2]$ $\mathbf{C}^{3.4}$. This complex was prepared in the same way as $\mathbf{C}^{3.3}$ using the ligand $\mathbf{L}^{3.4}$ (0.083 g, 0.4 mmol) to afford the pure complex as a yellow solid (yield >90%) (Found: C, 39.57; H, 5.30; N, 16.49. Calc. for $C_{11}H_{18}Cl_2N_4Zn \cdot 0.25CH_3CN$: C, 39.15; H, 5.36; N, 16.87%).

^1H NMR (CD_3CN, 360.1 MHz): δ_H (ppm) 7.61 (t, $J = 7.2$ Hz, 1H, py'-H3), 6.69 (t, $J =$ 7.9 Hz, 2H, py'-H5 and py'-H4), 5.89 (br, 2H, py'-NH_2) 3.82 (s, 2H, NCH_2-py'), 3.10, 2.77 and 2.57–2.47 (m, 2H, 2H and 4H, $N(CH_2CH_2)_2NCH_3$), 2.24 (s, 3H, NCH_3). ^{13}C NMR (CD_3CN, 90.5 MHz): δ_C (ppm) 159.8 (py'-C2), 151. 0 (py'-C6), 142.4 (py'-C3), 112.9 and 111.7 (py'-C4 and py'-C5), 62.6 (NCH_2-py'), 54.7 and 54.3 ($N(CH_2CH_2)_2NCH_3$), 45.8 (NCH_3). ESI-MS (+ ion): Found 305.2 (100%), Calc. 305.05 $\{(\mathbf{L}^{3.4})ZnCl\}^+$. Found 343.2 (100%), Calc. 343.02 $[(\mathbf{L}^{3.4})Zn(Cl)_2]H^+$ (50% intensity relative to $\{(\mathbf{L}^{3.4})ZnCl\}^+$), and matches theoretical isotope distribution.

$[(\mathbf{L}^{3.5})Zn(Cl)_2]$ $\mathbf{C}^{3.5}$. This complex was prepared in the same way as $\mathbf{C}^{3.3}$ using the ligand $\mathbf{L}^{3.5}$ (0.111 g, 0.4 mmol) to afford the pure complex as a white solid (yield >90%)

(Found: C, 43.86; H, 5.60; N, 10.12. Calc. for $C_{15}H_{23}Cl_2N_3OZn$: C, 43.55; H, 5.60; N, 10.16%).

^{1}H NMR (CD_3CN, 360.1 MHz): δ_H (ppm) 9.21 (s, 1H, NH), 8.14 (d, J = 8.6, 1H, py′-H5), 8.02 (t, J = 7.6 Hz, 1H, py′-H4), 7.24 (d, J = 7.5 Hz, 1H, py′-H3), 4.00 (s, 2H, NCH_2-py′), 3.92, 3.10 and 2.66 (m, 4H, 2H and 2H, N(CH_2CH_2)$_2$O), 1.32 (s, 9H, C(CH_3)$_3$). ^{13}C NMR (CD_3CN, 62.9 MHz, 298 K): δ_C (ppm) 178.6 (C=O), 152.5 and 152.4 (py′-C2 and py′-C6), 144.0 (py′-C3), 120.5 and 117.4 (py′-C4 and py′-C5), 63.1 (NCH_2-py′), 66.1 and 55.0 (N(CH_2CH_2)$_2$O), 40.9 (C(CH_3)$_3$), 27.2 (C(CH_3)$_3$). ESI-MS (+ ion): Found 376.2 (100%), Calc. 376.08 {(**L**$^{3.5}$)ZnCl}$^+$, and matches theoretical isotope distribution.

[(L$^{3.6}$)Zn(Cl)$_2$] C$^{3.6}$. This complex was prepared in the same way as **C**$^{3.3}$ using the ligand **L**$^{3.6}$ (0.077 g, 0.4 mmol) to afford the pure complex as a white solid (yield >90%) (Found: C, 36.57; H, 4.52; N, 12.68. Calc. for $C_{10}H_{15}Cl_2N_3OZn$: C, 36.45; H, 4.59; N, 12.75%).

^{1}H NMR (CD_3CN, 360.1 MHz): δ_H (ppm) 7.63 (dd, J = 8.3, 7.2 Hz, 1H, py′-H3), 6.69 (t, J = 7.9 Hz, 2H, py′-H5 and py′-H4), 5.87 (br, 2H, py′-NH_2) 3.80 (s, 2H, NCH_2-py′), 3.94, 3.1 and 2.61 (m, 4H, 2H and 2H, N(CH_2CH_2)$_2$O). ^{13}C NMR (CD_3CN, 90.5 MHz): δ_C (ppm) 159.8 and 151.0 (py′-C2 and py′-C6), 142.5 (py′-C3), 113.1 and 111.8 (py′-C4 and py′-C5), 63.0 (NCH_2-py′), 66.2 and 54.8 (N(CH_2CH_2)$_2$O). ESI-MS (+ ion): Found 291.9 (100%), Calc. 292.02 {(**L**$^{3.6}$)ZnCl}$^+$, and matches theoretical isotope distribution.

3.4.4 X-Ray Crystallography

Crystals suitable for X-ray diffraction studies of $\mathbf{C}^{3.3-3.6}$ were grown by slow evaporation of acetonitrile or acetonitrile–water solutions at room temperature.

Intensity data for $\mathbf{C}^{3.3-3.6}$ were collected at 150 K using a Bruker-AXS SMART APEX area detector diffractometer with graphite-monochromated Mo-Kα radiation (λ = 0.71073 Å). The structures of $\mathbf{C}^{3.3-3.6}$ were solved by direct methods and refined to convergence against F^2 data using the SHELXTL suite of programs. Data were corrected for absorption applying empirical methods using the program SADABS,[25] and the structures were checked for higher symmetry using the program PLATON.[26] All non-hydrogen atoms were refined anisotropically unless otherwise noted. Hydrogen atoms were placed in idealized positions and refined using a riding model with fixed isotropic displacement parameters. The N–H hydrogens were located in the difference map and refined isotropically.

References

[1] G. C. Pimentel and A. L. McClellan, *The hydrogen bond*, Freeman, San Francisco, 1960.

[2] G. A. Jeffrey and W. Saenger, *'Hydrogen Bonding in Biological Structures'*, Springer, 1991.

[3] G. R. Desiraju, *"The weak hydrogen bond: in structural chemistry and biology"*, Oxford University Press, Oxford, 2001.

[4] (*a*) L. Brammer, D. Zhao, F. T. Ladipo and J. Braddock-Wilking, *Acta Crystallogr., Sect B*, 1995, **51**, 632; (*b*) J. C. Mareque Rivas and L. Brammer, *Coord. Chem. Rev.*, 1999, **183**, 43; (*c*) L. M. Epstein and E. S. Shubina, *Coord. Chem. Rev.*, 2002, **231**, 165; (*d*) R. H. Crabtree, E. M. Per Siegbahn, O. Eisenstein, A. L. Rheingold and T. F. A Koetzle, *Acc. Chem. Res.*, 1996, **29**, 348; (*e*) A. J. Lough, S. Park, R. Ramachandran and R. H. Morris, *J. Am. Chem. Soc.*, 1994, **116**, 8356; (*f*) G. Aullon, D. Bellamy, G. A. Orpen, L. Brammer and E. A., *Chem. Commun.*, 1998, 653.

[5] (*a*) J. C. Mareque Rivas and L. Brammer, *Inorg. Chem.*, 1998, **37**, 4756; (*b*) A. L. Gillon, G. R. Lewis, A. G. Orpen, S. Rotter, J. Starbuck, X.-M. Wang, Y. Rodriguez-Martin and C. Ruiz-Perez, *Dalton Trans.*, 2000, 3897; (*c*) L. Brammer, J. K. Swearingen, E. A. Bruton and P. Sherwood, *Proc. Natl. Acad. Sci. USA*, 2002, **99**, 4956.

[6] (*a*) A. J. Canty and G. van Koten, *Acc. Chem. Res.*, 1995, **28**, 406; (*b*) W. N. Lipscomb and N. Straeter, *Chem. Rev.* 1996, **96**, 2375; (*c*) M. Filizola and G. H. Loew, *J. Am. Chem. Soc.*, 2000, **122**, 18; (*d*) B. D. Dunietz, M. D. Beachy, Y. Cao, D. A. Whittington, S. J. Lippard and R. A. Friesner, *J. Am. Chem. Soc.*, 2000, **122**, 2828; (*e*) R. Krämer, *Coord. Chem. Rev.*, 1999, 243; (*f*) D. K. Garner, S. B. Fitch, L. H. McAlexander, L. M.

Bezold, A. M. Arif and L. M. Berreau, *J. Am. Chem. Soc.*, 2002, **124**, 9970; (*g*) M. Wall, B. Linkletter, D. Williams, A.-M. Lebuis, R. C. Hynes and J. Chin, *J. Am. Chem. Soc.*, 1999, **121**, 4710; (*h*) F. Mancin and J. Chin, *J. Am. Chem. Soc.*, 2002, 10496; (*i*) J. Chin, S. Chung and D. H. Kim, *J. Am. Chem. Soc.*, 2002, 10498; (*j*) C. E. MacBeth, A. P. Golombek, V. G. Young, Jr., C. Yang, K. Kuczera, M. P. Hendrich and A. S. Borovik, *Science*, 2000, **289**, 938; (*k*) A. Wada, M. Harata, K. Hasegawa, K. Jitsukawa, H. Masuda, M. Mukai, T. Kitagawa and H. Einaga, *Angew Chem., Int. Ed.*, 1998, **37**, 798.

[7] L. Brammer, J. C. Mareque Rivas, R. Atencio, S. Fang and F. C. Pigge, *Dalton Trans.*, 2000, 3855.

[8] (*a*) I.D. Dance in *Perspectives in Supramolecular Chemistry*: Vol. 2, ed. G. R. Desiraju, Wiley, 1996; (*b*) L. Brammer, *Dalton Trans.*, 2003, 3145.

[9] (*a*) D. W. Christianson and W. N. Lipscomb, *Acc. Chem. Res.*, 1989, **22**, 62; (*b*) H. Kim and W. N. Lipscomb, *Biochemistry*, 1991, **30**, 8171.

[10] X. Iturrioz, R. Rozenfeld, A. Michaud, P. Corvol and C. Llorens-Cortes, *Biochemistry*, 2001, **40**, 14440.

[11] A. D. Pannifer, T. Y. Wong, R. Schwarzenbacher, M. Renatus, C. Petosa, J. Blenkowska, D. B. Lacy, R. J. Collier, S. Park, S. H. Leppla, P. Hanna and R. C. Liddington, *Nature*, 2001, **414**, 229.

[12] U. Baumann, S. Wu, K. M. Flaherty and D. B. McKay, *EMBO J.*, 1993, **12**, 3357.

[13] H. M. Holden, D. E. Tronrud, A. F. Monzingo, L. H. Weaver and B. W. Matthews, *Biochemistry*, 1987, **26**, 8542.

[14] C. J. Boxwell and P. H.Walton, *Chem. Commun.*, 1999, 647.

[15] E. Kövári and R. Krämer, *J. Am. Chem. Soc.*, 1996, 118, 12704.

[16] (*a*) D. K. Garner, R. A. Allred, K. J. Tubbs, A. M. Arif and L. M. Berreau, *Inorg. Chem.*, 2002, **41**, 3533; (*b*) L. M. Berreau, M. M. Makowska-Grzyska and A. M. Arif, *Inorg. Chem.*, 2001, **40**, 2212.

[17] E. Peris, J. C. Lee, Jr., J. R. Rambo, O. Eisenstein and R. H. Crabtree, *J. Am. Chem. Soc.*, 1995, **117**, 3485.

[18] L. M. Berreau, M. M. Makowska-Grzyska and A. M. Arif, *Inorg. Chem.*, 2000, **39**, 4390.

[19] J. C. Mareque Rivas, R. Torres Martín de Rosales and S. Parsons, *Dalton Trans.*, 2003, 2156.

[20] M. Rozenberg, A. Loewenschuss and Y. Marcus, *Phys. Chem. Chem. Phys.*, 2000, **2**, 2699.

[21] J. C. Mareque Rivas, E. Salvagni, R. Torres Martín de Rosales and S. Parsons, *Dalton Trans.*, 2003, 3339.

[22] A. V. Iogansen, G. A. Kurkchi, V. M. Furman, V. P. Glazunov and S. E. Odinokov, *Zhurnal Prikladnoi Spektroskopii*, 1980, **33**, 460.

[23] A. V. Iogansen, *Spectrochim. Acta A*, 1999, **55**, 1585.

[24] See for example: (*a*) E. I. Gutsul, N. V. Belkova, M. S. Sverdlov, L. M. Epstein, E. S. Shubina, V. I. Bakhmutov, T. N. Gribanova, R. M. Minyaev, C. Bianchini, M. Peruzzini and F. Zanobini, *Chem. Eur. J.*, 2003, **9**, 2219-2228; (*b*) S. G. Kazarian, P. A. Hamley and M. Poliakov, *J. Am. Chem. Soc.*, 1993, 115, 9069.

[25] G. M. Sheldrick, *SADABS, Empirical absorption correction program,* University of Göttingen, based upon the method of Blessing, 1995.

[26] A. L. Spek, *Acta Crystallogr., Sect. A*,. 1990, **46**, C43.

Chapter 4

Investigating the effect of hydrogen bonding environments in amide cleavage reactions

4.1 Introduction

As mentioned in previous chapters, peptidases commonly require a zinc(II) ion as essential co-factor for the hydrolysis of peptide bonds, polypeptides and proteins. Several of the ways by which the Lewis acidic zinc(II) ion(s) are believed to promote amide bond cleavage involve co-ordination of the amide oxygen are shown in Scheme 2.1 (chapter 2).

A different way is by providing a nucleophile (OH^-) at neutral pH. Although metal ions can drastically reduce the basicity of a coordinated hydroxide, and in less extent its nucleophilicity, the considerable increase in concentration of the metal-hydroxide species at neutral pH, [M-OH]>>[OH] = 10^{-7}, more than compensate the decrease in nucleophilicity.[1]

In the active site of the enzymes, also the amino-acid residues around the metal centre and not coordinated are thought to play a key role.[2] These residues offer functionalities with hydrogen bonding capabilities within hydrogen bonding distances of the metal bound nucleophilic water and/or carbonyl group of the substrate scissile amide unit. This hydrogen bonding environment, which belongs to the '*microenvironment* or *second coordination sphere*', is a common structural/functional feature of metalloproteases,[3] and could be indicative of the functional importance of these interactions.[4] In fact, the replacement of these amino acid residues by others unable to hydrogen bond to the nucleophilic zinc-bound water molecule can substantially reduce the efficiency with which the substrate is hydrolysed.[5]

4.1.1 Previous Model Studies on Cooperation of H-bonds and Metal Ions

Studies on synthetic metallonucleases showed how H-bonds and metal ions can cooperate towards hydrolysis of phosphodiester bonds.[3b,4,6] Nucleases are enzymes that cleave nucleic acids (DNA, RNA), more specifically they hydrolyse phosphodiester bonds which join nucleosides in DNA and RNA. Phosphodiester bonds are extremely robust and their hydrolysis at neutral pH and 25 °C proceeds very slowly having estimated half lives of 2 million and 100 years for DNA[7] and RNA,[8] respectively. Such great stability to hydrolysis is partly due to the repulsion between the nucleophile and the negatively charged backbone.[3b] Several model systems providing simultaneously a metal centre and H-bond interactions have been investigated and it has been demonstrated that the rate of phosphate cleavage can be significantly increased. Studies on cleavage of phosphate esters have shown that two Cu(II) ions with simultaneous hydrogen bonding to local ammonium groups, $-NMe_2H^+$ (half of the dimer is shown in Fig. 4.1), can bind and remarkably accelerate (4×10^7-fold) the hydrolysis of bis(*p*-nitrophenyl) phosphate (BNPP), substrate commonly used as model for DNA.[9] The excellent reactivity of this dicopper(II) complex was explained in terms of the additional electrostatic activation provided by the N-H···O-P hydrogen bonding.

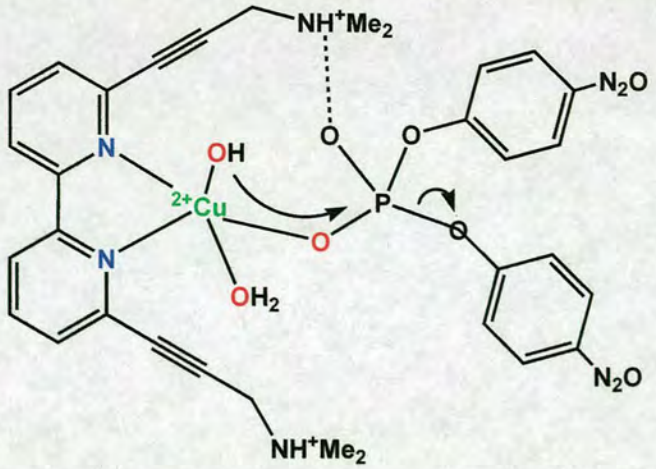

Fig. 4.1 Postulated reaction mechanism for the hydrolysis of BNPP by a Cu(II) complex.

Chin and co-workers[10] proved that an intramolecular hydrogen bonding, due to an amino group of a phenanthroline derivative copper complex (Fig. 4.2), lowers the pK_a of the metal-bound water molecule, and provides notable acceleration (1 x 10^9-fold) for the hydrolysis of 2′,3′-cAMP. The increase in reactivity was attributed to the hydrogen bonds that acidify the metal bound hydroxide thus making it more prone to deprotonation and hence facilitating the expulsion of the leaving group.

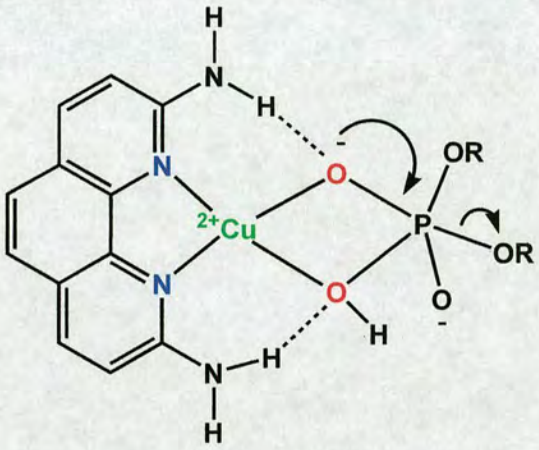

Fig. 4.2 Amino groups acting as H-bond donors increase rate of the hydrolysis of 2′,3′-cAMP.

More recent works have reported that also mononuclear zinc(II) complexes supported by tetradentate tripodal ligands can promote cleavage of phosphodiester bonds promoted. Ligands with a higher number of coordination sites reduce the Lewis activity of the metal ion and generally lead to less active species. On the other hand the higher stability of these complexes allows to work at lower concentrations of metal or ligand. It was demonstrated that hydrogen bonding environments around a zinc-water unit enhance its acidity and contribute with the metal for the activation and cleavage of phosphodiester bonds.[11-14]

As the number of $-NH_2$ functionalities in close proximity of a zinc(II)-bound water molecule increases from 1 to 3, its pK_a is lowered with an overall effect of *ca.* 2 units

(Fig. 4.3).[12] This result was rationalised in terms of intramolecular N-H···O(H)$_n$-Zn H-bond interactions. In this model system amino groups operate as H-bond donors and further stabilise the zinc-hydroxide species, which can act as double H-bond acceptors.

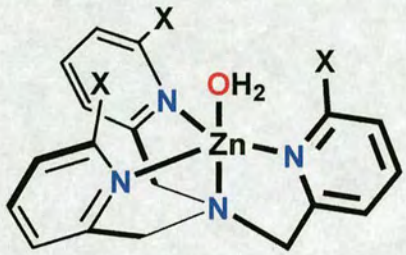

X = H, NH_2

Fig. 4.3 -NH_2 groups around a metal-bound water molecule enhance its acidity and promote catalytic cleavage of phosphodiester bonds.

In addition, when three amino groups are present the zinc-aqua complex proved to enhance the catalytic cleavage of 2-hydroxypropyl 4-nitrophenyl phosphate (substrate model for RNA cleavage) of 750 fold, compared to the relative complex bearing no functional groups (Fig. 4.4).[13] This example represents the most reactive zinc(II) complex reported to date towards cleavage of this specific substrate.

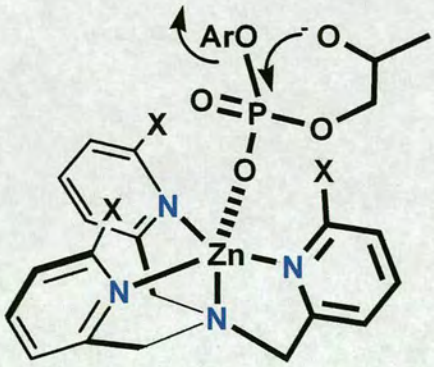

X = H, NH_2
Ar = 4-nitrophenyl

Fig. 4.4 Cleavage of 2-hydroxypropyl 4-nitrophenyl phosphate promoted by the $LZnOH_2$ complex.

Mancin *et al.*[14] observed that zinc(II) complexes with two $-NH_2$ and a nucleophilic hydroxyl group promote a similar effect, although smaller, towards the pK_a of a metal-bound water molecule which was decreased of 0.6-0.7 units going as the number of H-bond functionalities increased (Fig. 4.5). These complexes also accelerate cleavage of BNPP, the products of the reaction for **4** and **5** were *p*-nitrophenol and *O*-phosphorylated ligands.

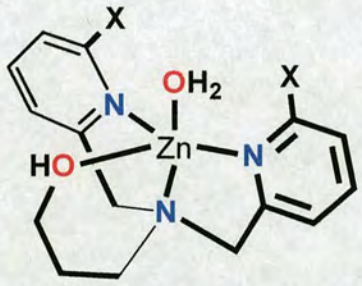

4, X = H

5, X = NH_2

Fig. 4.5 -NH_2 groups enhance acidity of metal-bound water molecule and contribute in substrate activation.

A remarkable result is in the effect of the H-bond donating amino groups that increase the reactivity of the cleavage of 230 fold comparing rate constants of **5** *vs.* **4**. Besides, it was also reported that **5** accelerates cleavage of BNPP with an increase in reactivity of six orders of magnitude when compared to the rate of spontaneous hydrolysis of BNPP at pH 7 and 25 °C. The proposed explanation for this outcome was that the NH_2 groups are suitably positioned to form H-bond interactions with the metal coordinated substrate; hence, cooperating with the metal, they contribute for further activation of the substrate.

All these studies suggest that, in principle, hydrogen bonding residues in cooperation with metal ion co-ordination could also be exploited to achieve more efficient amide bond cleavage by affecting nucleophile, electrophile and/or transition state species. If

so, the incorporation of hydrogen bonding features around metal complexes may lead to the design of more efficient artificial peptide cleaving agents, which is an area of considerable current interest.[15] In addition, activation of carbonyl compounds toward nucleophilic attack by double hydrogen bonding is a common tactic in modern carbonyl chemistry. For instance, in the 1980s Hine *et al.* showed that 1,8-biphenylene diols can be used as a catalyst to activate epoxides towards nucleophilic attack and later on in the 1990s Kelly and coworkers exploited similar catalysts to promote activation of carbonyl group for the Diels-Alder reaction (Scheme 4.1).[16]

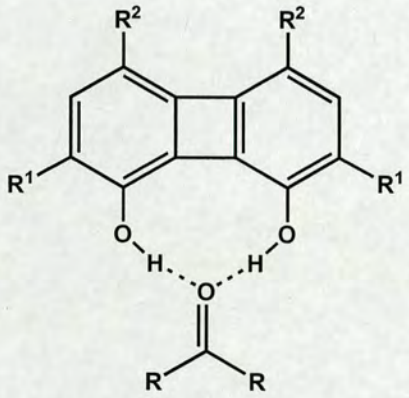

$R^1 = R^2 = H$
Hine biphenylenediol catalyst

$R^1 = n$Pr, $R^2 = NO_2$
Kelly biphenylenediol catalyst

Scheme 4.1 Organic catalysts able to activate a C=O group by double hydrogen bonding.

As an approach to induce intramolecular hydrogen bonding to an amide bond we use the ligand unit (6-pivaloylamido-2-pyridylmethyl)amine. In the previous chapters it has be shown that this unit is suitable to induce intramolecular amide oxygen co-ordination to a zinc(II) ion.[17] This ligand moiety as part of polydentate ligands with and without additional coordinating groups allowed the formation of zinc(II) complexes with different co-ordination environments which underwent amide methanolysis with rates spanning two orders of magnitude.[18]

Strategies to induce hydrogen bonding to a zinc(II)-bound amide oxygen, as well as the effect of the hydrogen bonding environments in the stability of the amide bond are herein examined. The structures and reactivity of zinc(II) complexes with amide oxygen co-ordination in the proximity of hydrogen bonding groups are reported. These studies provide experimental evidence that hydrogen bonding environments can both accelerate and slow down amide bond cleavage reactions at zinc(II) sites.

Importantly, the magnitude of the effects associated with the hydrogen bonding environments, was found to be significant, 800-fold rate difference, and can be similar to those associated with the coordinated ligands. This result highlights the importance of hydrogen bonding environments around metal centres in amide cleavage reactions, which may be relevant to the chemistry of natural metalloproteases and applicable to the design of more efficient artificial protein cleaving agents.

4.2 Results and Discussion

4.2.1 Design and Synthesis

The ligand unit (6-pivaloylamido-2-pyridylmethyl)amine ideally positions an amide oxygen for intramolecular metal co-ordination, a structural-functional feature of metalloproteases. This ligand unit also offers the possibility of investigating the effect of hydrogen bonding environments in amide cleavage reactions at a zinc(II) centre. For this purpose we have followed two different approaches; incorporation of amino hydrogen bond donors as part of the ligand with the (6-pivaloylamido-2-pyridylmethyl)amine unit, and as part of an external chelating ligand. $L^{4.2}$ and $L^{4.3}$ (Scheme 4.2) rigidly pre-organise amino and amide groups perpendicular to the N3 pyridine co-ordination plane, of an overall N4O ligand environment.

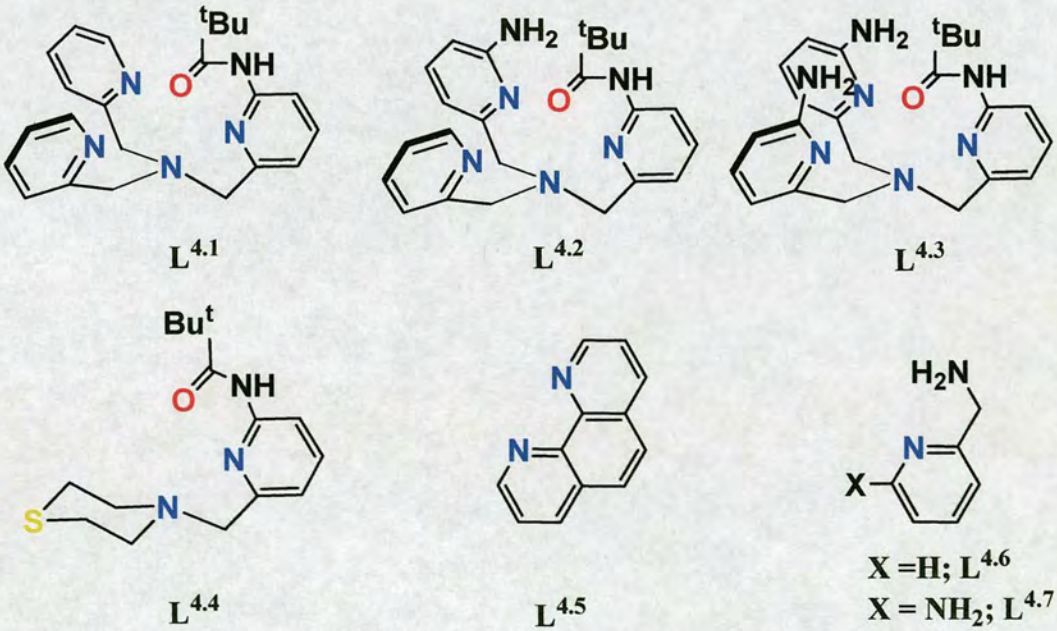

$L^{4.1}$ $L^{4.2}$ $L^{4.3}$

$L^{4.4}$ $L^{4.5}$

Scheme 4.2

The combination of the thiomorpholine based N2O chelating ligand $\mathbf{L}^{4.4}$ and the N2 chelating ligand $\mathbf{L}^{4.7}$ (Scheme 4.2) provides a more flexible N4O ligand environment and the possibility of a different relative arrangement of amino and amide groups. Recently, we reported that the reaction of $[Zn(NCCH_3)_4](PF_6)_2$ or $Zn(ClO_4)_2{\cdot}6H_2O$ in CH_3CN with the tripodal N4 ligand *N*, *N*-bis(2-pyridylmethyl)-*N*-(6-pivaloylamido-2-pyridylmethyl)amine $\mathbf{L}^{4.1}$ (Scheme 4.2) affords the $[(\mathbf{L}^{4.1})Zn]^{2+}$ cation $\mathbf{C}^{4.1}$, in which the zinc(II) centre is in a N4O trigonal bipyramidal co-ordination environment.[17]

In this study we use *N*-(6-amino-2-pyridylmethyl)-*N*, *N*-bis(6-pivaloylamido-2-pyridylmethyl)amine $\mathbf{L}^{4.2}$ and *N*, *N*-bis(6-amino-2-pyridylmethyl)-*N*-(6-pivaloylamido-2-pyridylmethyl)amine $\mathbf{L}^{4.3}$ to form $[(\mathbf{L}^{4.2,\ 4.3})Zn]^{2+}$ cations $\mathbf{C}^{4.2}$, $\mathbf{C}^{4.3}$ in which the amino hydrogen bonding group(s) are along the same axis than the metal-bound amide group. Also recently, we reported that the reaction of equimolar amounts of $Zn(ClO_4)_2{\cdot}6H_2O$ and $\mathbf{L}^{4.4}$ (Scheme 4.2) affords a mononuclear complex that can be viewed as a five coordinate $[(\mathbf{L}^{4.4})Zn(OH_2)(NCCH_3)]^{2+}$ dication in which $\mathbf{L}^{4.4}$ occupies three co-ordination sites, or a six coordinate $[(\mathbf{L}^{4.4})Zn(OH_2)(NCCH_3)]^{2+}$ cation $\mathbf{C}^{4.4}$ with a weakly coordinated perchlorate anion.[18]

Herein, we use chelating N2 ligands without amino hydrogen bonding groups such as 1,10-phenanthroline $\mathbf{L}^{4.5}$ and 2-(aminomethyl)pyridine $\mathbf{L}^{4.6}$ for control experiments and 6-amino-2-(aminomethyl)pyridine $\mathbf{L}^{4.7}$ (Scheme 4.2) as co-ligands of $\mathbf{L}^{4.4}$ around a zinc(II) ion. Perchlorate salts containing $\mathbf{L}^{4.4}$, Zn(II) and $\mathbf{L}^{4.5-\ 4.7}$ in a 1:1:1 ratio were assembled by stirring a mixture containing equimolar amounts of $\mathbf{L}^{4.4}$, $\mathbf{L}^{4.5-\ 4.7}$, and $Zn(ClO_4)_2{\cdot}6H_2O$ in dry CH_3CN.

4.2.2 X-Ray Crystallography

Crystal data for $[(\mathbf{L}^{4.2})Zn](ClO_4)_2 \cdot CH_3CN$ $\mathbf{C}^{4.2} \cdot (ClO_4)_2 \cdot CH_3CN$, $[(\mathbf{L}^{4.3})Zn](ClO_4)_2 \cdot CH_3CN$ $\mathbf{C}^{4.3} \cdot (ClO_4)_2 \cdot CH_3CN$, $[(\mathbf{L}^{4.4})Zn(\mathbf{L}^{4.5})ClO_4](ClO_4) \cdot CH_3CN$ $\mathbf{C}^{4.5} \cdot (ClO_4) \cdot CH_3CN$ and $[(\mathbf{L}^{4.4})Zn(\mathbf{L}^{4.7})](ClO_4)_2$ $\mathbf{C}^{4.7} \cdot (ClO_4)_2$ is listed in Table 4.1. Single crystals suitable for X-ray diffraction were grown by slow evaporation of acetonitrile or acetonitrile/ether solutions.

4.2.2.1 Structures of $\mathbf{C}^{4.2}$ and $\mathbf{C}^{4.3}$

A thermal ellipsoid plot of the molecular structures of $[(\mathbf{L}^{4.2})Zn]^{2+}$ $\mathbf{C}^{4.2}$ and $[(\mathbf{L}^{4.3})Zn]^{2+}$ $\mathbf{C}^{4.3}$ is shown in Fig. 4.6 and a list with selected distances and angles is given in Table 4.2. Like in $\mathbf{C}^{4.1}$,[17] the zinc(II) centre in $\mathbf{C}^{4.2}$ and $\mathbf{C}^{4.3}$ is in a predominantly trigonal bipyramidal co-ordination environment formed by three pyridine nitrogen atoms in the trigonal plane, and the bridgehead nitrogen of the tripodal ligand and amide oxygen in the axial positions.

The degree of trigonality was evaluated by means of the angular structural parameter $\tau = (\beta-\alpha)/60$ introduced by Addison *et al.*,[19] where α and β represent the two largest angles around the central atom with $\beta>\alpha$. A perfect trigonal bipyramidal geometry is associated with $\tau = 1$, while $\tau = 0$ is indicative of a perfect square pyramidal geometry. τ values for $\mathbf{C}^{4.1}$- $\mathbf{C}^{4.3}$ are quite similar; 0.74 ($\mathbf{C}^{4.1}$), 0.77 ($\mathbf{C}^{4.2}$) and 0.71 ($\mathbf{C}^{4.3}$).

The average Zn-N_{py} is 2.039 Å in $\mathbf{C}^{4.2}$ and 2.047 Å in $\mathbf{C}^{4.3}$, compared to 2.036 Å in $\mathbf{C}^{4.1}$, whereas the Zn-$N_{bridgehead}$ distances follow the sequence Zn-N(1) 2.1750(18) Å in $\mathbf{C}^{4.1}$, 2.143(2) Å in $\mathbf{C}^{4.2}$and 2.1218(15) Å in $\mathbf{C}^{4.3}$. The progressive slight shortening of the Zn-N(1) bond is accompanied by a progressive also slight lengthening of the *trans*

Zn-O(8) distance; 2.0005(16) Å in $\mathbf{C}^{4.1}$, 2.0236 (16) Å in $\mathbf{C}^{4.2}$ and 2.0437 (12) Å in $\mathbf{C}^{4.3}$.

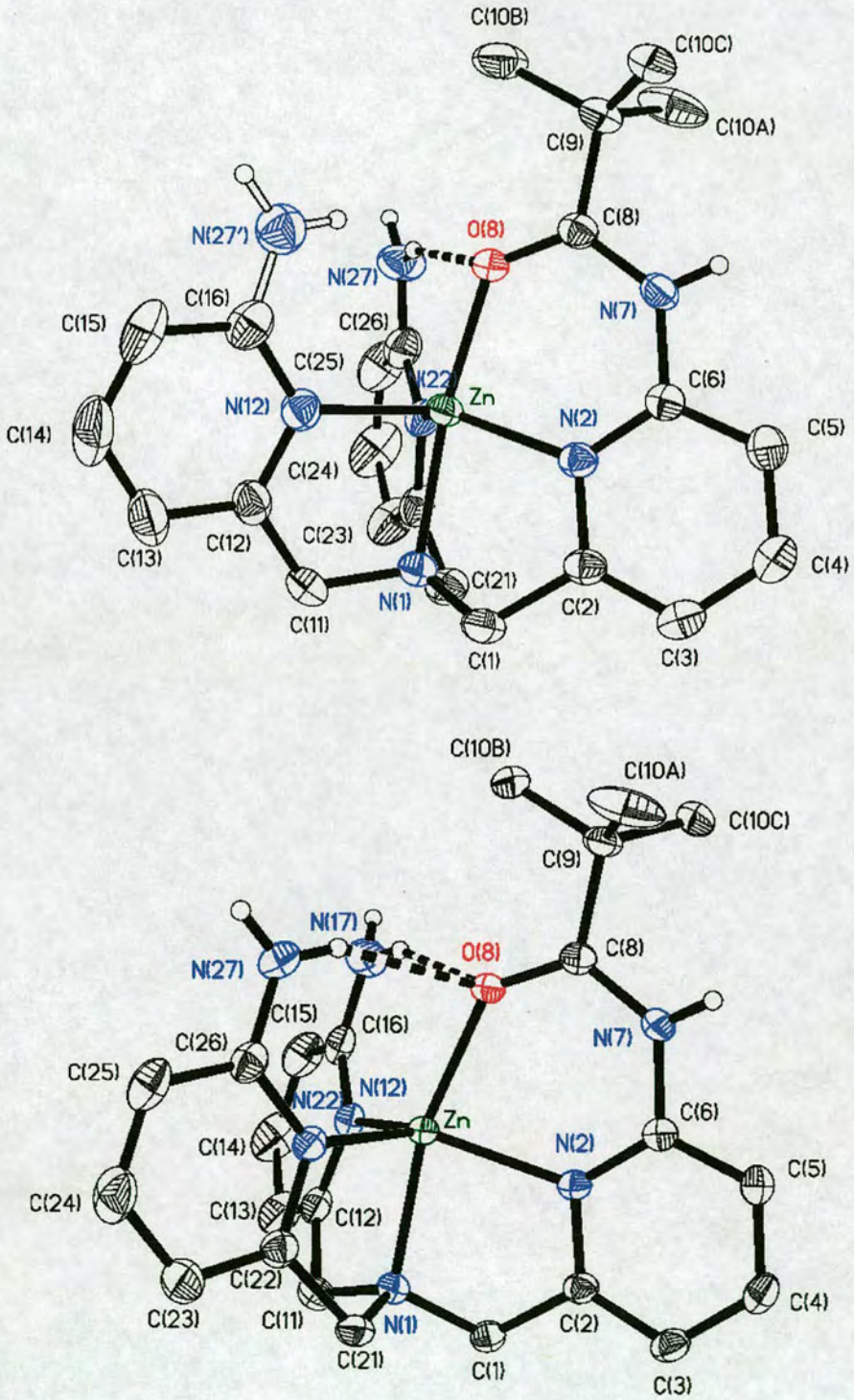

Fig. 4.6 Thermal ellipsoid plot drawn with 50% probability ellipsoids of the molecular structure of $[(\mathbf{L}^{4.2})\mathrm{Zn})]^{2+}$ $\mathbf{C}^{4.2}$ (*top*) showing the N-H···O hydrogen bonding (the NH_2 is disordered over two positions; solid line 77%, empty line 23%), and $[(\mathbf{L}^{4.3})\mathrm{Zn}]^{2+}$ $\mathbf{C}^{4.3}$ (*bottom*) showing double N-H···O hydrogen bonding. C-H hydrogen atoms are omitted for clarity.

Table 4.1 Crystallographic data and structure refinement details for $\mathbf{C}^{4.2}\cdot(ClO_4)_2\cdot CH_3CN$, $\mathbf{C}^{4.3}\cdot(ClO_4)_2\cdot CH_3CN$, $\mathbf{C}^{4.5}\cdot(ClO_4)\cdot CH_3CN$ and $\mathbf{C}^{4.7}\cdot(ClO_4)_2$.

	$\mathbf{C}^{4.2}\cdot(ClO_4)_2\cdot CH_3CN$	$\mathbf{C}^{4.3}\cdot(ClO_4)_2\cdot CH_3CN$	$\mathbf{C}^{4.5}\cdot(ClO_4)\cdot CH_3CN$	$\mathbf{C}^{4.7}\cdot(ClO_4)_2$
Empirical Formula	$C_{25}H_{28}Cl_2N_7O_9Zn$	$C_{25}H_{32}Cl_2N_8O_9Zn$	$C_{29}H_{34}Cl_2N_6O_9SZn$	$C_{21}H_{32}Cl_2N_6O_9SZn$
Formula	709.84	724.86	778.95	680.86
T/K	150(2)	150(2)	150(2)	150(2)
Crystal system	Triclinic	Triclinic	Triclinic	Triclinic
Space group	$P\bar{1}$	$P\bar{1}$	$P\bar{1}$	$P\bar{1}$
Crystal size/mm	0.68x0.62x0.24	0.48x0.22x0.20	0.29x0.18x0.13	0.19x0.18x0.14
A/Å	9.8999(4)	10.0798(2)	10.5300(6)	10.0729(12)
B/Å	11.5861(4)	11.7300(3)	12.0767(7)	10.6189(12)
C/Å	14.3217(5)	14.2630(3)	13.7292(8)	14.2244(16)
α/°	72.330(1)	71.377(1)	88.641(1)	87.826(2)
β/°	75.593(1)	75.058(1)	73.037(1)	85.209(2)
γ/°	86.876(2)	87.706(1)	88.069(1)	69.217(2)
V/Å^3	1515.6(1)	1542.42(6)	1668.83(17)	1417.5(3)
Z	2	2	2	2
D_{calc}/g cm^{-3}	1.555	1.561	1.550	1.595
μ/mm^{-1}	1.049	1.034	1.020	1.188
Reflections measured, unique	14264, 7045	18392, 7310	14951, 7775	10285, 4928
R_{int}	0.0207	0.0282	0.0196	0.0560
$R_1(F)^a$	0.0521	0.0383	0.0495	0.1073
$wR_2(F^2)^a$ (all data)	0.1139	0.0892	0.1152	0.1393
$S(F^2)^a$ (all data)	1.044	1.060	1.046	1.192
Largest difference peak, hole/ e Å^3	0.815,-0.608	0.612, -0.388	1.324, -0.487	0.878, -0.543

[a] $R_1(F) = \Sigma(|F_0| - |F_c|)/\Sigma(|F_0|$; $wR_2(F^2) = [\Sigma w (F_0^2 - F_c^2)^2/\Sigma wF_0^4]^{1/2}$; $S(F^2) = [\Sigma w (F_0^2 - F_c^2)^2/(n-p)]^{1/2}$.

Table 4.2 Selected bond lengths (Å) and angles (°) for zinc(II) complexes $\mathbf{C^{4.1}}$- $\mathbf{C^{4.3}}$.

	$\mathbf{C^{4.1}}$	$\mathbf{C^{4.2}}$	$\mathbf{C^{4.3}}$
Distances			
Zn-N(2)	2.0590(18)	2.057(2)	2.0924(14)
Zn-N(12)	2.0227(19)	2.035(2)	2.0590(15)
Zn-N(22)	2.0272(19)	2.026(2)	2.0399(15)
Zn-N(1)	2.1750(18)	2.143(2)	2.1218(15)
Zn-O(8)	2.0005(16)	2.0236(16)	2.0437(12)
Angles			
N(2)-Zn-N(12)	118.08(8)	122.31(8)	123.33(6)
N(2)-Zn-N(22)	123.53(7)	125.73(8)	124.29(6)
N(12)-Zn-N(22)	110.12(8)	106.50(8)	107.04(6)
N(1)-Zn-N(2)	80.12(7)	82.01(8)	81.32(6)
N(1)-Zn-N(12)	81.09(7)	82.70(8)	83.43(6)
N(1)-Zn-N(22)	80.01(7)	82.13(8)	82.44(6)
N(1)-Zn-O(8)	167.75(6)	168.92(7)	166.46(5)
O(8)-Zn-N(2)	88.59(7)	87.50(7)	85.23(5)
O(8)-Zn-N(12)	108.69(7)	100.10(8)	102.85(6)
O(8)-Zn-N(22)	102.67(7)	107.06(8)	106.67(6)

This structural feature may indicate that the amide oxygen binds somewhat more weakly to the zinc(II) centre of $\mathbf{C^{4.3}}$ than to that of $\mathbf{C^{4.2}}$ and $\mathbf{C^{4.1}}$. Arguably the most important difference between the co-ordination environments of $\mathbf{C^{4.2}}$ and $\mathbf{C^{4.3}}$ compared to $\mathbf{C^{4.1}}$ is N-H···O hydrogen bonding (Fig 4.5, $\mathbf{C^{4.2}}$: 77% site occupancy N(27)···O(8) 2.977(4) Å, H(27A)···O(8) 2.03 Å, N(27)-H(27A)···O(8) 154.6 °, 23% site occupancy N(27')···O(8) 2.82(1) Å, H(27C)···O(8) 1.98 Å, N(27')-H(27C)···O(8) 138.4 °; $\mathbf{C^{4.3}}$: N(17)···O(8) 2.881(2) Å, H(17A)···O(8) 1.93 Å, N(17)-H(17A)···O(8) 156.3 °, N(27)···O(8) 3.047(2) Å, H(27A)···O(8) 2.11 Å, N(27)-H(27A)···O(8) 152.9 °; for N-H distances extended/normalized to 1.01 Å).[20]

Hydrogen bonding to the zinc-bound amide oxygen could explain the slight lengthening of the Zn-O bond and affect the reactivity of the amide group (*vide infra*). Thus, recently we have reported the progressive lengthening of the Zn(II)-Cl bond length by internal N-H···Cl-Zn hydrogen bonding.[21]

4.2.2.2 Structures of $C^{4.5}$ and $C^{4.7}$

Thermal ellipsoid plots of the X-ray structures of the $[(\mathbf{L}^{4.4})Zn(\mathbf{L}^{4.5})ClO_4]^+$ $\mathbf{C}^{4.5}$ and $[(\mathbf{L}^{4.4})Zn(\mathbf{L}^{4.7})]^{2+}$ $\mathbf{C}^{4.7}$ cations are shown in Fig. 4.7 and selected distances and angles are given in Table 4.3.

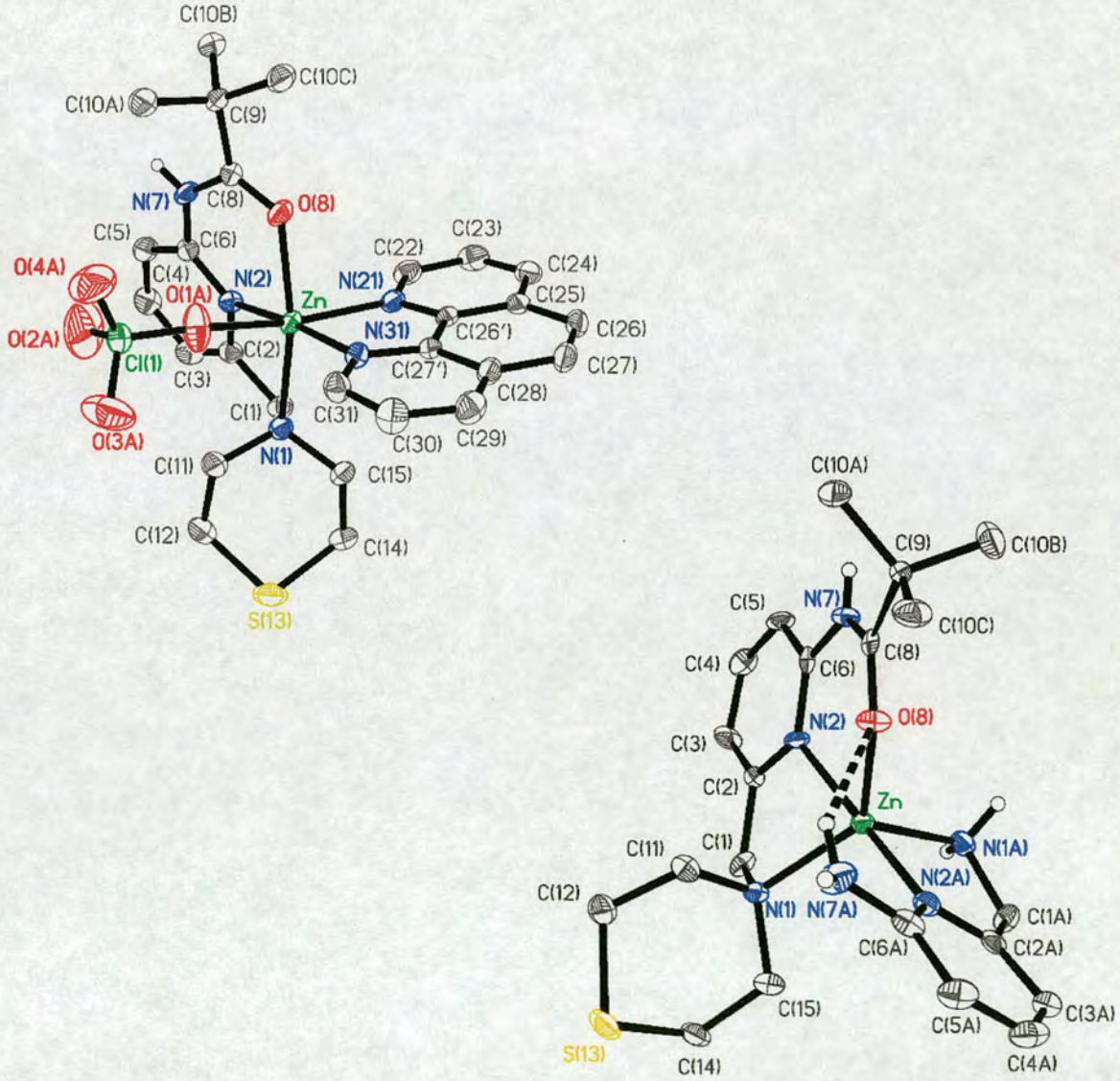

Fig. 4.7 Thermal ellipsoid plot drawn with 50% probability ellipsoids of the molecular structure of $[(\mathbf{L}^{4.4})Zn(\mathbf{L}^{4.5})(ClO_4)]^+$ $\mathbf{C}^{4.5}$ (*top left*) and $[(\mathbf{L}^{4.4})Zn(\mathbf{L}^{4.7})]^{2+}$ $\mathbf{C}^{4.7}$ (*bottom right*) showing the N-H···O hydrogen bonding. C-H hydrogen atoms are omitted for clarity.

Table 3. Selected bond lengths (Å) and angles (°) for zinc(II) complexes $\mathbf{C}^{4.5}$ and $\mathbf{C}^{4.7}$.

	$\mathbf{C}^{4.5}$	$\mathbf{C}^{4.7}$
Distances		
Zn-N(1)	2.2405(19)	2.134(5)
Zn-N(2)	2.0911(19)	2.082(5)
Zn-N(21 or 1A)	2.132(2)	2.050(5)
Zn-N(31 or 2A)	2.1062(19)	2.058(5)
Zn-O(8)	2.0900(17)	2.051(4)
Zn-O(1A)	2.219(2)	N/A
Angles		
N(2)-Zn-N(21 or 1A)	101.70(7)	104.01(19)
N(2)-Zn-N(31 or 2A)	174.90(7)	172.36(19)
N(21 or 1A)-Zn-N(31 or 2A)	79.14(7)	82.3(2)
N(1)-Zn-N(2)	79.17(7)	78.39(18)
N(1)-Zn-N(21 or 1A)	96.97(7)	116.3(2)
N(1)-Zn-N(31 or 2A)	95.74(7)	102.88(18)
N(1)-Zn-O(8)	163.20(7)	128.61(17)
O(8)-Zn-N(2)	84.10(7)	82.91(17)
O(8)-Zn-N(21 or 1A)	87.88(7)	114.6(2)
O(8)-Zn-N(31 or 2A)	100.98(7)	90.57(17)
O(1A)-Zn-O(8)	81.44(9)	
O(1A)-Zn-N(2)	94.92(8)	
O(1A)-Zn-N(21)	159.21(9)	
O(1A)-Zn-N(31)	85.42(8)	

In the crystal structure, the co-ordination geometry of the zinc(II) centre of $\mathbf{C}^{4.5}$ may be best described as distorted octahedral with a weakly coordinated perchlorate counter ion (Zn-O(1A) 2.219(2) Å). In $\mathbf{C}^{4.7}$ the zinc(II) centre is in a distorted trigonal bipyramidal (τ = 0.73) environment with the two pyridine groups comprising the axial ligands (N(2)-Zn-N(2A) 172.36(19) °). In both cases, $\mathbf{L}^{4.4}$ provides N2O co-ordination.

The higher co-ordination number of $\mathbf{C}^{4.5}$ seems compensated by longer Zn-N and Zn-O distances than $\mathbf{C}^{4.7}$. Thus, the average Zn-N distances are 2.142 Å in $\mathbf{C}^{4.5}$ and 2.081 Å in $\mathbf{C}^{4.7}$. Similarly, the Zn-O(8) distance is 2.0900(17) Å in $\mathbf{C}^{4.5}$ and 2.051(4) Å in $\mathbf{C}^{4.7}$. An important structural parameter of these cations is the angle between the amino and

amide coordinating groups, N(1)-Zn-O(8), as it is between these groups where nucleophile species would be most suitably positioned for attack on the C=O group (*vide infra*). This angle is 164.33(8) ° and 128.61(17) ° in $\mathbf{C}^{4.5}$ and $\mathbf{C}^{4.7}$, respectively. In principle the smaller N(1)-Zn-O(8) could be better to position zinc-interacting nucleophile species closer to the amide carbonyl unit, and N(7A) closer to the transition state species after nucleophilic attack (*vide infra*).

An important difference between the co-ordination environment of $\mathbf{C}^{4.7}$ compared to $\mathbf{C}^{4.5}$ is the hydrogen bonding interaction between the amide oxygen of $\mathbf{L}^{4.4}$ and the 6-amino group of $\mathbf{L}^{4.7}$ (N(7A)···O(8) 3.042(7) Å, H(7NA)···O(8A) 2.19 Å, N(7A)-H(7NA)···O(8) 141.1 ° for a N(7A)-H(7NA) normalized/extended to 1.01 Å). This hydrogen bonding interaction may explain the unusually small N(1)-Zn-O(8) angle (*vide supra*) and may also lead to differences in the reactivity of the amide bond (*vide infra*). Internal hydrogen bonds with donor:acceptor distances of as long as 3.4 Å have been reported to have an important effect on the properties of metal-bound molecules.[22]

4.2.3 NMR Studies

4.2.3.1 Solution Structures

Like in $\mathbf{L}^{4.1}$ and $\mathbf{L}^{4.4}$ the arrangement of the amide group of the metal-free ligands $\mathbf{L}^{4.2}$ and $\mathbf{L}^{4.3}$ is such that allows the intramolecular interaction of H5 with the amide oxygen on the same pyridine ring. This deduction is based on the downfield appearance of the H5 proton resonance relative to that of adjacent H4 (see chapter 2).[17] Zinc(II) complexes $\mathbf{C}^{4.1}$ - $\mathbf{C}^{4.7}$ in acetonitrile solutions are all characterized by ^{1}H NMR resonances shifted downfield relative to the corresponding ligands, a feature consistent

with metal binding. In all cases the H4 proton resonance appears downfield of H5, indicative of the C=O group being oriented in opposite direction than in the free ligand; an orientation ideal for amide oxygen co-ordination to the zinc(II) ion (see chapter 2).[17]

The position of the carbonyl resonances in the ^{13}C NMR spectra of $\mathbf{C^{4.1}}$, $\mathbf{C^{4.2}}$ and $\mathbf{C^{4.3}}$ in acetonitrile of 187.1, 185.7 and 187.2 ppm, respectively, compared to 176.9 ppm for $\mathbf{L^{4.1}}$, 178.0 ppm for $\mathbf{L^{4.2}}$ and 178.4 ppm for $\mathbf{L^{4.3}}$ provides additional evidence[(a)] of solution carbonyl binding in $\mathbf{C^{4.1}}$ - $\mathbf{C^{4.3}}$. Similarly, the carbonyl resonances are 183.4 ppm for $\mathbf{C^{4.5}}$ and $\mathbf{C^{4.6}}$, and 184.9 ppm for $\mathbf{C^{4.7}}$, compared to 177.9 ppm for $\mathbf{L^{4.4}}$.

4.2.3.2 Amide Cleavage Reactions.

Catalytic zinc sites possess a predominantly N-coordinating ligand environment.[23] In addition, the common presence of active-sites residues within hydrogen bonding distances to metal-bound substrate and/or nucleophile species could be indicative of the functional importance of the microenvironment.[3] In chapter 2 it has been reported that the intramolecular *tert*-butyl amide group of $\mathbf{C^{4.1}}$ is cleaved predominantly to methyltrimethylacetate in methanol at 50(1) °C upon addition of $Me_4NOH{\cdot}5H_2O$ (1 equiv.) at a rate faster than the intramolecular *tert*-butyl amide group of a complex with N/S ligation and much faster than that of $\mathbf{C^{4.4}}$, which has an accessible and flexible zinc(II) co-ordination site.[18] Overall, these major changes in the first co-ordination sphere of the zinc(II) ion led to an overall change in the stability of the amide bond of

(a) IR studies are also indicative of amide oxygen coordination; ν_{CO} 1684 ± 4 cm^{-1} for $\mathbf{L^{4.1-4.4}}$, 1646 ± 4 cm^{-1} for $\mathbf{C^{4.1}}$- $\mathbf{C^{4.3}}$ and 1662-1642 ± 4 cm^{-1} for $\mathbf{C^{4.5}}$- $\mathbf{C^{4.7}}$.

ca. 300-fold. In an attempt to gain insights into possible cooperation mechanisms of metals and hydrogen bonding groups, and the relative importance of the zinc ligands and the active site microenvironment in the stability of amide groups, in this study we compare the ability of $\mathbf{C}^{4.1}$- $\mathbf{C}^{4.3}$ and $\mathbf{C}^{4.5}$- $\mathbf{C}^{4.7}$ to undergo amide methanolysis under the same experimental conditions (Scheme 4.3).

Amide bond cleaving conditions : $Me_4N^+OH^-5H_2O$ (1 equiv.), MeOH, 50 °C

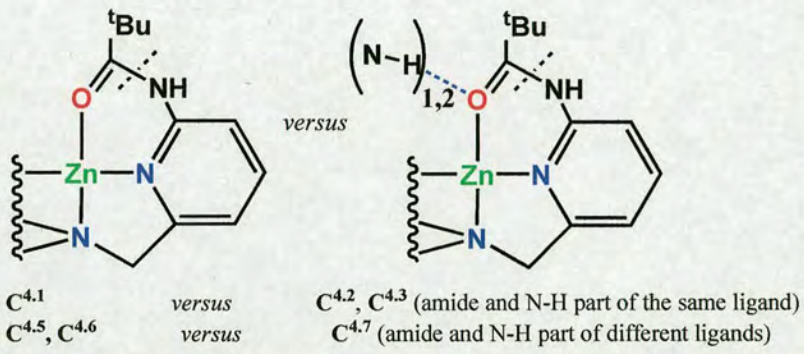

$\mathbf{C}^{4.1}$ *versus* $\mathbf{C}^{4.2}$, $\mathbf{C}^{4.3}$ (amide and N-H part of the same ligand)

$\mathbf{C}^{4.5}$, $\mathbf{C}^{4.6}$ *versus* $\mathbf{C}^{4.7}$ (amide and N-H part of different ligands)

Scheme 4.3

Under these conditions it was found that $\mathbf{C}^{4.2}$ and $\mathbf{C}^{4.3}$ undergo amide cleavage slower than $\mathbf{C}^{4.1}$. To our knowledge this is the first evidence that N-H···O=C hydrogen bonding can deactivate a metal-bound carbonyl group of an amide unit toward nucleophilic attack. Thus, the half-life of the amide bond, $t_{1/2}$, is 9 h for $\mathbf{C}^{4.2}$ and 320 h for $\mathbf{C}^{4.3}$ compared to 0.4 h for $\mathbf{C}^{4.1}$. It is remarkable to observe that a hydrogen bonding environment can affect the reactivity of a local zinc(II)-bound peptide bond by *ca.* 800-fold.[b] By comparison, major changes in the ligand environment of the zinc(II) centre led to a change in amide bond stability of *ca.* 300-fold.[18] There is evidence that amide oxygen co-ordination facilitates deprotonation of the amide N-H, and that this event de-activates the amide bond toward nucleophilic attack.[24]

[b] Electronic effect of the amino groups on the pyridine ring may also partly contribute to affect the rate of cleavage.

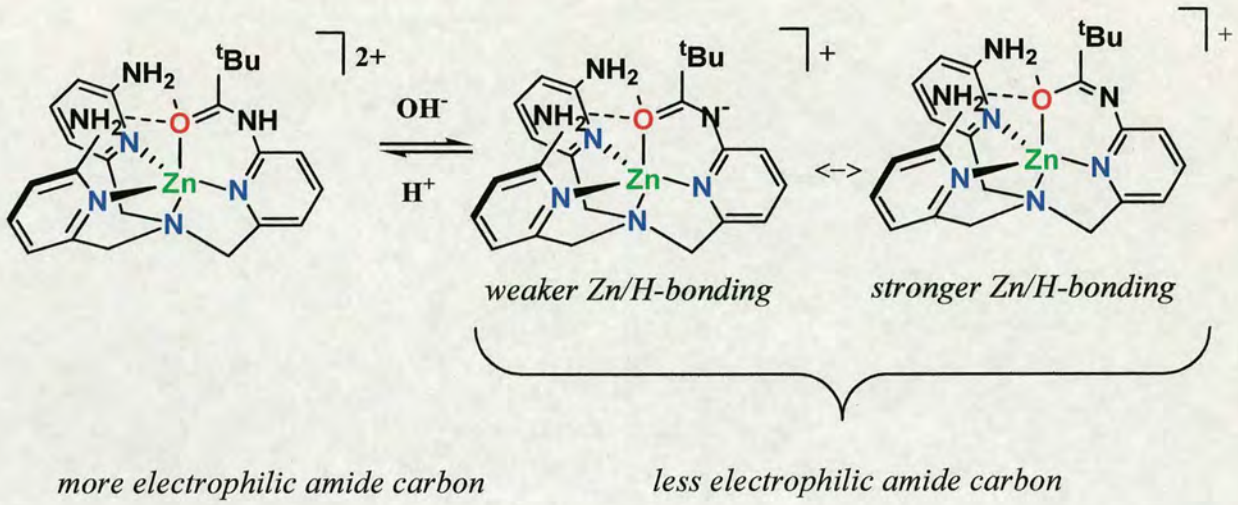

Scheme 4.4

For $\mathbf{C}^{4.2}$, ESI-MS (+ ion) analysis of the reaction mixture showed an isotope cluster at m/z 467.2 (100%), a mass consistent with $[(\mathbf{L}^{4.2}(-H^+))Zn]^+$ (calcd. value 467.15) and matches theoretical isotope distribution. Similarly, for $\mathbf{C}^{4.3}$ ESI-MS (+ ion) analysis of the reaction mixture showed an isotope cluster at m/z 482.2 (100%) (calcd. 482.16 for $[(\mathbf{L}^{4.3}(-H^+))Zn]^+$). Hence, a reasonable explanation for the observed reactivity of $\mathbf{C}^{4.2}$ and $\mathbf{C}^{4.3}$ is that the combination of zinc-binding and hydrogen bonding stabilises a -N=C(^{t}Bu)-O$^-$ resonance form (Scheme 4.4), which is less susceptible to nucleophilic attack. This result is important in that it suggests that protonation of the amide N-H may be a key requirement for efficient amide bond cleavage. In fact, in the active site of carboxypeptidase A and thermolysin Glu-270 and Glu-143, respectively are believed to be involved in protonation of the amide NH.[3c,25,26] This result may explain also why cleavage of peptide bonds of polypeptides using Pt(II) and Pd(II) complexes proceeds faster in acidic solutions.[27]

It is possible that the rigidity of $\mathbf{L}^{4.2}$ and $\mathbf{L}^{4.3}$ does not allow the amino groups to interact with nucleophile and/or transition state species, which presumably would lead

to faster amide bond cleavage reactions. To test this hypothesis we have investigated the reactivity when amino hydrogen bonding groups are given the opportunity to adopt a different orientation relative to the scissile amide bond using more flexible co-ordination environments. Under the same experimental conditions the half-life of the amide bond of $\mathbf{C}^{4.5}$ and $\mathbf{C}^{4.6}$ which do not have a hydrogen bonding environment is 7.4 h and 20 h, respectively, compared to 1.60 h for $\mathbf{C}^{4.7}$ which has an amino hydrogen bonding group. Thus the presence of the amino group causes in this case a 12.5-fold rate enhancement ($\mathbf{C}^{4.6}$ *versus* $\mathbf{C}^{4.7}$). The different reactivity may be due to the flexible co-ordination environment offering amino hydrogen bonding group and scissile amide bond the possibility to adopt a wide range of orientations relative to one another. These orientations may include one that would allow the interaction with the transition state species, which was impossible in the $[(\mathbf{L}^{4.2,\,4.3})\mathrm{Zn}]^{2+}$ cations due to the rigidity imposed by $\mathbf{L}^{4.2,\,4.3}$.

4.3 Conclusion and Future Work

Catalytic zinc sites in Nature possess a predominantly N-coordinating ligand environment and hydrogen bonding microenvironments around the zinc(II) centre.[3,23] Hydrogen bonding is also a common tactic for carbonyl activation in organic synthesis.[15] This study has explored the effect of a zinc(II) ion and local hydrogen bonding groups in amide bond cleavage reactions.

The approach consisted of using the ligand unit (6-pivaloylamido-2-pyridylmethyl)amine as a method to induce intramolecular amide oxygen co-ordination to a zinc(II) centre, and additional ligands that provide a hydrogen bonding environment around the zinc(II)-bound amide. N-H···O=C(amide) was accomplished following two different strategies; one in which amide and amino groups are fixed to

the same ligand framework and another in which they are part of different ligands. This work shows that the hydrogen bonding environment around the zinc-bound amide can affect the stability of the amide bond to the same and even greater extent than major changes in the first co-ordination sphere of the zinc(II) ion. This result may explain the abundance of hydrogen bond donating microenvironments in the active sites of metalloproteases.

Importantly, this study shows that hydrogen bonding can both activate and deactivate the carbonyl unit of amide groups around metal sites. The deactivation of the amide group was consistent with metal/hydrogen bonding-induced deprotonation of the amide N-H and stabilisation of its -N=C(^{t}Bu)-O$^-$ resonance form. Hence, protonation of the amide N-H is revealed as a major requirement for efficient amide bond cleavage. This result is consistent with some proposed catalytic mechanisms of zinc-requiring proteases where glutamate residues are believed to effect protonation of the amide N-H.[2c,25,26] This result is also consistent with recent work in which Pt(II) and Pd(II) compounds effect peptide bond cleavage under acidic conditions.[27] When amino and amide groups were allowed to freely orient relative to one another amide at the zinc(II) centre, amide cleavage occurred faster than in similar compounds without the hydrogen bonding groups. Therefore we propose that the orientation of the hydrogen bonding groups relative to the amide bond may be an important parameter to allow the cooperation of metal ions and hydrogen bonding groups toward more effective peptide bond cleavage.

In view of these outcomes, a logical consequence would be to methylate the nitrogen of the peptide bond in order to prevent deprotonation of the amide N-H and consequent

stabilisation of its -N=C(^{t}Bu)-O$^-$ resonance form. Remarkably, preliminary results showed that cleavage of the methylated (CH_3-N(*py*)-C(^{t}Bu)=O) amide bond for $\mathbf{C}^{4.1}$ carried out at room temperature and under the same experimental conditions was almost complete after only 1 minute. Therefore, it would be interesting to investigate the effect promoted by the hydrogen bond environment of the corresponding amide methylated species of $\mathbf{C}^{4.2}$ and $\mathbf{C}^{4.3}$. Unfortunately initial attempts to synthesise the desired compounds were unsatisfactory, and lack of time did not allow completion of these studies. Hence, future work should focus to find a suitable way to methylate the nitrogen of the amide bond of $\mathbf{L}^{4.2}$ and $\mathbf{L}^{4.3}$ and explore the ability of their relative metal complexes to stabilise and cleave the scissile peptide bond.

4.4 Experimental

4.4.1 General

Reagents were obtained from commercial sources and used as received unless otherwise noted. Solvents were dried and purified under N_2 by using standard methods[28] and were distilled immediately before use. All compounds were prepared under N_2 unless otherwise mentioned. $\mathbf{L}^{4.4}$ and $\mathbf{L}^{4.7}$ were synthesized according to recently reported procedures.[11a,17,18,29] The NMR spectra were obtained using a Bruker DPX 360 at 20 °C in CD_3CN unless otherwise noted. ^{13}C and ^{1}H chemical shifts are referenced with respect to the carbon (δ_C 1.32 and 118.26 ppm) and residual proton (δ_H 1.94 ppm) solvent peaks. Sample concentrations for the NMR studies were 0.02-0.04 M. The half-life of the amide bond, $t_{1/2}$ was determined by ^{1}H NMR by integration of *tert*-butyl resonances. Infrared spectra were recorded with a JASCO FTIR-410 spectrometer between 4000 and 250 cm^{-1} as KBr pellets (solid state) or as acetonitrile solutions in KBr cells. Elemental analyses were carried out by the microanalyses service provided by the School of Chemistry at the University of Edinburgh.

4.4.2 Synthesis

$\mathbf{L}^{4.2}$. A solution of 2-(pivaloylamido)-6-(bromo-methyl)pyridine (7.8 mmol, 2.11 g) in CH_3CN (60 cm^3) was added dropwise over a period of 1.5 h to a solution containing 2-(aminomethyl)pyridine (15.7 mmol, 1.689 g) and Na_2CO_3 (15.7 mmol, 1.66 g) in CH_3CN (110 cm^3) at 40 °C. The insoluble white solid was removed by filtration and the filtrate evaporated under vacuum. The crude material was purified by flash chromathography (alumina, EtOAc:DCM 8:2) to obtain *N*-(6-pivaloylamido-2-

pyridylmethyl)-*N*-(2-pyridylmethyl)amine as a yellow oil (1.111 g , 42 %). *N*-(6-Pivaloylamido-2-pyridylmethyl)-*N*-(2-pyridylmethyl)amine (3.3 mmol, 1.111 g) was dissolved in 2 M HCl (20 cm^3) and the solution was refluxed for 24 h. The solution was allowed to cool to room temperature, after which, 1M NaOH was added until ~ pH 14. The product was extracted with CH_2Cl_2 (3 x 100 cm^3). The combined organic phases were dried over Na_2SO_4 and evaporated to dryness under reduced pressure to afford *N*-(6-amino-2-pyridylmethyl)-*N*-(2-pyridylmethyl)amine as a brown oil (0.477 g, 67 %). *N*-(6-Amino-2-pyridylmethyl)-*N*-(2-pyridylmethyl)amine (0.4 mmol, 0.086 g) and Na_2CO_3 (0.4 mmol, 0.042 g) were dissolved in CH_3CN (~10 cm^3). To this solution was added 2-(pivaloylamido)-6-(bromo-methyl)pyridine (0.4 mmol, 0.109 g). The resulting mixture was stirred at room temperature for about 3 h, after which, the solid was filtered off. The solution evaporated under vacuum to yield a brown oil. This oil was dissolved in a minimum amount of CH_3CN (*ca.* 5 cm^3); diethyl ether was then added until a white/yellow precipitate was formed. The solid was collected by filtration and the solution was evaporated to give a brown oil; this solution was treated as above, and the same process was repeated 4 times. The combined solids were treated with 1M NaOH (10 cm^3) and extracted with CH_2Cl_2 (3 x 30 cm^3). The combined organic layers were dried over Na_2SO_4, and evaporated to dryness under reduced pressure to afford the ligand as brown oil (120 mg, 75 %).

^{1}H NMR (CD_3CN, 360.1 MHz) δ_H (ppm) 8.46 (m, 1H, py-*H*), 8.37 (br s, 1H, py-N*H*), 7.94 (d, *J* = 7.9 Hz, 1H, py-*H*), 7.71-7.61 (m, 2H, py-*H*), 7.57 (d, *J* = 7.9 Hz, 1H, py-*H*), 7.37 (dd, J = 8.3 and 7.6 Hz, 1H, py-*H*), 7.29 (d, 7.6 Hz, 1H, py-*H*), 7.18 (m, 1H, py-*H*), 6.80 (d, J = 7.2 Hz, 1H, py-*H*), 6.36 (d, J = 7.9 Hz, 1H, py-*H*), 4.96 (br, 2H, py-N*H*$_2$), 3.80 (s, 2H, NC*H*$_2$-py), 3.71 (s, 2H, NC*H*$_2$-py), 3.56 (s, 2H, NC*H*$_2$-py), 1.26 (s, 9H, C-(C*H*$_3$)$_3$). ^{13}C NMR (CD_3CN, 90.5 MHz) δ_C (ppm) 178.0 (*C*=O), 160.4 (py-*C*),

159.9 (py-*C*), 159.0 (py-*C*), 158.3 (py-*C*), 152.2 (py-*C*), 149.8 (py-*C*H), 139.5 (py-*C*H), 138.8 (py-*C*H), 137.4 (py-*C*H), 123.8 (py-*C*H), 122.9 (py-*C*H), 119.4 (py-*C*H), 112.8 (py-*C*H), 112.6 (py-*C*H), 60.7, 60.6 and 60.3 (N*C*H_2-py), 40.3 (*C*-(CH_3)$_3$), 27.4 (C-(*C*H_3)$_3$). FTIR (KBr, cm^{-1}) 1684 ± 4 (ν_{CO}). ESI-MS (+ion) Found 405.2 (100%), Calcd. 405.24 (100%) for $[(\mathbf{L}^{2})H]^{+}$, and matches theoretical isotope distribution.

L$^{4.3}$. A solution of 2-(pivaloylamido)-6-(bromo-methyl)pyridine (4 mmol, 1.084 g) in CH_3CN (60 cm^3) was added dropwise over a period of 1.5 h to a solution containing (6-pivaloylamido-2-methylpyridyl)amine (8 mmol, 1.656 g) and Na_2CO_3 (8 mmol, 0.85 g) in CH_3CN (110 cm^3) at 60 °C. The insoluble white solid was removed by filtration and the filtrate evaporated under vacuum. The crude material was purified by flash chromathography (alumina, DCM:EtOAc 8:2) to obtain bis(6-pivaloylamido-2-pyridylmethyl)amine as a yellow oil (0.7 g, 73 %). Bis(6-pivaloylamido-2-pyridylmethyl)amine (0.8 mmol, 0.320 g) was dissolved in 2 M HCl (20 cm^3) and the solution was refluxed for 48 h. The solution was allowed to cool to room temperature, after which, 1M NaOH was added until ~ pH 14. The product was extracted with CH_2Cl_2 (3 x 50 cm^3). The combined organic phases were dried over Na_2SO_4 and evaporated to dryness under reduced pressure to afford bis(6-amino-2-pyridylmethyl)amine a brown oil (0.129 g, 70 %). Bis(6-amino-2-pyridylmethyl)amine (0.56 mmol, 0.129 g) and Na_2CO_3 (0.56 mmol, 0.060 g) were dissolved in CH_3CN (~20 cm^3). To this solution was added 2-(pivaloylamido)-6-(bromo-methyl)pyridine (0.56 mmol, 153 mg). The resulting mixture was stirred at room temperature for 3 h, after which, the solid was filtered off. The solution evaporated under vacuum. The oil formed was dissolved in a minimum amount of CH_3CN (*ca.* 5 cm^3); diethyl ether was then added until a white/yellow precipitate was formed. The solid was collected by

filtration and the solution was evaporated to give a brown oil again; this solution was treated as above, and the same process was repeated 4 times. The combined solids were treated with 1M NaOH (10 cm^3) and extracted with CH_2Cl_2 (3 x 30 cm^3). The combined organic layers were dried over Na_2SO_4, and evaporated to dryness under reduced pressure to afford the ligand as brown oil (0.15 mg, 64 %).

^{1}H NMR (CD_3CN, 360.1 MHz) δ_H (ppm) 8.18 (br, 1H, py-N*H*), 7.97 (d, J = 8.4 Hz, 1H, py-*H*), 7.67 (t, J = 8.4 Hz, 1H, py-*H*), 7.39 (m, 3H, py-*H*), 6.86 (d, J = 7.6 Hz, 2H, py-*H*), 6.36 (d, J = 8.3 Hz, 2H, py-*H*), 4.8 (br, 2H, py-NH_2), 3.69 (s, 2H, NCH_2-py), 3.60 (s, 4H, NCH_2-py), 1.29 (s, 9H, C-(CH_3)$_3$). ^{13}C NMR (CD_3CN, 90.5 MHz) δ_C (ppm) 178.4 (*C*=O), 160.3 (py-*C*), 158.5 (py-*C*), 157.6 (py-*C*), 152.8 (py-*C*), 139.6 (py-*C*H), 139.0 (py-*C*H), 120.0 (py-*C*H), 113.7 (py-*C*H), 112.9 (py-*C*H), 107.9 (py-*C*H), 60.5 and 60.3 (N*C*H_2-py), 40.5 (*C*-(CH_3)$_3$), 27.5 (C-(*C*H_3)$_3$). FTIR (KBr, cm^{-1}) 1684 ± 4 (ν_{CO}). ESI-MS (+ion) Found 420.2 (100%), Calcd. 420.25 (100%) for $[(\mathbf{L}^3)H]^+$, and matches theoretical isotope distribution.

$[(\mathbf{L}^{4.2})Zn](ClO_4)_2$ $\mathbf{C}^{4.2}$. $Zn(ClO_4)_2 \cdot 6H_2O$ (37.2 mg, 0.1 mmol) and $\mathbf{L}^{4.2}$ (40.5 mg, 0.1 mmol) were dissolved in acetonitrile (10 cm^3) and the solution was stirred for 1 h at room temperature. The solvent evaporated under vacuum to yield the pure product as a yellow solid in quantitative yield. (Found: C, 41.0; H, 4.2; N, 13.1. Calc. for $C_{23}H_{28}Cl_2N_6O_9Zn$: C, 41.30; H, 4.22; N, 12.57).

^{1}H NMR (CD_3CN, 360.1 MHz) δ_H (ppm) 9.61 (br s, 1H, py-N*H*), 8.61 (d, J = 6Hz, 1H, py-*H*), 8.1 (t, *J* = 8.3 Hz, 2H, py-*H*), 7.65-7.57 (m, 3H, py-*H*), 7.51 (d, *J* = 8.3 Hz, 1H, py-*H*), 7.40 (d, J = 7.9 Hz, 1H, py-*H*), 6.72 (m, 2H, py-*H*), 5.96 (br, 2H, py-NH_2), 4.2-4.05 (s, 6H, py-CH_2N), 1.50 (s, 9H, C-(CH_3)$_3$). ^{13}C NMR (CD_3CN, 90.5 MHz) δ_C (ppm) 187.1 (*C*=O), 160.6 (py-*C*), 156.1 (py-*C*), 153.9 (py-*C*), 152.4 (py-*C*), 151.9

(py-*C*), 149.3 (py-*C*H), 144.5 (py-*C*H), 142.8 (py-*C*H), 126.3 (py-*C*H), 125.9 (py-*C*H), 122.5 (py-*C*H), 117.5 (py-*C*H), 113.5 (py-*C*H), 112.5 (py-*C*H), 57.9, 57.3 and 57.2 (N*C*H_2-py), 42.5 (*C*-(CH_3)$_3$), 27.1 (C-(*C*H_3)$_3$). FTIR (KBr, cm^{-1}) 1646 ± 4 (ν_{CO}).

[($L^{4.3}$)Zn](ClO_4)$_2$ $C^{4.3}$. $Zn(ClO_4)_2 \cdot 6H_2O$ (18.6 mg, 0.05 mmol) and $L^{4.3}$ (21 mg, 0.05 mmol) were dissolved in acetonitrile (5 cm^3) and the solution was stirred for 1 h at room temperature. The solution was filtered through celite and the solvent evaporated under vacuum to yield the pure product as a yellow solid in quantitative yield. (Found: C, 41.0; H, 4.4; N, 15.1. Calc. for $C_{23}H_{29}Cl_2N_7O_9Zn \cdot CH_3CN$: C, 41.42; H, 4.45; N, 15.46).

^{1}H NMR (CD_3CN, 360.1 MHz) δ_H (ppm) 9.69 (br, 1H, py-N*H*), 8.13 (dd, J = 8.3 and 7.5 Hz, 1H, py-*H*), 7.64 (dd, J = 8.3 and 7.2 Hz, 2H, py-*H*), 7.56 (d, J = 8.3, 1H, py-*H*), 7.44 (d, J = 7.6 Hz, 1H, py-*H*), 6.75 (d, J = 8.5 Hz, 2H, py-*H*), 6.70 (d, J = 7.3 Hz, 2H, py-*H*), 4.2 (br, 2H, py-NH_2), 3.96 (s, 4H, N*C*H_2-py), 1.47 (s, 9H, C-(*C*H_3)$_3$). ^{13}C NMR (CD_3CN, 90.5 MHz) δ_C (ppm) 187.2 (*C*=O), 160.6 (py-*C*), 153.9 (py-*C*), 152.2 (py-*C*), 152.0 (py-*C*), 144.5 (py-*C*H), 142.7 (py-*C*H), 123.0 (py-*C*H), 117.7 (py-*C*H), 113.6 (py-*C*H), 112.5 (py-*C*H), 56.8 and 56.3 (N*C*H_2-py), 42.3 (*C*-(CH_3)$_3$), 27.0 (C-(*C*H_3)$_3$). FTIR (KBr, cm^{-1}) 1646 ± 4 (ν_{CO}).

[($L^{4.4}$)Zn($L^{4.5}$)](ClO_4)$_2$ $C^{4.5}$·(ClO_4)$_2$. To a solution of $L^{4.4}$ (58.6 mg, 0.2 mmol) in dry CH_3CN (10 mL) was added solid $Zn(ClO_4)_2 \cdot 6(H_2O)$ (74.4 mg, 0.2 mmol). The solution was stirred for ~ 10 min after which $L^{4.5}$ (39.7 mg, 0.3 mmol) was added. The resulting reaction mixture was stirred for ~1 h at room temperature. The solvent was evaporated under vacuum to yield the product as a yellow solid in quantitative yield. (Found: C, 44.20; H, 4.37; N, 10.51. Calc. for $C_{26}H_{29}Cl_2N_5O_9SZn \cdot CH_3CN$: C, 43.96; H, 4.22; N, 10.99).

^{1}H NMR (CD_3CN, 360.1 MHz) δ_H (ppm) 9.23 (br s, 1H, N*H*), 8.64 (m, 4H, phen-C*H*), 8.26 (s, 2H, phen-C*H*), 8.24 (t, J = 7.6 Hz, 1H, py-C*H*), 8.09 (dd, J = 5.0, 7.9 Hz, 2H, phen-C*H*), 7.56 and 7.54 (m, 1H and 1H, py-C*H*), 4.38 and 4.14 (br, 2H, NCH_2-py), 3.04-2.81 and 2.29 (m, 6H and 2H, NCH_2CH_2S), 0.68 (s, 9H, C-(CH_3)$_3$). ^{13}C NMR (CD_3CN, 90.5 MHz, 298 K) δ_C (ppm) 184.4 (*C*=O), 152.9, 152.6 (py-*C*), 150.1 (phen-*C*H), 144.1 (py-*C*H), 141.8 (phen-*C*H), 141.4 (phen-*C*), 130.6 (phen-*C*), 130.6 (phen-*C*), 128.4 and 126.9 (phen-*C*H), 122.5 and 117.6 (py-*C*H), 55.5 (N*C*H_2-py), 54.3 and 21.1 (N*C*H_2*C*H_2S), 40.9 (*C*-(CH_3)$_3$), 26.1 (C-(*C*H_3)$_3$). FTIR (KBr, cm^{-1}) 1658 ± 4 (ν_{CO}).

[($L^{4.4}$)Zn($L^{4.6}$)](ClO_4)$_2$ $C^{4.6}$·(ClO_4)$_2$. To a solution of $L^{4.4}$ (29.3 mg, 0.1 mmol) in dry CH_3CN (5 cm^3) was added solid Zn(ClO_4)$_2$·6(H_2O) (37.2 mg, 0.1 mmol). The resulting mixture was stirred for ~ 10 minutes after which time $L^{4.6}$ (10.8 mg, 0.1 mmol) was added. The reaction mixture was stirred for ~1 h at room temperature. At this time, Et_2O (50 cm^3) was added, resulting in the formation of white precipitate. The solution was kept at –20 °C for 48 h after which it was filtered. The precipitate was then dried under vacuum to afford the product as a white solid in 90% yield. (Found: C, 39.28; H, 5.13; N, 9.91. Calc. for $C_{21}H_{31}Cl_2N_5O_9Zn$·0.5Et_2O: C, 39.30; H, 5.16; N, 9.96).

^{1}H NMR (CD_3CN, 360.1 MHz) δ_H (ppm) 9.17 (br s, 1H, N*H*), 8.14 (t, J = 7.9 Hz, 1H, py-C*H*), 8.08 (d, J = 6 Hz, 1H, py-C*H*), 8.03 (m, 1H, py-C*H*), 7.55 (d, J = 7.9 Hz, 1H, py-C*H*), 7.44 (m, 3H, py-C*H*), 4.29 (t, J = 6.5 Hz, 2H, py-CH_2NH_2), 4.25 (s, 2H, NCH_2-py), 3.59 (t, J = 6.5 Hz, 2H, py-CH_2NH_2), 3.12-2.96 and 2.16 (m, 6H and 2H, NCH_2CH_2S), 1.07 (s, 9H, C-(CH_3)$_3$). ^{13}C NMR (CD_3CN, 90.5 MHz, 298 K) δ_C (ppm) 183.4 (*C*=O), 157.6, 152.8 and 152.6 (py-*C*), 147.6, 144.0, 141.5, 125.4, 125.0, 122.2

and 117.3 (py-*C*H), 54.7 and 43.6 (N*C*H_2-py), 53.9 and 20.7 (N*C*H_2*C*H_2S), 41.3 (*C*-(CH_3)$_3$), 26.6 (C-(*C*H_3)$_3$). FTIR (KBr, cm^{-1}) 1665 ± 4 (ν_{CO}).

[($L^{4.4}$)Zn($L^{4.7}$)](ClO_4)$_2$ $C^{4.7}$·(ClO_4)$_2$. To a solution of $L^{4.4}$ (88 mg, 0.3 mmol) in dry CH_3CN (10 mL) was added solid $Zn(ClO_4)_2$·6(H_2O) (112 mg, 0.3 mmol). The solution was stirred for ~ 10 min after which $L^{4.7}$ (37 mg, 0.3 mmol) was added. The resulting reaction mixture was stirred for ~1 h at room temperature. The solvent was evaporated under vacuum to yield the pure product as a yellow solid in quantitative yield. (Found: C, 36.92; H, 4.70; N, 12.36. Calc. for $C_{21}H_{32}Cl_2N_6O_9SZn$: C, 37.04; H, 4.74; N, 12.34). ^{1}H NMR (CD_3CN, 360.1 MHz) δ_H (ppm) 9.50 (br s, 1H, N*H*), 8.14 (br, 1H, py-C*H*), 7.70 (d, J = 7.6 Hz, 1H, py-C*H*), 7.50 and 7.45 (br, 1H and 1H, py-C*H*), 6.76 (m, 2H, py-C*H*), 5.38 (br s, 2H, NH_2), 4.32 and 4.14 (br, 2H and 2H, py-C$H_2$$NH_2$ and NCH_2-py), 3.64 (br, 2H, py-CH_2NH_2), 3.10-2.96 and 2.19 (m, 6H and 2H, N*C*H_2*C*H_2S), 1.27 (s, 9H, C-(CH_3)$_3$). ^{13}C NMR (CD_3CN, 90.5 MHz, 298 K) δ_C (ppm) 184.7 (*C*=O), 159.4, 154.4, 153.4 and 152.3 (py-*C*), 147.6, 142.5, 122.1, 117.2, 112.9 and 111.2 (py-*C*H), 54.7 and 44.1 (N*C*H_2-py), 53.4 and 20.5 (N*C*H_2*C*H_2S), 41.6 (*C*-(CH_3)$_3$), 26.8 (C-(*C*H_3)$_3$). FTIR (KBr, cm^{-1}) 1642 ± 4 (ν_{CO}).

4.4.3 X-ray Crystallography

Crystals suitable for X-ray diffraction studies were grown by slow evaporation of acetonitrile or acetonitrile/ether solutions at room temperature.

Intensity data for [($L^{4.2}$)Zn](ClO_4)$_2$·CH_3CN $C^{4.2}$·(ClO_4)$_2$·CH_3CN, [($L^{4.3}$)Zn](ClO_4)$_2$·CH_3CN $C^{4.2}$·(ClO_4)$_2$·CH_3CN, [($L^{4.4}$)Zn($L^{4.5}$)(ClO_4)](ClO_4)·CH_3CN $C^{4.5}$·(ClO_4)·CH_3CN and [($L^{4.4}$)Zn($L^{4.7}$)](ClO_4)$_2$ $C^{4.7}$·(ClO_4)$_2$ were collected at 150 K

using a Bruker AXS SMART APEX area detector diffractometer with graphite-monochromated Mo Kα radiation (λ = 0.71073 Å). The structures were solved by direct methods and refined to convergence against F^2 data using the SHELXTL suite of programs.[30] Data were corrected for absorption applying empirical methods using the program SADABS,[31,32] and the structures were checked for higher symmetry using the program PLATON.[33] All non-hydrogen atoms were refined anisotropically unless otherwise noted. Hydrogen atoms were placed in idealized positions and refined using a riding model with fixed isotropic displacement parameters. The N-H hydrogens were located in the difference map and refined isotropically. Difference maps of the crystal structure of $\mathbf{C}^{4.2}\cdot(ClO_4)_2\cdot CH_3CN$ revealed disorder affecting the Py-NH_2, which refined to 77% (N(27)) and 23% (N(27')) site-occupancies.

References

[1] L. M. Sayre, *J. Am. Chem. Soc.*, 1986, **108**, 1632.

[2] (*a*) R. Holm, P. Kennepohl and E. I. Solomon, *Chem. Rev.*, 1996, **96**, 2239; (*b*) Y. Lu and J. S. Valentine, *Curr. Opin. Struct. Biol.*, 1997, **7**, 495; (*c*) M. F. Perutz, G. Fermi, B. Luisi, B. Shaanan and R. C. Liddington, *Acc. Chem. Res.*, 1987, **20**, 309; (*d*) A. Ivanchich, K. Artz, J. C. Williams, J. P. Allen and T. A. Mattioli, *Biochemistry*, 1998, **37**, 11812; (*e*) K. Rose, S. E. Shadle, M. K. Eidsness, D. K. Kurtz Jr., E. A. Scott, B. Hedman, K. A. Hodgson and E. I. Solomon, *J. Am. Chem. Soc.*, 1998, **120,** 10743; (*f*) K. C. Vance and A. –F. Miller, *Biochemistry*, 2001, **40**, 13079.

[3] (*a*) W. N. Lipscomb and N. Straeter, *Chem. Rev.*, 1996, **96**, 237; (*b*) E. L. Hegg and J. N. Burstyn, *Coord. Chem. Rev.*, 1998, **173**, 133; (*c*) D. W. Christianson and W. N. Lipscomb, *Acc. Chem. Res.*, 1989, **22**, 62; (*d*) H. Kim and W. N. Lipscomb, *Biochemistry*, 1991, **30**, 8171; (*e*) X. Iturrioz, R. Rozenfeld, A. Michaud, P. Corvol and C. Llorens-Cortes, *Biochemistry*, 2001, **40**, 14440; (*f*) A. D. Pannifer, T. Y. Wong, R. Schwarzenbacher, M. Renatus, C. Petosa, J. Blenkowska, D. B. Lacy, R. J. Collier, S. Park, S. H. Leppla, P. Hanna and R. C. Liddington, *Nature*, 2001, **414**, 229; (*g*) U. Baumann, S. Wu, K. M. Flaherty and D. B. McKay, *EMBO J.*, 1993, **12**, 3357.

[4] R. Krämer, *Coord. Chem. Rev.*, 1999, 243.

[5] J. H. Cho, D. H. Kim, K. J. Lee and K. Y. Choi, *Biochemistry* 2001, **40**, 10197.

[6] J. R. Morrow and O. Iranzo, *Curr. Op. in Chem. Biol.*, 2004, **8**, 192.

[7] J. Chin, B. Banaszczyk, V. Jubian and X. Zou, *J. Am. Chem. Soc.*, 1989, **111**, 186.

[8] N. H. Williams and J. Chin, *Chem. Commun.*, 1989, 131.

[9] E. Kövári and R. Krämer, *J. Am. Chem. Soc.*, 1996, **118**, 12704.

[10] M. Wall, B. Linkletter, D. Williams, A. M. Lebuis, R. C. Hynes and J.Chin, *J. Am. Chem. Soc*, 1999, **121**, 4710.

[11] H. Aït-Haddou, J. Sumaoka, S. L. Wiskur, J. F. Folmer-Andersen and E. V. Anslyn, *Angew. Chem. Int. Ed.*, 2002, **41**, 4014.

[12] (*a*) J. C. Mareque-Rivas, R. Prabaharan and R. Torres-Martín-de-Rosales, *Chem. Commun.*, 2004, 76; (*b*) J. C. Mareque-Rivas, R. Prabaharan and S. Parsons, *Dalton Trans.*, 2004, 1648.

[13] G. Feng, J. C. Mareque-Rivas, R. Torres-Martín-de-Rosales and N. H. Williams, *J. Am. Chem. Soc.*, (submitted).

[14] M. Livieri, F. Mancin, U. Tonellato and J. Chin, *Chem. Commun.*, 2004, 2862.

[15] (*a*) N. M. Milovic, J. D. Badjic and N. M. Kostic, *J. Am. Chem. Soc.*, 2004, **126**, 696; (*b*) G. Allen, *Met. Ions Biol Syst.*, 2001, **38**, 197; (*c*) S. A. Datwyler and C. F. Meares, *Met. Ions Biol Syst.*, 2001, **38**, 213.

[16] P. M. Pihko, *Angew. Chem. Int. Ed.*, 2004, **43**, 2062.

[17] (*a*) J. C. Mareque-Rivas, R. Torres-Martín-de-Rosales and S.Parsons, *Dalton Trans.*, 2003, 2156; (*b*) J. C.Mareque-Rivas, E. Salvagni, R. Torres-Martín-de-Rosales and S. Parsons, *Dalton Trans.*, 2003, 3339.

[18] (*a*) J. C. Mareque-Rivas, E. Salvagni, R. Prabaharan, R. Torres-Martin-de-Rosales and S. Parsons, *Dalton Trans.*, 2004, 172; (*b*) L. M. Berreau, M. M. Makowska-Grzyska and A. M. Arif, *Inorg. Chem.*, 2000, **39**, 4390.

[19] A. W. Addison, T. N. Rao, J. Reedijk, J. van-Rijn and G. C. Werchoor, *J. Chem. Soc., Dalton Trans.*, 1984, 1349.

[20] F. H. Allen, O. Kennard, D. G. Watson, L. Brammer, A. G. Orpen and R. Taylor, *J. Chem. Soc. Perkin Trans.*, 1987, **2** , S1.

[21] J. C. Mareque-Rivas, R. Prabaharan, R. Torres-Martin-de-Rosales, L. Metteau and S. Parsons, *Dalton Trans.*, 2004, 2800.

[22] N. Suzuki, T. Higuchi, Y. Urano, K. Kikuchi, H. Uekusa, Y. Ohashi, T. Uchida, T. Kitagawa and T. Nagano, *J. Am. Chem. Soc.*, 1999, **121**, 11571.

[23] B. L. Valle and D. S. Auld, *Proc. Natl. Acad. Sci. USA*, 1990, **87**, 220.

[24] J. T. Groves, R. Rife and R. Chambers, Jr., *J. Am. Chem. Soc.*, 1984, **106**, 630.

[25] A. F. Monzigo and B. W. Matthews, *Biochemistry*, 1984 **23**, 5724.

[26] D. G. Hangauer, A. F. Monzigo and B. W. Matthews, *Biochemistry*, 1984, **23**, 5730.

[27] N. M. Milovic and N. M. Kostic, *J. Am. Chem. Soc.*, 2002, **124**, 4759.

[28] W. L. F. Armarego and D. D. Perrin, *Purification of Laboratory Chemicals*, Butterworth-Heinemann Ed., Oxford, 1997.

[29] L. M. Berreau, S. Mahapatra, J. A. Halfen, V. G. Young, Jr.and W. B. Tolman, *Inorg. Chem.*, 1996, **35**, 6339.

[30] G. M. Sheldrick, *SHELXS and SHELXL 97*, University of Göttingen, 1997.

[31] G. M. Sheldrick, *Empirical absorption correction program*, University of Göttingen, based upon the method of Blessing, 1995.

[32] R. H. Blessing, *Acta Crystallogr., Sect. A*, 1995, **51**, 33.

[33] A. L. Spek and PLATON, *Acta Crystallogr., Sect. A.*, 1990, **46**, C.

Chapter 5

Structures and reactivity of synthetic zinc(II) complexes resembling the active sites and reaction intermediates of aminopeptidases

5.1 Introduction

This study reports the first crystallographic characterization and hydrolysis of a synthetic zinc(II) complex that resembles the active site and reaction intermediates proposed for aminopeptidases.

There is great interest in designing metal complexes that resemble the active site of metallopeptidases and capable of hydrolysing unactivated peptide bonds.[1] Such complexes not only could be useful in elucidating fundamental aspects of the enzyme chemistry but also find important applications in protein sequencing. Metallopeptidases typically require a zinc(II) ion with a co-ordination environment consisting of a glutamate and two histidine residues.[2] In addition, active-site residues participate in substrate binding and/or co-operate with the zinc(II) ion towards facilitating the amide hydrolysis reaction, but the effects associated with the second co-ordination sphere are not well understood.[3] An example of zinc metallopeptidase for which this co-ordination environment has been proposed is aminopeptidase A (APA), which specifically cleaves *in vitro* the N-terminal glutamyl or aspartyl residue from peptide substrates (Scheme 5.1).[4]

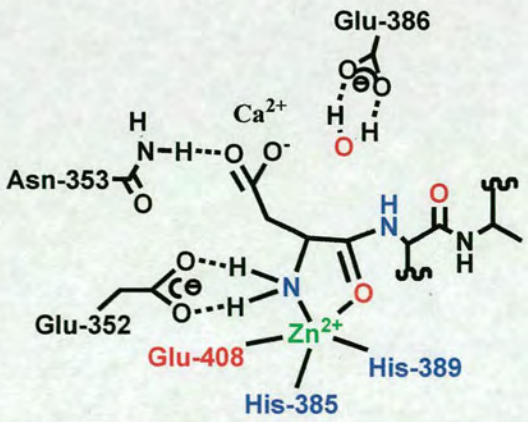

Scheme 5.1

APA has been found in many tissues such as renal epithelial cells, vascular endothelium and in brain nuclei. Brain APA is also involved in the central control of blood pressure, it has been, therefore, suggested that it is a possible target for the treatment of hypertension.[4c]

5.1.1 Catalytic Mechanism of Aminopeptidase A

Because the APA active site shares many similarities with that of thermolysin, a proposed catalytic mechanism of action was based on X-ray diffraction data from thermolysin and taking into account site-directed mutagenesis studies (Scheme 5.2).[4c]

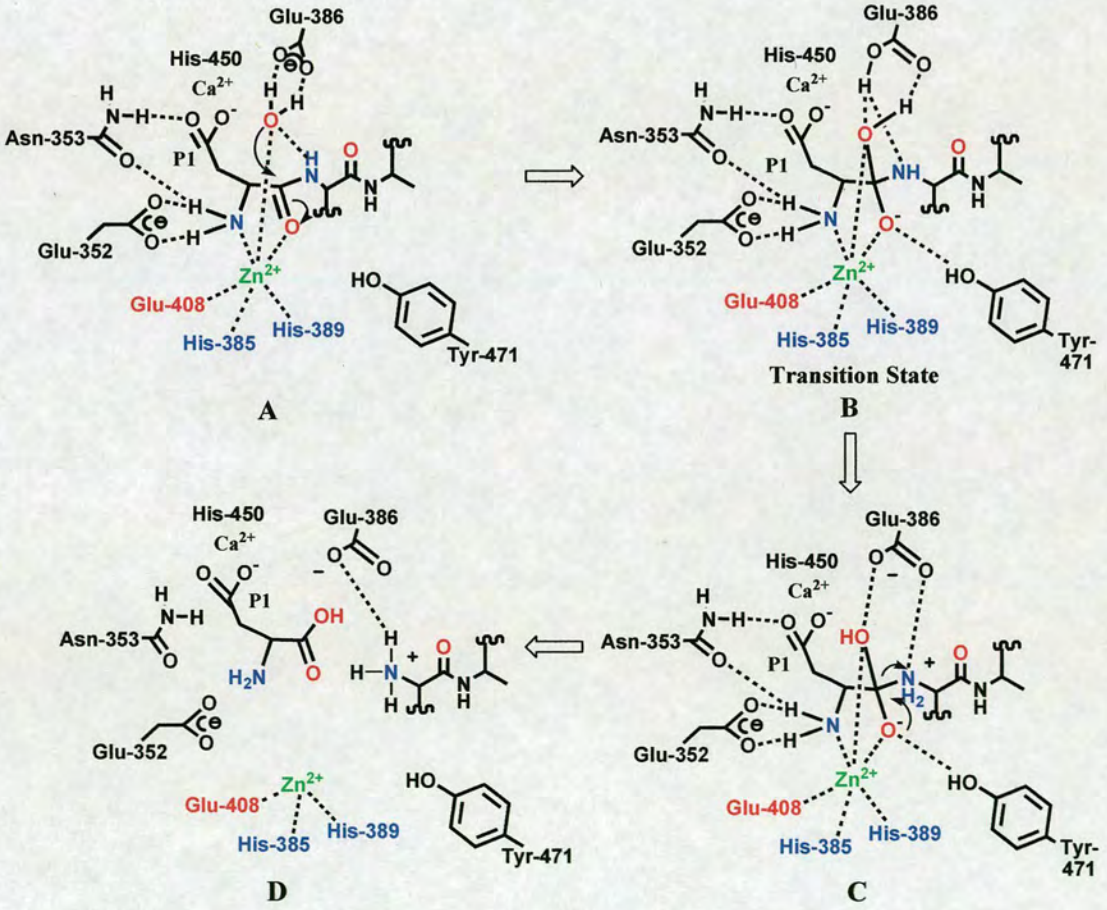

Scheme 5.2

The zinc ion is initially tetracoordinated by three amino acids residues (His 385, His 389 and Glu 408) and a water molecule. As the substrate enters the active site, is recognized, positioned and oriented by several residues: Ca^{2+} and His 450 interact with the P1 carboxylate of the side chain, Glu 352 hydrogen bond the free N-terminal of the substrate so does Asn-353, which simultaneously hydrogen bonds also to the P1 carboxylate. Then, the substrate coordinates through the carbonyl of the scissile amide bond and the unprotonated N-terminal to the zinc ion, which becomes hexacoordinated (Scheme 5.2 **A**). The negatively charged Glu 386 further polarises the zinc coordinated water molecule which performs its nucleophilic attack on the electrophilic amide carbon of the scissile peptide bond. The tetrahedral intermediate formed is stabilised by the zinc ion and hydrogen bonds interactions with Glu 386, Tyr 471 and Glu 352 (Scheme 5.2 **B**). At this point Glu 386 acts as a general acid and donates a proton to the amino leaving group, thus promoting the cleavage of the scissile amide group (Scheme 5.2 **C**). The products are then released and the active site is ready for a new cycle (Scheme 5.2 **D**).

5.1.2 Previous Studies

Several metal complexes have been used as synthetic models for metallopeptidases. Substitutionally inert metal complexes of Co(III) have demonstrated that amide hydrolysis can be promoted through activation of the carbonyl and/or intramolecular attack of a metal bound hydroxide (see chapter 2).[5a,5b] Complexes of Cu(II) and Zn(II) were also used to study the mechanism and reaction intermediates of metal-promoted amide-bond hydrolysis (see chapters 1 and 2).[6] Because of the great stability of peptide bonds, however, these studies generally involved activated amides.

Recently, it has been shown that Pd(II) complexes spontaneously bind to the side chains of methionine and histidine residues and effect hydrolytic cleavage of short peptides (see chapter 1).[7] To our knowledge the only metal complexes of biologically relevant Zn(II) and Cu(II) ions that are able to cleave unactivated peptides and/or proteins have been two Cu(II) complexes of two N_3 ligands.[8, 9]

One of these model systems was investigated by Hegg and Burstyn. They observed that hydrolysis of Gly-Gly incubated with 1 equivalent of 1,4,7-triazacyclononane dichloride copper(II) (Cu([9]aneN_3)-Cl_2) complex (Fig. 5.1) at 50 °C and at pH = 8.1 takes place in *ca.* 15% yield after 7 days.[8]

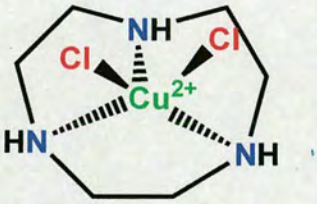

Fig. 5.1 The (Cu([9]aneN_3)-Cl_2) complex.

The second example was given by Fujii and coworkers, who reported that hydrolysis of Gly-Gly incubated with 1 equivalent of *cis, cis*-1,3,5-triaminocyclohexane-copper(II) $[Cu(tach)]^{2+}$ complex at the same pH and 70 °C after 1 day is about 18% (Fig. 5.2).[9]

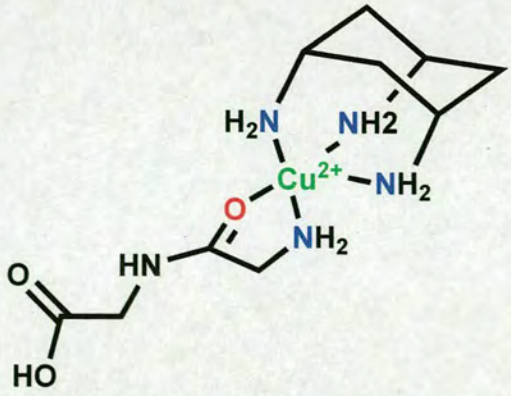

Fig. 5.2 The $[Cu(tach)(glygly)]^{+}$ complex.

Thus to date, no synthetic zinc(II) complex with double nitrogen and single carboxylate ligation has been reported. This work shows the structure of two zinc(II) complexes that resemble quite faithfully the zinc(II) ligation and several of the peripheral active site features of APA. Furthermore, we demonstrate that these complexes have the ability to hydrolyse the unactivated dipeptide glycylglycine (Gly-Gly) to glycine (Gly).

5.2 Results and Discussion

Perchlorate salts of $[(\mathbf{L}^{5.1}H^{+})_2Zn_2(Gly\text{-}Gly)_2]^{4+}$ $\mathbf{C}^{5.1}$ and $[(\mathbf{L}^{5.1}H^{+})Zn(Gly)]^{2+}$ $\mathbf{C}^{5.2}$ ($\mathbf{L}^{5.1}$ = 1-methyl-4-(6-amino-2-pyridinylmethyl)-piperazine; Gly = glycine anion, Gly-Gly = glycylglycine anion) were assembled by stirring a mixture of equimolar amounts of $\mathbf{L}^{5.1}$, $Zn(ClO_4)_2{\cdot}6H_2O$ and Gly-Gly for $\mathbf{C}^{5.1}$ and Gly for $\mathbf{C}^{5.2}$ in methanol (Fig. 5.3).

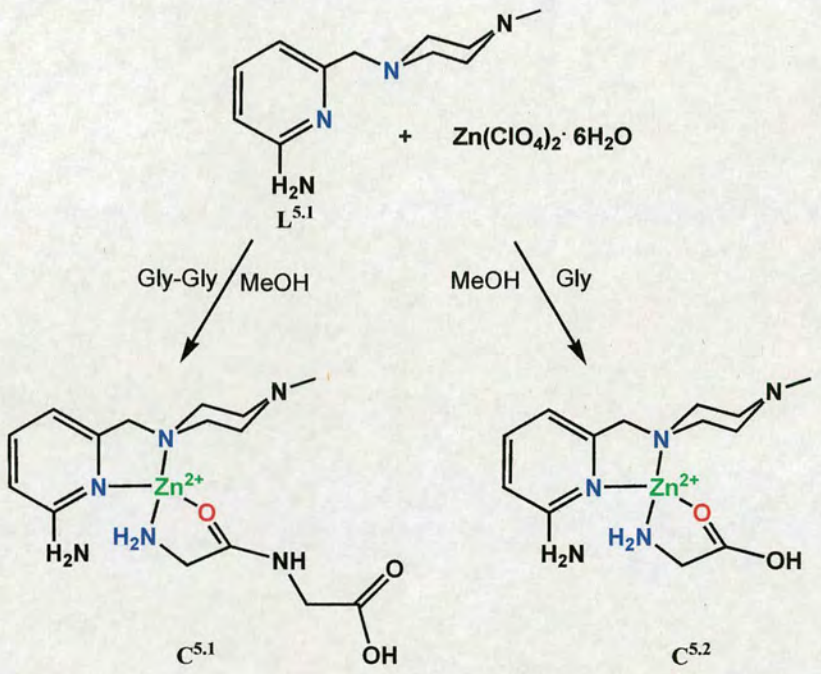

Fig. 5.3 The half dimers $[(\mathbf{L}^{5.1})Zn(Gly\text{-}Gly)]^{2+}$ ($\mathbf{C}^{5.1}$) complex and the $[(\mathbf{L}^{5.1})Zn(gly)]^{2+}$ ($\mathbf{C}^{5.2}$) complex.

Crystals of the two complexes were grown by slow evaporation of a MeOH–water solution at room temperature and their structures were determined by X-ray crystallography (Table 5.1).

Table 5.1 Crystallographic data and structure refinement details for $\mathbf{C}^{5.1}\cdot(ClO_4)_4\cdot 4H_2O$ and $\mathbf{C}^{5.2}\cdot(ClO_4)_2$.

	$\mathbf{C}^{5.1}\cdot(ClO_4)_4\cdot 4H_2O$	$\mathbf{C}^{5.2}\cdot(ClO_4)_2$
Empirical Formula	$C_{30}H_{60}Cl_4N_{12}O_{26}Zn_2$	$C_{13}H_{23}Cl_2N_5O_{10}Zn$
Formula	1277.44	545.63
T/K	150(2)	150(2)
Crystal system	Triclinic	Monoclinic
Space group	$P\bar{1}$	$P2_1/n$
λ(Mo-Kα) /Å	0.71073	0.71073
A/Å	9.0776(10)	16.0691(10)
B/Å	10.2002(11)	7.9677(5)
C/Å	14.5845(16)	16.3441(10)
α/°	104.467(2)	90
β/°	101.407(2)	96.9230(10)
γ/°	98.007(2)	90
V/Å^3	1256.2(2)	2077.3(2)
Z	1	4
D_{calc}/g cm^{-3}	1.689	1.745
μ/mm^{-1}	1.265	1.502
Reflections measured, unique	11411, 5900	18298, 5145
R_{int} (all data)	0.0274	0.0260
$R_1(F)^a$ (all data)	0.0657	0.0389
$wR_2(F^2)^a$ (all data)	0.1438	0.0909
$S(F^2)^a$ (all data)	1.069	1.047
Largest difference peak, hole/ e Å^3	1.317,-0.550	0.885, -0.504

[a] $R_1(F) = \Sigma(||F_o| - |F_c||)/\Sigma(|F_o|)$; $wR_2(F^2) = [\Sigma w (F_o^2 - F_c^2)^2/\Sigma wF_o^4]^{1/2}$; $S(F^2) = [\Sigma w (F_o^2 - F_c^2)^2/(n-p)]^{1/2}$.

In the crystal structures of $\mathbf{C}^{5.1}$ and $\mathbf{C}^{5.2}$ the zinc(II) centre is in a co-ordination environment between square pyramidal and trigonal bipyramidal (Figs. 5.4 (i) and 5.5 (i)). Whereas $\mathbf{C}^{5.1}$ adopts a dimeric structure of formulation $[(LH^+)_2Zn_2(Gly\text{-}Gly)_2](ClO_4)_4\cdot 2H_2O$ (Fig. 5.4 (ii)), $\mathbf{C}^{5.2}$ is a $[(LH^+)Zn(Gly)](ClO_4)_2$'polymer'(Fig. 5.5 (ii)). The Zn–N distances of Zn–N(1) 2.185(3) Å and Zn–N(2) 2.085(3) Å for $\mathbf{C}^{5.1}$ are slightly shorter than those of $\mathbf{C}^{5.2}$, (Zn–N(1) 2.1996(17) Å and Zn–N(2) 2.0957(16) Å) presumably because Gly is a slightly stronger ligand than Gly-Gly (Tables 5.2 and 5.3). As expected, Zn–N distances in $\mathbf{C}^{5.1}$ and $\mathbf{C}^{5.2}$ are longer than those of the tetrahedral complex $(L)Zn(Cl)_2$.[10] Binding provided by $\mathbf{L}^{5.1}$ mimics the bis-histidine zinc-ligation in aminopeptidases. Binding of the Gly and Gly-Gly through the COO^- group mimics glutamate binding to the zinc(II) centres of aminopeptidases.

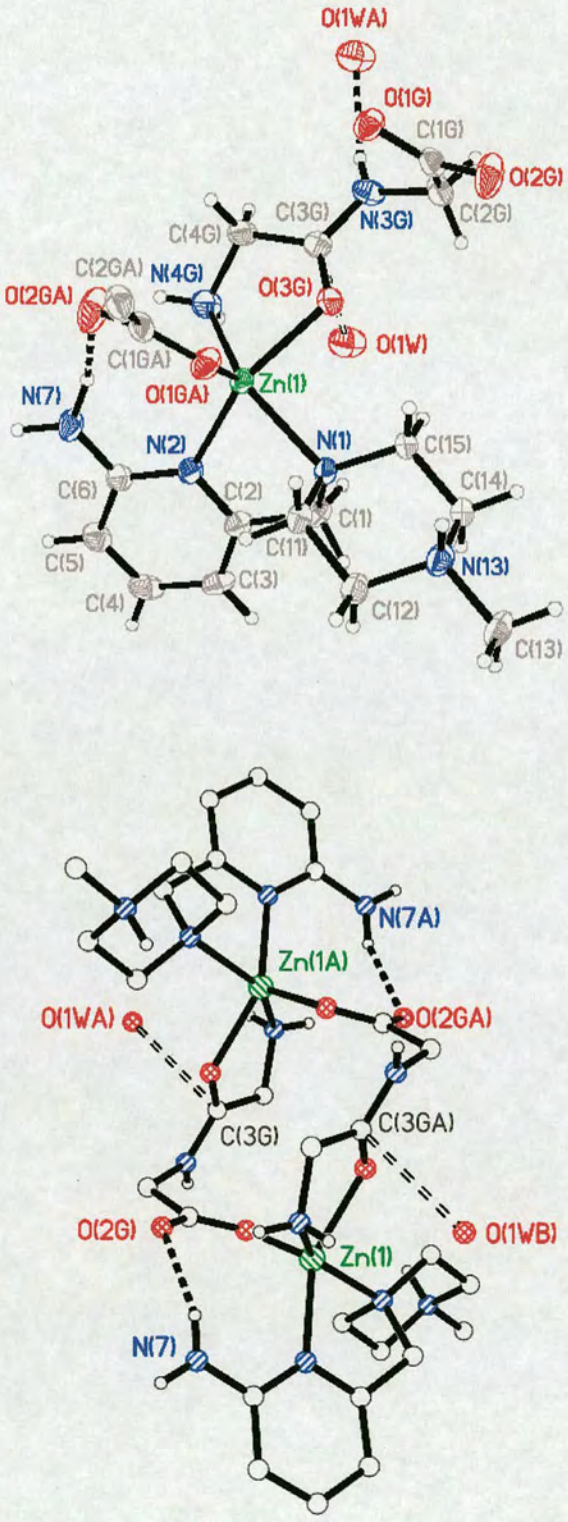

Fig. 5.4 (i) Thermal ellipsoid plot (50% probability) showing the zinc(II) co-ordination environment of **C**[5.1]; (ii) structure of the $[(LH^{+})_2Zn_2(Gly\text{-}Gly)_2]^{4+}$ cation with water molecules close to the amide bond.

Table 5.2 Selected bond lengths (Å) and angles (°) for zinc(II) complexes $\mathbf{C}^{5.1}$.

	$\mathbf{C}^{5.1}$
Distances	
Zn(1)-N(1)	2.185(3)
Zn(1)-N(2)	2.085(3)
Zn-N(4G)	2.099(3)
Zn-O(1GA)	1.952(2)
Zn-O(3G)	2.094(2)
Angles	
O(1GA)-Zn-N(2)	112.98(11)
O(1GA)-Zn-N(4G)	115.76(13)
O(1GA)-Zn-O(3)	94.14(10)
O(1GA)-Zn-N(1)	98.61(10)
N(2)-Zn-O(3G)	151.52(11)
N(2)-Zn-N(4G)	95.38(11)
N(2)-Zn-N(1)	78.78(10)
O(3G)-Zn-N(4G)	79.54(11)
O(3G)-Zn-N(1)	89.08(10)
N(4G)-Zn-N(1)	144.29(13)

In $\mathbf{C}^{5.1}$, the peptide (Gly-Gly) is co-ordinated through the terminal NH_2 group and the carbonyl amide oxygen atom. This mode of co-ordination was recently suggested to account for the ease of hydrolysis of Gly-Gly with the $[Cu(tach)]^{2+}$ complex (Fig. 5.2),[9] and also resembles the peptide binding mode proposed for APA. It is interesting that the proposed H-bonding between Glu-386 and Glu-352 of APA and the nucleophilic water/hydroxide and co-ordinated NH_2 from the peptide substrates (Scheme 5.1), which are believed to be functionally critical,[11] are mimicked by similar H-bonds to the perchlorate anions in the crystal structure of $\mathbf{C}^{5.1}$.

Remarkably, the positioning of a water molecule O(1W) in the crystal structure of $\mathbf{C}^{5.1}$ would be suitable for attack on the carbonyl carbon atom C(3G) (Fig. 5.4, O(1W)···

C(3G) 3.050 Å), which should be activated for nucleophilic attack by the zinc(II) centre. Moreover, like in the case of Gly-Gly hydrolysis with the $[Cu(tach)]^{2+}$ complex, the peptide chelate ring would not be required to be broken for hydrolysis to occur, as shown by the retention of this chelation motif in crystal structure of **C**[5.2]. Thus Gly is chelated to one zinc(II) ion *via* the nitrogen atom and oxygen atom of the carboxylate, and bridges to the next zinc *via* the other oxygen atom.

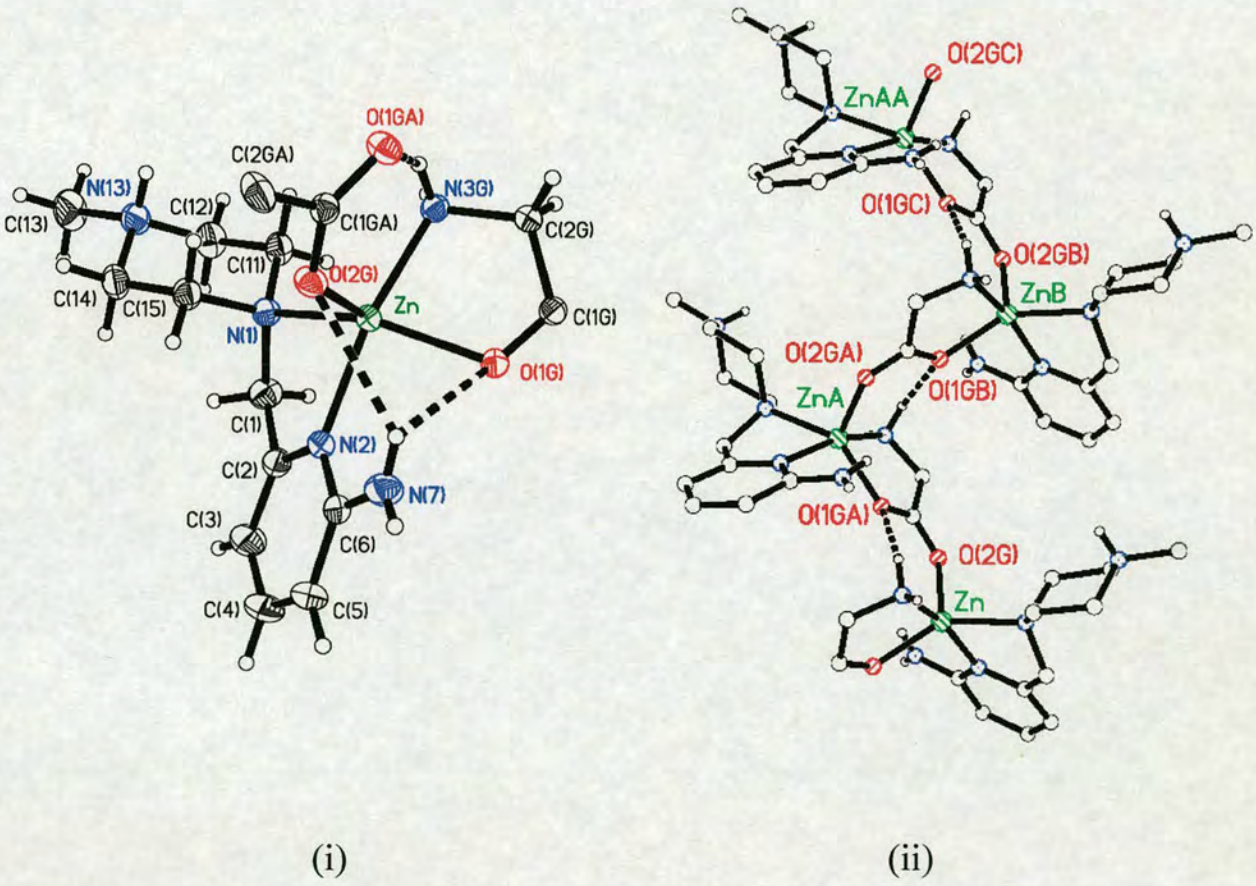

Fig. 5.5 (i) Thermal ellipsoid plot (50% probability) showing the zinc(II) co-ordination environment of **C**[5.2]; (ii) The polymeric chain structure of the $[(LH^{+})Zn(gly)]^{2+}$ cation.

To our knowledge the only other example with this polymeric chain structure is $[Cu(Gly)(NO_3)(H_2O)]$.[12] The positioning of the NH_2 group of the ligand in **C**[5.2] is such that forms hydrogen bonding with both of the oxygens of the carboxylate group of Gly

(N(7)···O(1G) 3.059 Å, N(7)···O(2G) 3.225 Å). Similarly, the amino group of the ligand in $\mathbf{C}^{5.1}$ is H-bonded to one of the oxygens of the zinc(II) bound carboxylate group of Gly-Gly (N(7)···O(2G) 2.957 Å). In principle, these H-bonding interactions may assist peptide binding and orient the bound peptide.

Table 5.2 Selected bond lengths (Å) and angles (°) for zinc(II) complexes $\mathbf{C}^{5.2}$.

	$\mathbf{C}^{5.2}$
Distances	
Zn-N(1)	2.1996(17)
Zn-N(2)	2.0957(17)
Zn-N(3G)	2.0799(17)
Zn-O(1G)	2.0645(14)
Zn-O(2GA)	2.0020(14)
Angles	
O(2GA)-Zn-O(1)	111.13(6)
O(2GA)-Zn-N(3G)	102.08(6)
O(1G)-Zn-N(3G)	81.41(6)
O(2GA)-Zn-N(2)	94.52(6)
O(1G)-Zn-N(2)	90.61(6)
O(2GA)-Zn-N(1)	103.88(6)
O(1G)-Zn-N(1)	143.95(6)
N(3G)-Zn-N(2)	163.24(7)
N(3G)-Zn-N(1)	99.79(7)
N(2)-Zn-N(1)	78.09(6)

We have investigated the hydrolysis of $\mathbf{C}^{5.1}$ by NMR and found that Gly-Gly is hydrolysed to Gly at 70 °C and pH 7 ± 0.1 (50 mM HEPES). After five days cleavage is almost 30%, much higher than the spontaneous hydrolysis which under the same conditions is only about 2% (Fig. 5. 6). Gly-Gly was cleaved at $\mathbf{C}^{5.1}$ and pH 7 with similar efficiency to two copper(II) complexes (*vide supra* Figs. 5.1 and 5.2).

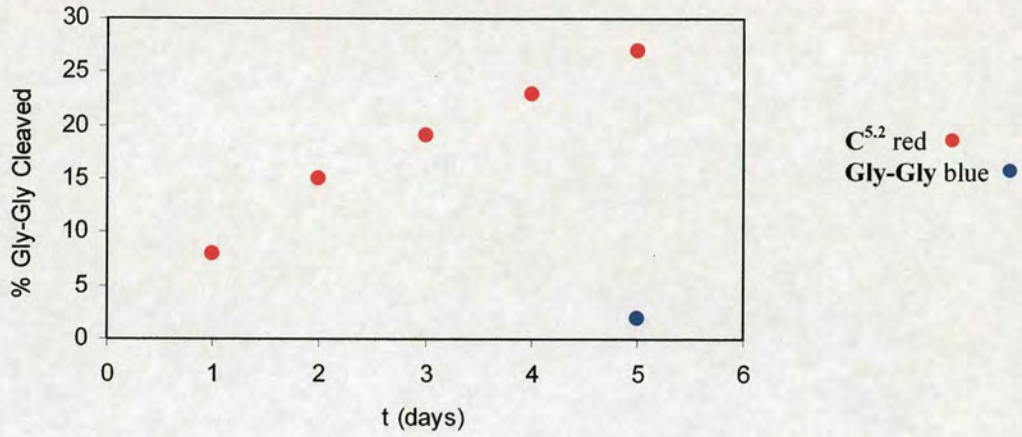

Fig. 5.6 Extent of hydrolysis of Gly-Gly of $\mathbf{C^{5.1}}$ and Gly-Gly to Gly at 70 °C and pH 7 ± 0.1 (50 mM HEPES) at different times.

Unlike previously reported synthetic model complexes of metallopeptidases or peptide cleaving agents, $\mathbf{C^{5.1}}$ utilizes a biologically-relevant metal ion, zinc(II), in a biologically-relevant co-ordination environment and achieves cleavage of an otherwise unactivated peptide bond under mild physiological conditions. In fact, the half-life of hydrolysis of Gly-Gly at pH 7 and 70 °C has been estimated to be *ca.* 2 years.[13]

5.3 Conclusion and Future Work

In summary, the structures of two zinc(II) complexes with Gly-Gly and Gly co-ordinated to the zinc(II) centre are reported. These two complexes represent the first crystallographically characterized zinc(II) complexes in which the zinc(II) centre is in co-ordination environment that closely resembles the active site and reaction intermediates proposed for aminopeptidases. Furthermore, hydrolysis of Gly-Gly at the zinc(II)–Gly-Gly complex is achieved at physiological pH. Thus, to our knowledge, this is the first example of an unactivated peptide being hydrolysed by a small biomimetic zinc(II) complex. For future work it would be interesting to investigate the

hydrolysis of Gly-Gly promoted by other mononuclear and dinuclear zinc(II) complexes bearing multiple hydrogen bond functionalities (Fig. 5.7).

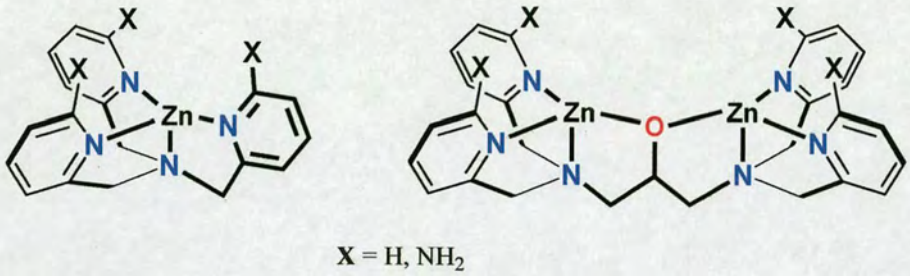

X = H, NH_2

Fig. 5.7 Mononuclear and dinuclear zinc(II) complexes for the hydrolysis of peptide bonds.

Preliminary studies showed that ^{1}H NMR spectra display peaks overlaps in the region of interest (3-4 ppm) between the complexes and the Gly-Gly and/or Gly, thus making difficult to evaluate accurately the extent of the hydrolysis. Therefore, an alternative route would be to monitor the cleavage reaction by HPLC. In order to do so Gly-Gly and Gly need to be made UV active by derivatisation with (dimethylamino)azobenzensulfonyl chloride (DABS-Cl) (Fig. 5.8).

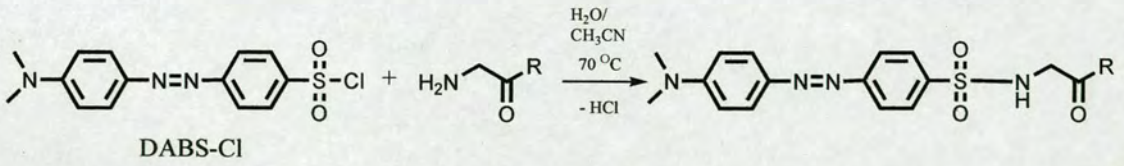

DABS-Cl

Gly: R = OH
Gly-Gly: R= Gly(-H)

Fig. 5.8 Derivatistion of Gly-Gly and Gly with DABS-Cl.

Initial experiments proved that DABS-Gly-Gly and DABS-Gly can be eluted with a 15%-30% water/acetonitrile gradient having retention times of 22 and 26 mins,

respectively. Unfortunately, lack of time did not permit to complete these studies and investigations are currently still in progress.

Once these aspects are elucidated it would be also interesting to explore the effect that these complexes might promote on the hydrolysis of different peptides, polypeptides and proteins.

5.4 Experimental

5.4.1 General

Reagents were obtained from commercial sources and used as received unless otherwise noted. Solvents were dried and purified under N_2 by using standard methods[1] and were distilled immediately before use. Buffer solutions of HEPES (2-(4-(2-hydroxyethyl)-1-piperazinyl)ethanesulfonic acid, (50 mM in H_2O) pH 7.0 were used for the hydrolysis studies. All compounds were prepared under N_2 unless otherwise mentioned. 1-Methyl-4-(-6-amino-2-pyridinylmethyl)-piperazine (L) was synthesized according to a recently reported procedure.[2] The NMR spectra were obtained using a Bruker DPX 360 at 20 °C in D_2O unless otherwise noted. ^{13}C and ^{1}H chemical shifts are referenced with respect to the carbon (δ_C 0 ppm) and proton resonances (δ_H 0.00 ppm) of TSP (external standard). Mass spectra were performed on a micromass Platform II system operating in Flow Injection Analysis mode with the electrospray method. Elemental analyses were carried out by the microanalyses service provided by the School of Chemistry at the University of Edinburgh.

5.4.2 Synthesis

$[((L^{5.1}H^{+})_2Zn_2(Gly\text{-}Gly)_2](ClO_4)_4(H_2O)_2$ **$C^{5.1}\cdot(ClO_4)_4(H_2O)_2$** $Zn(ClO_4)_2 \cdot 6H_2O$ (74.5 mg, 0.2 mmol) and 1-methyl-4-(-6-amino-2-pyridinylmethyl)-piperazine (**$L^{5.1}$**) (41.3 mg, 0.2 mmol) were dissolved in MeOH (10 mL). After 10 min, glycylglycine (26.4 mg, 0.2 mmol) was added and the reaction mixture was stirred at room temperature until a white cloudy solution was formed (ca. 1h). The precipitate was isolated by centrifugation and dried under vacuum to afford the pure compound as a white solid

(115 mg, 95%) (Found: C, 29.25; H, 4.34; N, 13.27. Calc. for $C_{30}H_{54}Cl_4N_{12}O_{24}Zn_2$: C, 29.07; H, 4.39; N, 13.56). ^{1}H NMR (D_2O, 360.1 MHz, 293 K) δ_H (ppm) 7.60 (dd, J = 8.3 and 7.2 Hz, 1H, py'-*H4*), 6.74 and 6.69 (d, J = 7.2 Hz, 1H and d, J = 8.3 Hz, 1H; py'-*H3* and py'-*H5*), 3.87 and 3.65 (s, 2H and 2H, CH_2 (Gly-Gly)), 3.74 (s, 2H, NCH_2-py'), 3.23 and 2.9 (br.s., 4H and 4H, N(CH_2CH_2)$_2$N-CH_3) and 2.78 (s, 3H, N(CH_2CH_2)$_2$N-CH_3). ^{13}C NMR (D_2O, 90.5 MHz, 293 K) δ_C (ppm); 179.4 and 176.4 (*C*=O (Gly-Gly)), 161.3 and 153.1 (py'-*C2* and py'-*C6*), 143.7 (py'-*C3*), 116.7 and 113.6 (py'-*C4* and py'-*C5*), 64.1 (N*C*H_2-py'), 54.9 and 52.7 (N(*C*H_2*C*H_2)$_2$N-CH_3), 45.9 (N(*C*H_2*C*H_2)$_2$N-*C*H_3), 46.4 and 43.4 (*C*H_2 (Gly-Gly)). ESI-MS (+ ion) Found 401.0, Calcd. for $[(L)Zn(Gly\text{-}Gly)]^+$ 401.1 (100%), and matches theoretical isotope distribution.

[((LH^+)Zn(Gly)](ClO$_4$)$_2$ C$^{5.2}$. $Zn(ClO_4)_2 \cdot 6H_2O$ (74.5 mg, 0.2 mmol) and 1-methyl-4-(-6-amino-2-pyridinylmethyl)-piperazine (**L**$^{5.1}$) (41.3 mg, 0.2 mmol) were dissolved in MeOH (10 mL). After 10 min glycine (15 mg, 0.2 mmol) was added and the reaction mixture was left stirring at room temperature until a white cloudy solution was formed (ca. 1h). The precipitate was isolated by centrifugation and dried under vacuum to afford the pure compound as a white solid (100 mg, 92%) (Found: C, 28.62; H, 4.21; N, 12.71. Calc. for $C_{13}H_{23}Cl_2N_5O_{10}Zn$: C, 28.62; H, 4.25; N, 12.84). ^{1}H NMR (D_2O, 360.1 MHz, 293 K) δ_H (ppm) 7.62 (t, J = 7.6 Hz, 1H, py'-*H4*), 6.78 and 6.70 (d, J = 7.2 Hz, 1H and d, J = 8.3 Hz, 1H; py'-*H3* and py'-*H5*), 3.71 (s, 2H, NCH_2-py'), 3.37 (s, 2H, CH_2 (Gly)), 3.21 and 2.9 (br.s., 4H and 4H, N(CH_2CH_2)$_2$N-CH_3) and 2.79 (s, 3H, N(CH_2CH_2)$_2$N-CH_3). ^{13}C NMR (D_2O, 90.5 MHz, 293 K) δ_C (ppm); 181.4 (*C*=O (Gly)), 161.2 and 153.9 (py'-*C2* and py'-*C6*), 143.2 (py'-*C3*), 117.1 and 113.1 (py'-*C4* and py'-*C5*), 63.4 (N*C*H_2-py'), 55.1 and 52.6 (N(*C*H_2*C*H_2)$_2$N-CH_3), 45.8

($N(CH_2CH_2)_2N$-CH_3), 44.6 (CH_2 (Gly)). ESI-MS (+ ion) Found 343.9, Calcd. for $[(L)Zn(Gly)]^+$ 344.10 (100%), and matches theoretical isotope distribution.

5.4.3 Hydrolysis Studies

NMR tubes containing $\mathbf{C}^{5.1}\cdot(ClO_4)_4\cdot 2H_2O$ or Gly-Gly (as control) in D_2O (25 mM) were incubated at 70 °C and pH 7.0 ± 0.1. Solutions were evaporated to dryness under vacuum, D_2O (0.6 cm^3) was added and the ^1H NMR spectra were recorded after 1, 3 and 5 days. This procedure, introducing D_2O after incubation at elevated temperatures, was adopted (1) to avoid solvent deuterium effects on reaction rates and (2) to avoid exchange of carbon-bound hydrogen atoms. Cleavage of the amide bond of Gly-Gly to Gly is indicated by the appearance of the proton resonance at 3.4 ppm of Gly, which grows over time. The identity of the product was confirmed by the detection of peaks due to the $[(L)Zn(Gly)]^+$ cation by ESI-MS (+ ion). The concentration of this hydrolysis product after 1, 3 and 5 days was determined from the integrated resonances of the glycine CH_2 protons and aromatic protons of the ligand $\mathbf{L}^{5.1}$. The concentration of Gly estimated in this way was used to determine the percentage of Gly-Gly cleaved. Each hydrolysis experiment was repeated at least three times. The pH of the solutions was checked periodically and remained constant throughout the hydrolysis reactions (± 0.2 pH units).

5.4.4 X-ray Crystallography

Crystals suitable for X-ray diffraction studies were grown by slow evaporation of water/methanol solutions at room temperature.

Intensity data for $[(LH^+)_2Zn_2(Gly\text{-}Gly)_2](ClO_4)_4\cdot 2H_2O$ $\mathbf{C}^{5.1}\cdot(ClO_4)_4\cdot 2H_2O$ and $[(LH^+)Zn(Gly)](ClO_4)_2$ $\mathbf{C}^{5.2}\cdot(ClO_4)_2$ were collected at 150 K using a Bruker-AXS

SMART APEX area detector diffractometer with graphite-monochromated Mo Kα radiation (λ = 0.71073 Å). The structures were solved by direct methods and refined to convergence against F^2 data using the SHELXTL suite of programs.[3] Data were corrected for absorption applying empirical methods using the program SADABS,[4] and the structures were checked for higher symmetry using the program PLATON.[5] All non-hydrogen atoms were refined anisotropically unless otherwise noted. Hydrogen atoms were placed in idealized positions and refined using a riding model with fixed isotropic displacement parameters. The N-H hydrogens were located in the difference map and refined isotropically. One of the ClO_4^- anions and one of the water molecules of $\mathbf{C}^{5.1}$ was disordered and modelled over two positions with 60% and 40% occupancy.

References

[1] E. L. Hegg and J. N. Burstyn, *Coord. Chem. Rev.*, 1998, **173**, 133.

[2] W. N. Lipscomb and N. Sträter, *Chem. Rev.*, 1996, **96**, 2375.

[3] R. Krämer, *Coord. Chem. Rev.*, 1999, **182**, 243.

[4] (*a*) I. Nagatsu, T. Nagatsu, T. Yamamoto, G. G. Glenner and J. W. Mehl, *Biochim. Biophys. Acta*, 1970, **198**, 255; (*b*) S. Wilk and D. Healy, *Adv. Neuroimmunol.*, 1993, **3**, 195; (*c*) X. Iturrioz, R. Rozenfeld, A. Michaud, P. Corvol and C. Llorens-Cortes, *Biochemistry*, 2001, **40**, 14440.

[5] (*a*) P. A. Sutton and D. A. Buckingham, *Acc. Chem. Res.*, 1987, **20**, 357; (*b*) J. T. Groves and L. A. Baron, *J. Am. Chem. Soc.*, 1989, **111**, 5442; (*c*) K. Takasaki, J. H. Kim, E. Rubin and J. Chin, *J. Am. Chem. Soc.*, 1993, **115**, 1157.

[6] (*a*) L. Meriwether and F. H. Westheimer, *J. Am. Chem. Soc.*, 1956, **78**, 5119; (*b*) W. A. Connor, M. M. Jones and D. L. Tuleen, *Inorg. Chem.*, 1965, **4**, 1129; (*c*) J. T. Groves and R. J. Rife Chambers, Jr., *J. Am. Chem. Soc.*, 1984, **106**, 630; (*d*) T. H. Fife and T. J. Przystas, *J. Am. Chem. Soc.*, 1986, **108**, 4631; (*e*) J. Chin, V. Jubian and K. Mrejen, *J. Chem. Soc., Chem. Commun.*, 1990, 1326; (*f*) B. F. Duerr and A. W. Czarnik, *J. Chem. Soc., Chem. Commun.*, 1990, 1707; (*g*) L. M. Sayre, K. V. Reddy, A. R. Jacobson and W. Tang, *Inorg. Chem.*, 1992, **31**, 935.

[7] T. N. Parac, G. M. Ullmann and N. K. Kostic, *J. Am. Chem. Soc.*, 1999, **121**, 3127.

[8] E. L. Hegg and J. N. Burstyn, *J. Am. Chem. Soc.*, 1995, **117**, 7015.

[9] X. S. Tan, Y. Fujii, T. Sato, Y. Nakano and M. Yashiro, *Chem. Commun.*, 1999, 881.

[10] J. C. Mareque Rivas, E. Salvagni, R. Torres Martín de Rosales and S. Parsons, *Dalton Trans.*, 2003, 3339.

[11] G. Vazeux, J. Wang, P. Corvol and C. Llorens-Cortes, *J. Biol. Chem.*, 1996, **271**, 9069.

[12] H. O. Davies, R. D. Gillard, M. B. Hursthouse, M. A. Mazid and P. A. Williams, *J. Chem. Soc., Chem. Comm.*, 1992, 226.

[13] A. Radzicka and R. Wolfenden, *J. Am. Chem. Soc.*, 1996, **118**, 6105.

Summary and Future Work

Amide oxygen metal coordination is considered to be one of the key factors of metallopeptidases, as is the stability of the scissile amide bond.

This thesis shows how amino hydrogen bonding groups adjacent to a zinc(II) ion, as well as different numbers and types of metal binding sites, affect binding and cleavage of peptide bonds. This study also shows that different hydrogen bond environments around a metal can drastically influence the stability of the intracomplex metal-bound amide bond, thus accelerating or slowing down the rate of its cleavage. In addition, this work demonstrates that zinc(II) complexes promote hydrolysis of exogenous peptides (Gly-Gly).

In view of this results, future studies could examine how positioning of several hydrogen bond functionalities local to metal centre(s) influence binding and cleavage of polypeptides and proteins. Therefore, further investigations could be undertaken by following two possible approaches. Firstly, a logical consequence would be to functionalise the complexes prepared in this work, and others providing different donor/acceptor hydrogen bonding groups such as carboxylate, guanidines, alkyl and aryl amines, and thioureas.

An alternative approach would be to investigate peptide binding and cleavage promoted by polymetallic complexes and the effect of hydrogen bonding groups in this environment.

These results may help elucidate the mechanism of action of peptidase, more specifically, the functional role of metal ion in cooperation with hydrogen bonding groups in the active site. A better understanding of these systems could provide essential information to develop new strategies for the design of novel synthetic peptidases, whose potential applications in biotechnology have been envisioned.